Vibration Frequencies of Rotating Tapered Beam Including Rotary Inertia and Transverse Shear Deformation

by

Abdelaziz Bazoune

A Thesis Presented to the

FACULTY OF THE COLLEGE OF GRADUATE STUDIES

KING FAHD UNIVERSITY OF PETROLEUM & MINERALS

DHAHRAN, SAUDI ARABIA

In Partial Fulfillment of the
Requirements for the Degree of

MASTER OF SCIENCE

In

MECHANICAL ENGINEERING

June, 1990

Order Number 1355725

Vibration frequencies of rotating tapered beam including rotary inertia and transverse shear deformation

Bazoune, Abdelaziz, M.S.

King Fahd University of Petroleum and Minerals (Saudi Arabia), 1990

U·M·I
300 N. Zeeb Rd.
Ann Arbor, MI 48106

Vibration Frequencies of Rotating Tapered Beam Including Rotary Inertia and Transverse Shear Deformation

BY

ABDELAZIZ BAZOUNE

A Thesis Presented to the

FACULTY OF THE COLLEGE OF GRADUATE STUDIES

KING FAHD UNIVERSITY OF PETROLEUM & MINERALS

DHAHRAN, SAUDI ARABIA

In Partial Fulfillment of the
Requirements for the Degree of

MASTER OF SCIENCE

In

MECHANICAL ENGINEERING

JUNE 1990

KING FAHD UNIVERSITY OF PETROLEUM & MINERALS

DHAHRAN, SAUDI ARABIA

This thesis, written by

ABDELAZIZ BAZOUNE

under the direction of his Thesis Advisor, and approved by his Thesis Committee, has been presented to and accepted by the Dean of the College of Graduate Studies, in partial fulfillment of the requirements for the degree of

MASTER OF SCIENCE IN MECHANICAL ENGINEERING

Thesis Committee

Chairman (Dr. Y. A. KHULIEF)

Member (Dr. A. K. KAR)

Member (Dr. R. R. GUNTUR)

Member (Dr. K. A. F. MOUSTAFA)

Department Chairman

Dean College of Graduate Studies

Date : 18 - 6 - 90

To my parents and my wife.

ACKNOWLEDGEMENT

Acknowledgement is due to King Fahd University of Petroleum and Minerals for the support of this research .

My deep appreciation and thanks are due to my thesis committee chairman and academic advisor Dr. Y. A. Khulief . He was generous in time and thought . My thanks are also due to other committee members : Dr. A. K. Kar , Dr. R. R. Guntur and Dr. K. A. F. Moustafa for their coordination .

Sincere thanks are due to department chairman Dr. Habib Abul hamayel for immeasurable cooperation.

Finally I thank my wife for her indispensable patience throughout this research work .

TABLE OF CONTENTS

LIST OF TABLES

LIST OF FIGURES

Figure *Page*

NOMENCLATURE

A	element cross-sectional area
$[B]$	strain displacement matrix
E	modulus of elasticity
F_x , F_z	centrifugal forces
G	modulus of rigidity
I	second moment of cross-sectional area
i	refers to the i th element
J	rotary inertia
$[K]$	global stiffness matrix
$[k_e]$	elastic stiffness matrix
$[k_s]$	shear stiffness matrix
$[k_c]$	centrifugal stiffness matrix
k'	shear correction factor
L	Lagrangian
L	truncated length of the beam
L_{oy}	untruncated length of the beam in the x-y plane
L_{oz}	untruncated length of the beam in the x-z plane
l^i	element length
$[M]$	global mass matrix
$[M_t]$	translational mass matrix
$[M_r]$	rotary inertia mass matrix
$[N]$	matrix of shape functions
n	total number of elements

$\{q\}$	vector of nodal coordinates
$\{\bar{q}\}$	vector of displacement amplitudes of vibration
r	position vector
r_g	radius of gyration of the cross-section $= \sqrt{(I/A)}$
t	time
T	kinetic energy
U	strain energy
u	axial displacement
V	potential energy due to centrifugal force
w	transverse displacement
(x, y, z)	local coordinate axes
(X, Y, Z)	global coordinate axes
α_i	constant
β_i	constant
γ	angle of distortion due to shear
γ_{xz}	unit shearing strain
δ	variation
$\varepsilon_{xx}, \varepsilon_{yy}$	unit elongation in x and y -directions
η	rotational speed parameter $= \Omega L^2 / \sqrt{EI_o / \rho A_o}$
θ	angle of rotation due to bending
κ	curvature
Λ_i	constant
λ	frequency parameter $= \omega \sqrt{\rho A_o L^4 / EI_o}$
μ_i	constant
ν	Poisson's ratio

ν_y	taper ratio in the x-y plane $= L / L_{oy}$
ν_z	taper ratio in the x-z plane $= L / L_{oz}$
ξ^i	nondimensional length $= x^i / l^i$
Π	total potetial energy $= U + V$
ρ	mass density
σ_{xx}	normal stress parallel to x -axis
τ_{xz}	shear stress
Φ	shear deformation parameter
Ψ	setting angle
Ω	rate of spin of the beam
ω	natural frequency of the beam
$[\ ]^T$	transpose of $[\ ]$

THESIS ABSTRACT

NAME OF STUDENT : *ABDELAZIZ BAZOUNE*

TITLE OF STUDY : *Vibration Frequencies of Rotating Tapered Beam Including Rotary Inertia and Transverse Shear Deformation .*

MAJOR FIELD : *Mechanical Engineering*

DATE OF DEGREE : *June, 1990*

The out-of-plane free vibration of a rotating tapered beam based on both Euler and Timoshenko theories are presented by means of the finite element technique . The beam which is assumed to be linearly tapered in two planes is discretized into a number of simple elements with four degrees of freedom each . The governing equations for the free vibrations of the rotating tapered beam are derived from Hamilton's principle . Explicit expressions for the finite element mass and stiffness matrices are derived by using a consistent mass formulation . The generalized eigenvalue problem is defined and numerical solutions are generated for a wide range of rotational speed and taper ratios . Results obtained include the first ten frequencies for both fixed and hinged end conditions . Comparisons are made whenever possible with exact solutions and with numerical results available in the literature . The results display high accuracy when compared with other numerical results .

MASTER OF SCIENCE DEGREE

KING FAHD UNIVERSITY OF PETROLEUM AND MINERALS

Dhahran , Saudi Arabia

June 1990

خلاصة الرسالة

اسم الطالب الكامل : عبدالعزيز بازون
عنوان الدراسة : ترددات الإهتزاز لعتبة دورانية متناقصة القطر ذات تشوه قصي وعطالة دورانية .
التخصص : هندسة ميكانيكية
تاريخ الشهادة : يونيو ١٩٩٠م .

طبقت تقنية العنصر المحدود على عتبة دورانية متناقصة القطر تهتز إهتزازاً حراً خارج المستوى بناءً على نظريتي (Euler) و (Timoshenko) . إن هذه العتبة المفترض أن تكون متناقصة القطر خطياً في سطحين مستويين أمكن تقسيمها إلى عدد من العناصر البسيطة لكل منها أربع درجات حرة . أما المعادلات التي تحكم الإهتزاز الحر في العتبة الدورانية فقد أمكن إشتقاقها من مبدأ (Hamilton) ، كما أشتقت العبارة الصريحة للعنصر المحدود لكل من مصفوفتي الصلبية والكتلة إعتماداً على التشكل الكتلي المتماسك ، وقد تم تعريف المشكل المميز (Eigenvalue Problem) ومنه وجدت الحلول الرقمية لمعدلات واسعة من السرعات الدورانية ونسب التناقص. والنتائج التي تم الحصول عليها تشمل الترددات العشر الأولى لكل من الحالات الثابتة والمعلقة النهاية ، كما تم عمل بعض المقارنات بقدر الإمكان مع الحلول الصحيحة والرقمية الموجودة في البحوث السابقة . وتعكس هذه النتائج تطابقاً كبيراً بالمقارنة مع النتائج الرقمية الأخرى .

درجة الماجستير في العلوم
جامعة الملك فهد للبترول والمعادن
الظهران – المملكة العربية السعودية
يونيو ١٩٩٠م .

CHAPTER ONE

INTRODUCTION

1.1 GENERAL

Many engineering systems have mechanical components , that can be modeled by rotating structural beams . Examples are turbomachines , turbine blades , aircraft propellers , helicopter rotors , high speed flexible mechanisms , robot manipulators , and spinning space structures .

The dynamic behaviour of beams and shafts has been the subject of intensive study for many years . The finite element method , in conjunction with digital computers , has been proven to be a powerful technique for the design of complex structures .

The lateral vibration of beams was usually approximated by the Bernoulli-Euler differential equation (Classical Theory) . Corrections due to the effect of rotary inertia (Rayleigh Theory) and transverse shear deformation (Timoshenko Theory) may be of importance if the effect of the cross-sectional dimensions on frequencies cannot be neglected , or when higher modes and frequencies of vibrations are desired . These effects may also cause appreciable perturbations of all modes when the theory of beams is employed as a basis for study of complicated structures ; such as wings of airplanes and missile structures . There has been a considerable interest recently in developing techniques for the solution of equations of rotating tapered beams .

Although analytical solutions may be possible for some special cases , numerical methods have become important due to the difficulties in the solution of tapered beams

Several studies were directed to the evaluation of natural frequencies and mode shapes of a rotating uniform beam undergoing transverse vibrations . Early investigations by Schilhansl [1] and Pruelli [2] have shown that rotation of a beam tended to increase its natural frequencies of flexural motion . Rotating flexible components are known to experience centrifugally induced tensile force that tend to increase the effective torsional and flexural stiffness . The rotary inertia is equivalent to an increase in mass and therefore will cause a decrease in natural frequency. Furthermore , the effect is more pronounced and influencial at the higher frequencies .

Vibrations of rotating beams have been extensively studied by numerous authors using a variety of methods ; for example , the Southwell principle , the Rayleigh-Ritz method , the perturbation technique , the Myklestad method , the transfer matrix approach , the method of integral equations , the Galerkin procedure and several forms of the finite element techniques [3] .

1.2 LITERATURE SURVEY

Untill the middle 1960s , most of the work was based on continuum methods such as Rayleigh-Ritz and Galerkin methods . More recently finite element methods are being introduced [4] .

1.2.1 NON-ROTATING BEAMS

Vibration analysis of non-rotating tapered beams has been addressed by a few investigators . A detailed literature review of this subject is given by Downs [5] .

The published material which is of relevance to this work can be classified under the following headings and is thoroughly reviewed in [6] :

1 - Uniform and tapered Bernoulli-Euler beams.

2 - Uniform Timoshenko beams.

3 - Tapered Timoshenko beams.

A considerable number of Timoshenko beam finite elements for use in vibration problems have been described in reference [7] . In a critical review of many of the uniform straight beam elements , it was shown that the elements could be classified as simple ; having two degrees of freedom at each of two end nodes , or complex ; with additional degrees of freedom , reference [7] . Dugundji [8] obtained simple expressions for vibration modes of uniform Euler beams . Lin [9] developed a finite element method for a uniformly loaded cantilever beam with a general cross-section . Heppler and Hansen [10] used trigonometric basis functions in developing a finite element method for a uniform Timoshenko beam . The properties and performance of these new elements were explored through a series of illustrative problems that treat both straight and curved geometries . Yuan and Miller [11] developed a higher order finite element for short beams .

Gallagher et al. [12] have employed the finite element method to estimate natural frequencies and mode shapes of a non-rotating tapered beam . Sato [13] examined natural frequencies of axially loaded tapered beams. The most recent work reported by Williams et al. [14] evaluated the first five natural frequencies of axially loaded tapered beams based on stepped representation approach . Although the methods presented in [13,14] consider axial loads , they are restricted to non-rotating tapered beams . Carnegie and Thomas [15] studied the influence of pretwist and taper of non-rotating beams . Goel [16] presented a study to obtain characteristic equations for linearly tapered beams with elastically restrained ends . Downs [5] determined the natural frequencies of an isotropic cantilever beams with doubly symmetric cross-section , based on both Euler and Timoshenko theories for 36 combinations of linear depth and breadth taper . Taber and Viano [17] calculated resonant frequencies and mode shapes by a transfer matrix technique for Timoshenko beams of varying cross-sections . With the non-uniform beam represented by a series of uniform segments , results were given for longitudinal , torsional and flexural vibration . To [18] , examined two integral parts : namely the examination and development of higher order tapered beam finite elements and the application of the higher order tapered beam elements to the transverse vibration of tapered cantilever beam structures with end mass and rotary inertia of the end mass representing a class of tapered mast antenna structures . Later , To [19] developed an explicit mass and stiffness matrices of a linearly tapered finite element in order to provide a means for incorporating , as well as investigating , the effect of the secondary contributions of shear deformation and rotary inertia in vibration analysis of a class of a mast antenna structures treated as linearly tapered cantilever beam structures . Vesniere de Irassar et al. [20] used the Ritz method to determine the fundamental frequency of the transverse vibration of tapered beams with one end restrained against rotation and carrying a mass at the free end .

1.2.2 ROTATING BEAMS

A vast amount of published work can be found in the field of beam vibrations dealing with analytical and numerical techniques . In these works , rotating beams with various geometries have been considered , added masses and springs , effect of pre-twist were also included .

Likins , Barbera and Baddeley [21] addressed the problem of mathematical modeling and modal coordinate selection for an elastic appendage attached to a rigid base which is constrained to rotate with a constant angular speed about a body-axis fixed in the inertial space . They concluded that the continuum model is ideal for an axial beam , and not infeasible for the radial beam (both within the usual limitations of beam theory) . Hoa [22] presented a finite element formulation for a uniform rotating beam with tip mass . Rao and Banerjee [23] developed a polynomial frequency equation to determine the natural frequencies of a cantilever blade with an asymmetric cross-section mounted on a rotating disc . Carnegie [24] evaluated the increase in potential energy due to rotation and estimated only the fundamental frequency of straight uniform beam . Schilhansl [1] used a successive iteration formula to find the first flexural frequency of a rotating cantilever beam . Khulief and Yi [25] developed a finite element formulation that represents vibrational response of a uniform rotating beam with tip mass during lead-lag motion . This formulation accounts for the centrifugal force field and the centripetal acceleration effects . Kammer and Schlack [26] presented a paper in which they studied the effects of a time-dependant angular velocity upon the vibration of a rotating Euler beam . They assumed that angular velocity can be expressed as the sum of a steady-state value and a relatively small periodic perturbation . A perturbation technique called the Krylov-Bogoliubov-Mitropolski (KBM) method was used to derive the general expressions for approximate solutions and instability region boundaries . Yokoyama [3] developed a finite element procedure for determining the free vibration characteristics of rotating uniform Timoshenko beams . The effects of hub radius , setting angle , shear deformation and rotary inertia on the natural frequencies of the rotating beams have been examined . The numerical results indicate that the natural frequencies increase with the rotational speed and / or the hub radius of the beam , that the effect of setting angle on the higher mode frequencies is insignificant and that the effects of shear deformation and rotary inertia on the natural frequencies increase appreciably with mode number . He concluded also that the effects of shear deformation are generally larger than the rotary inertia for non-rotating beams , but their relative effects may be reversed for the higher mode frequencies of the rotating beams owing to the centrifugal stiffness effects . Finally he emphasized that ; although the numerical examples have been limited to the uniform rotating cantilever beams , the technique described therein can readily be applied to non-uniform rotating beams with discontinuities , as well as with other end conditions .

Wright et al. [27] applied the method of Frobenius to obtain exact solutions for the frequencies and mode shapes of rotating beam in which both flexural rigidity and mass distribution vary linearly . Although the method developed in [27] can be applied to a rotating tapered beam , it is confined , however , to such beams in which flexural rigidity vary linearly. Swaminathan and Rao [28] computed the first three frequencies of a pretwisted , tapered and rotating blade using the Rayleigh-Ritz method including the effects of the speed of rotation , pretwist angle and width of taper . Murty and Murthy [4] developed a simple finite element scheme for vibration analysis of rotors and numerical results have been given for the case of tapered cantilever rotors They presented two charts which can be used for quick estimation of the fundamental frequency parameter of rotating tapered beams with small taper . Magari et al. [29] developed a rotating blade finite element with coupled bending and torsion . Stori and Aboelnaga [30] studied the transverse deflections of a straight tapered symmetric beam attached to a rotating hub as a model for the bending vibration of blades in turbomachinery . They obtained a broad class of blade shapes for which the equation of motion can be solved analytically in terms of hypergeometric functions . Based on this analytic solution , they presented an algorithm for computing the natural bending frequencies and mode shapes as a function of setting angle and rotation rate . Khulief [31] derived explicit expressions for the finite element mass and stiffness matrices using consistent mass formulation for the vibration of rotating tapered beam . The results obtained by Khulief display high accuracy when compared with the exact solutions given by Wright et al. [27] .

1.3 PROPOSED RESEARCH

The few studies reported on rotating tapered beams have been concerned with obtaining the modal frequencies only for out-of-plane vibration with zero setting angle, and have neglected the effects of shear deformation and rotary inertia .

The purpose of the present study is to develop a finite element procedure for analyzing the vibration characteristics (i.e. the natural frequencies and associated mode shapes) of a rotating tapered beam including shear deformation and rotary inertia effects . This formulation is based on a consistent mass approach that accounts for the centrifugal force field .

The governing differential equations for the free vibrations of a rotating beam undergoing in-plane and out-of-plane deformations are derived using Hamilton's principle . The effect of setting angle , shear deformation and rotary inertia are incorporated into the finite element model . Explicit expressions for the inertia and stiffness properties of a linearly tapered rotating beam are derived . The generalized eigenvalue problem is formulated and solved for a wide range of parameter changes . Numerical results are presented and compared with other solutions in the literature whenever possible .

CHAPTER TWO

THEORY

2.1 INTRODUCTION

The classical Bernoulli-Euler theory predicts the frequencies of flexural vibration of the lower modes of slender beams with adequate te precision . However , because in this theory the effects of transverse shear deformation and rotary inertia are neglected , the errors associated with it become increasingly large as the beam depth inceases and as the wavelength of vibration decreases .

In Timoshenko theory , the rotation of the neutral axis , $\partial w/\partial x$ is the sum of the shearing angle , γ , and the rotation of the cross-section due to bending , θ , (where w is the transverse displacement and x is the longitudinal axis) . (See Fig. 2.3) . The problem is thus governed by two variables , w and θ say , rather than by w alone as in Bernoulli-Euler theory .

In this chapter , the general assumptions are stated .The strain and stress relations are presented . The strain , kinetic and potential energy equations are obtained , and finally , the general governing differential equations for the rotating tapered beam are derived by means of the extended Hamilton's principle .

The system to be analyzed is shown in Fig. 2.1 . The beam has a length L and spins at a constant angular speed Ω about an axis fixed in the space undergoing vibrational motion in a plane fixed in a local system rotating with the beam .

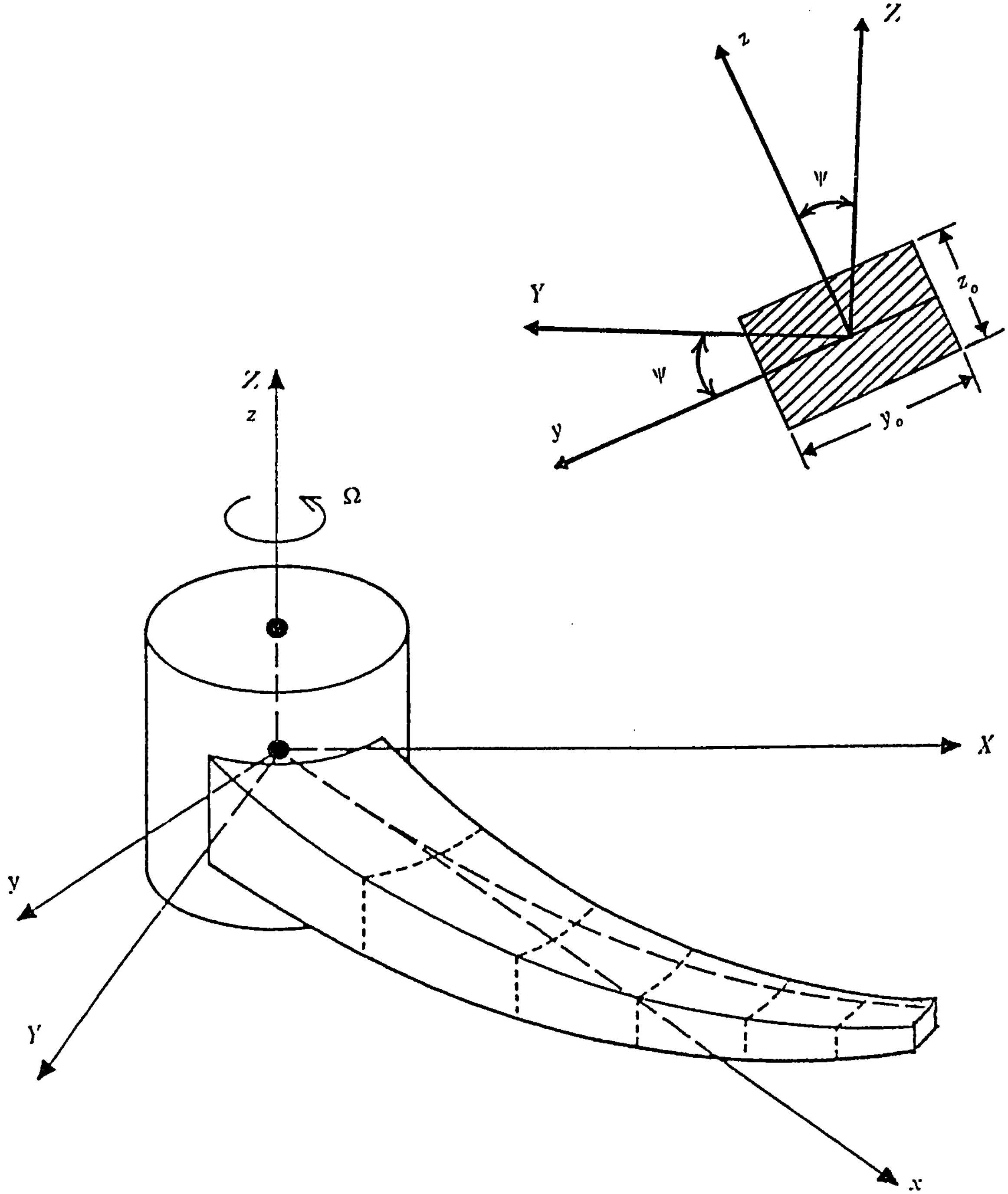

Fig. 2.1 Coordinate frame of a rotating tapered beam .

As shown in Fig. 2.1 , the beam rotates about the global Z -axis . (X,Y,Z) is called a system of global coordinate axes while (x,y,z) is a system of body (local) coordinate axes with origin coinciding with the former (i.e; at the center of the rotating disc) . In this study , we have followed the same notations adopted by Khulief [31] .

The beam is considered to be inextensible , and oriented along the major dimensions ; i.e. the x -axis is along the length of the beam , the y -axis is along the width and the z -axis is along the thickness . The mid-plane of the beam is inclined to the plane of rotation at an angle ψ . For $\psi = \pi / 2$, the transversal motion of the beam exists in the x-y plane and therefore , is purely lead-lag ; for $\psi = 0$, the motion is confined to the x-z plane and is purely flapping .

2.2 GENERAL ASSUMPTIONS

1) - The material of the beam is elastic , homogeneous and isotropic .

2) - The transverse displacements of the beam are sufficiently small .

3) - The cross-sections initially perpendicular to the neutral axis of the beam remain plane , but no longer perpendicular to the neutral axis during bending .

4) - The deflection of the beam is produced by the displacement of points of the centerline normal to its initial straight position .

5) - The hub radius of the rotating disc is neglected .

2.3 FORCES ACTING ON THE BEAM

The radial component of the centrifugal force per unit volume acting on an element of the beam at x is given by

$$F_r = \rho A(x) \Omega^2 x \tag{2.1}$$

where ρ is the mass density of the beam .

As can be seen from Fig. 2.2 , a displacement of w along the z direction would result in a component ($-w \sin \psi$) in the Y direction and a component ($w \cos \psi$) in the Z direction .

The force F_r can be resolved into two components along the Y and X directions :

$$F_X = F_x \approx \rho A(x)\Omega^2 x \tag{2.2}$$

$$F_Y = \rho A(x)\Omega^2 x \{ -w \sin \psi / x \} = -\rho A(x)\Omega^2 w \sin \psi \tag{2.3}$$

The force F_Y can be resolved into components along the y and z directions ; i.e.,

$$F_y = F_Y \cos \psi = -\rho A(x)\Omega^2 w \sin \psi \cos \psi \tag{2.4}$$

$$F_z = -F_Y \sin \psi = \rho A(x)\Omega^2 w \sin^2 \psi \tag{2.5}$$

2.4 STRAIN AND STRESS RELATIONS

Fig. 2.3 shows a beam element before and after deformation . The beam is originally straight and lies along the longitudinal axis : the element length is dx, while w is the total lateral displacement of the section , parallel to z- axis . The angle of rotation due to bending is θ , while the angle of distortion due to shear is γ . The total angle can be written as

$$\frac{\partial w}{\partial x} = \theta + \gamma \tag{2.6}$$

It is assumed that displacement components u and w are independent of y coordinate . It is accepted that u is a linear function of z coordinate and w is independent of z coordinate , where u and w are the longitudinal and lateral displacements of the beam , respectively .

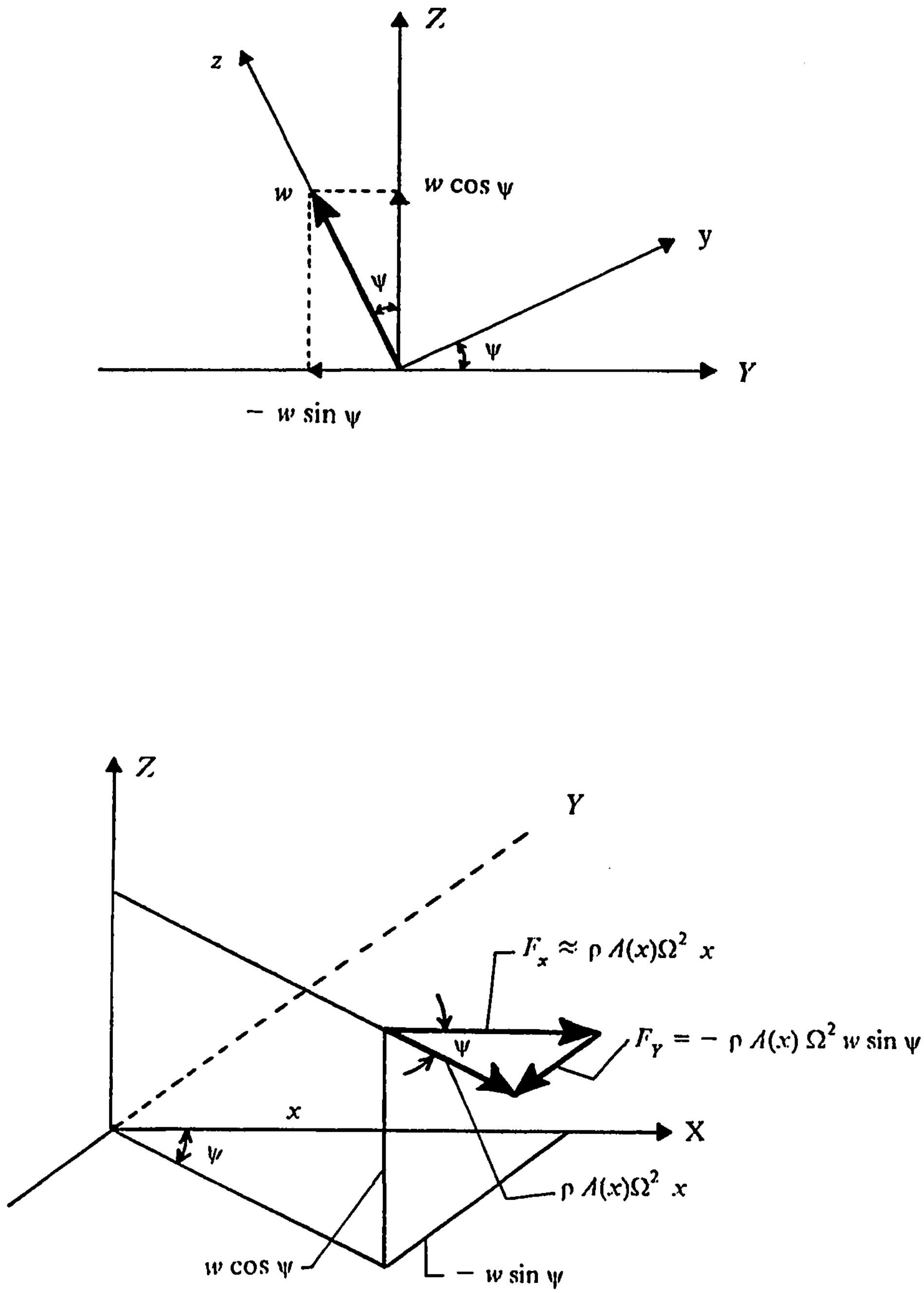

Fig. 2.2 Displacement and force components .

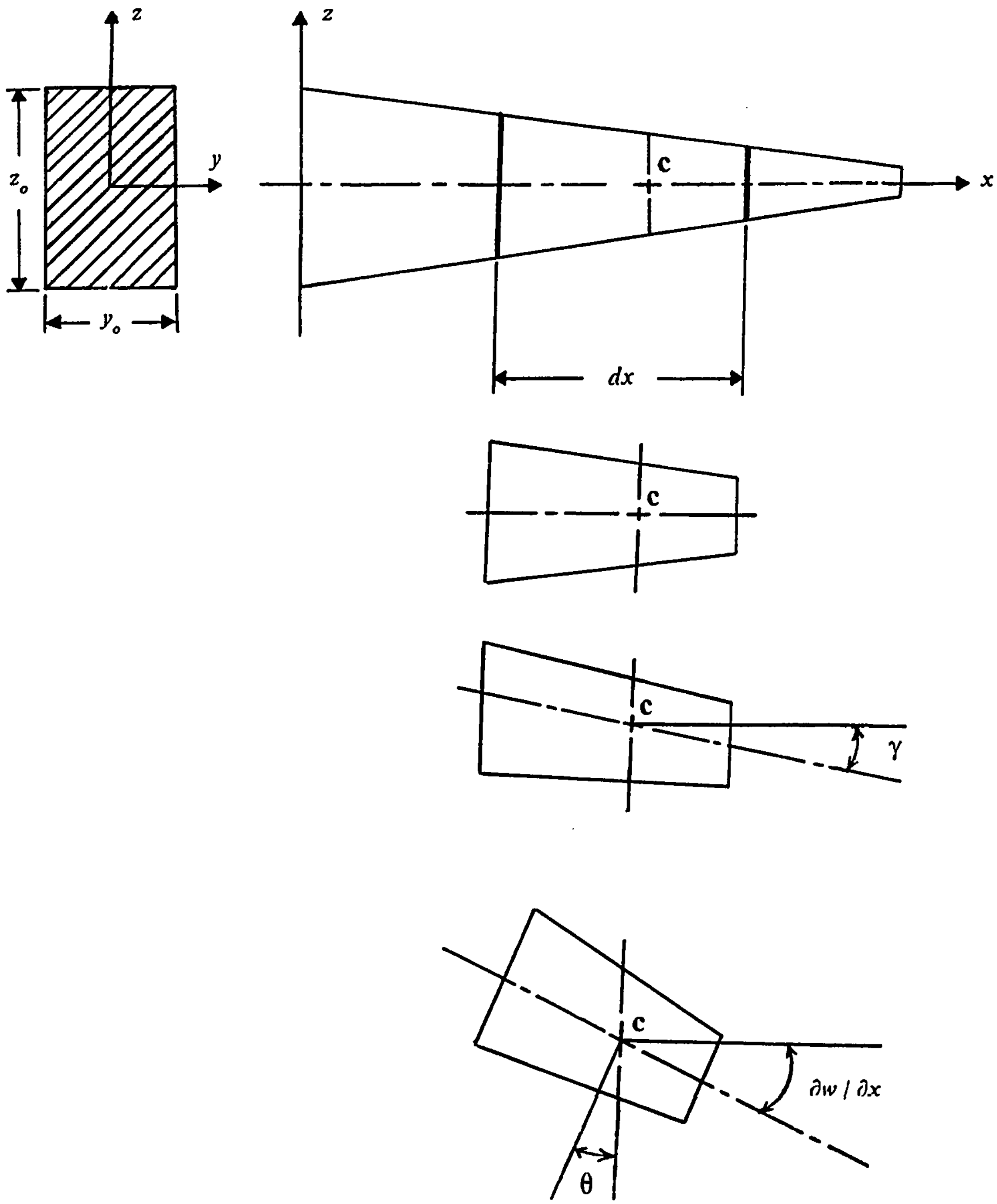

Fig. 2.3 Deformation , displacement and rotation of an element by shear followed by bending .

There is no relative motion in the y-direction at any time of points in the cross-section of the beam ($\varepsilon_{yy} = 0$) , and it may be concluded that the displacement component v is zero , where ε_{yy} and v are the unit elongation per unit length of the beam and the displacement of the beam , respectively , in the y-direction . Therefore , displacement components can be written as :

$$u(x,y,z,t) = -z\theta(x,t) \quad , \quad v(x,y,z,t) = 0 \quad , \quad w(x,y,z,t) = w(x,t) \qquad (2.7)$$

where the functions are dependent of time .

Using the strain-displacement relations , a unit elongation in the x-direction is obtained as :

$$\varepsilon_{xx} = \frac{\partial u}{\partial x} = -z\frac{\partial \theta}{\partial x} \qquad (2.8)$$

and a unit shearing strain in the x-z plane is obtained as :

$$\gamma_{xz} = \gamma = \frac{\partial u}{\partial z} + \frac{\partial w}{\partial x} = -\theta + \frac{\partial w}{\partial x} \qquad (2.9)$$

Applying Hooke's law , stress-strain relations can be written as :

$$\sigma_{xx} = E\varepsilon_{xx} \quad , \quad \tau_{xz} = G\gamma_{xz} \qquad (2.10)$$

where for an isotropic material

$$G = E\,/\,2(1+\nu) \qquad (2.11)$$

where ν is Poisson's ratio .

Let us write equations (2.8) , (2.9) and (2.10) in terms of angle of rotation and angle of distortion as :

$$\sigma_{xx} = -Ez\frac{\partial \theta}{\partial x} \quad , \quad \tau_{xz} = G\gamma \qquad (2.12)$$

Using equations (2.12) , the moment and shear force expressions for a tapered beam can be written in terms of displacement and rotational components as follows :

$$M(x) = \int_{-z_o/2}^{z_o/2} \sigma_{xx}\, z_o\, y_o\, dz = -\, E\, I(x)\, \frac{\partial \theta}{\partial x} \tag{2.13}$$

$$Q(x) = \int_{-z_o/2}^{z_o/2} \tau_{xz}\, y_o\, dz = k'\, G\, A(x)\, \gamma = k'\, G\, A(x) \left(\frac{\partial w}{\partial x} - \theta \right) \tag{2.14}$$

where z_o and y_o are the the thickness and the width of the beam respectively , $E\,I(x)$ is the flexural rigidity , $G\,A(x)$ is the shear rigidity and k' is the shear constant which is inserted as a correction factor to account for the fact that τ_{xz} is not in reality uniform over the height of the cross-section , [36] . It is also mentioned in reference [34] , that k' depends mainly on the cross-section and is given by :

$$k' = \frac{10\,(1+\nu)}{12+11\nu} \quad \textit{for rectangular cross-section} \tag{2.15}$$

and

$$k' = \frac{6\,(1+\nu)}{7+6\nu} \quad \textit{for circular cross-section} \tag{2.16}$$

The variations of the shear correction factor as a function of Poisson's ratio are shown in Fig. 2.4

2.5 HAMILTON'S PRINCIPLE

The equations of motion can be derived by using the extended Hamilton's principle [36] which states :

" Of all admissible configurations that the body can take as it goes from configuration 1 at time t_1 to configuration 2 at time t_2, the path that satisfy Newton's law at each instant during the interval (and is thus the actual locus of configurations) is the path that extremizes the time integral of the Lagrangian during the interval " .

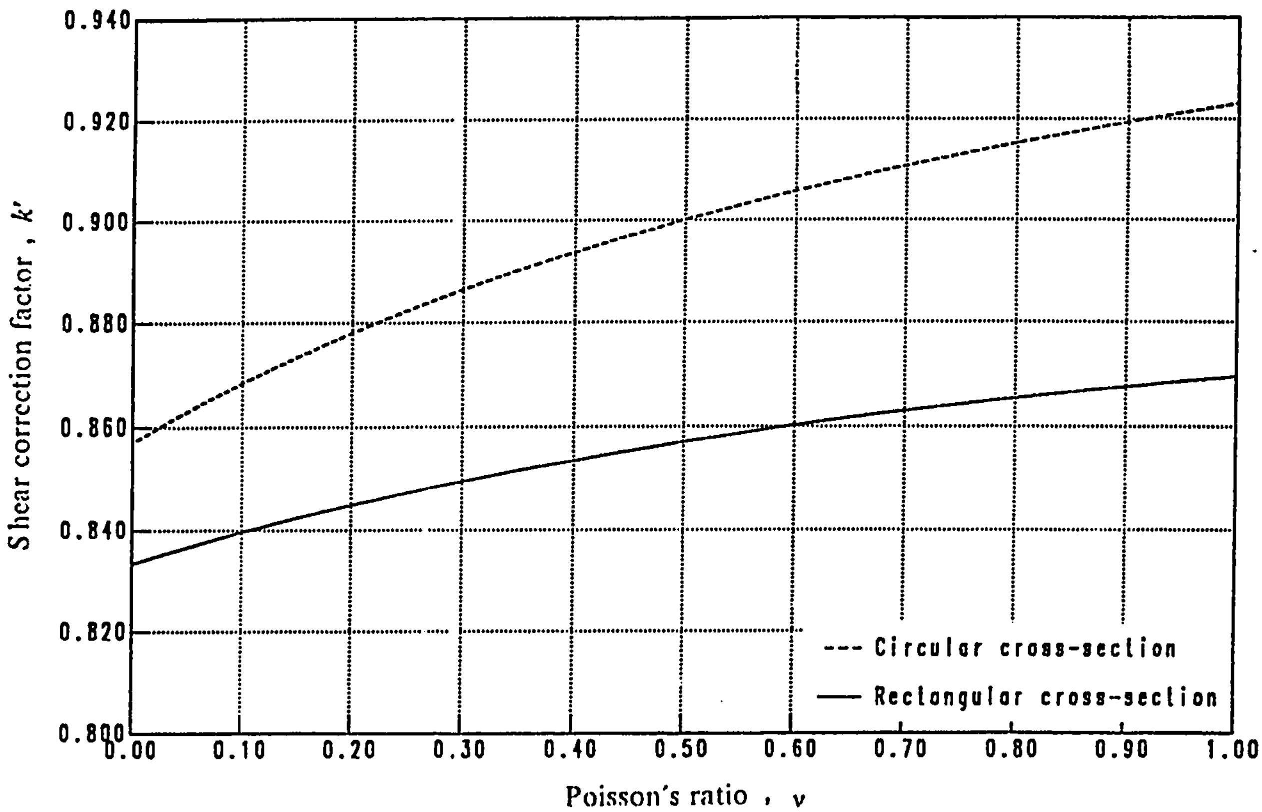

Fig. 2.4 Variation of the shear correction factor as a function of Poisson's ratio

This can be written in mathematical form as :

$$\delta \int_{t_1}^{t_2} (T - \Pi)\, dt = \delta \int_{t_1}^{t_2} L\, dt = 0 \tag{2.17}$$

where

δ = *variation*

T = *kinetic energy*

Π = *total potential energy* = $U + V$

U = *strain energy*

V = *potential energy*

L = *Lagrangian* = $T - \Pi$

2.6 STRAIN , KINETIC AND POTENTIAL ENERGY

The contribution of the kinetic enrgy of the tapered beam due to translation and rotation is expressed as :

$$T = \left(\frac{1}{2}\right)\int_0^L \rho A(x) \left(\frac{\partial w}{\partial t}\right)^2 dx + \left(\frac{1}{2}\right)\int_0^L J(x) \left(\frac{\partial \theta}{\partial t}\right)^2 dx \tag{2.18}$$

where L is the the length of the beam and $J(x)$ is the mass moment of inertia per unit length about the neutral axis of the beam .

But $J(x)$ is related to $I(x)$ by

$$J(x) = \rho I(x) \tag{2.19}$$

where $I(x)$ is the area moment of inertia of the beam .

Now , the kinetic energy can be written in the form :

$$T = \left(\frac{1}{2}\right)\int_0^L \rho A(x) \left(\frac{\partial w}{\partial t}\right)^2 dx + \left(\frac{1}{2}\right)\int_0^L \rho I(x) \left(\frac{\partial \theta}{\partial t}\right)^2 dx \tag{2.20}$$

The total strain energy of the spinning beam is composed of flexural strain energy , shear strain energy and strain energy due to the centrifugal force F_x . Because Ω is constant , the centrifugal force is also approximately constant , and may be treated as an axial load that creates strain energy .

$$U = (\frac{1}{2})\int_0^L E\,I(x)\,(\frac{\partial\theta}{\partial x})^2\,dx + (\frac{1}{2})\int_0^L k'\,G\,A(x)\,(\frac{\partial w}{\partial x} - \theta)^2\,dx + (\frac{1}{2})\int_0^L F_x(\frac{\partial w}{\partial x})^2\,dx \quad (2.21)$$

where F_x is the centrifugal force given by equation (2.2)

The potential energy V due to the centrifugal force F_z per unit volume acting on the beam in the z direction is given by [3] :

$$V = -(\frac{1}{2})\int_0^L F_z\,w\,A(x)\,dx \quad (2.22)$$

where F_z is given by equation (2.5) .

2.7 ELASTODYNAMIC EQUATIONS

Substitute equations (2.20) , (2.21) and (2.28) into equation (2.17) , one can obtain :

$$\delta\int_{t_1}^{t_2} L\,dt = \delta\int_{t_1}^{t_2} \{(\frac{1}{2})\int_0^L \rho\,A(x)\,(\frac{\partial w}{\partial t})^2\,dx + (\frac{1}{2})\int_0^L \rho\,I(x)\,(\frac{\partial\theta}{\partial t})^2\,dx$$

$$- (\frac{1}{2})\int_0^L E\,I(x)\,(\frac{\partial\theta}{\partial x})^2\,dx - (\frac{1}{2})\int_0^L k'\,G\,A(x)\,(\frac{\partial w}{\partial x} - \theta)^2\,dx$$

$$- (\frac{1}{2})\int_0^L F_x(\frac{\partial w}{\partial x})^2\,dx + (\frac{1}{2})\int_0^L F_z\,w\,A(x)\,dx\,\}\,dt = 0 \quad (2.23)$$

Performing the variation in the above equation we obtain :

$$\delta\int_{t_1}^{t_2} L\,dt = \int_{t_1}^{t_2} \{\int_0^L \rho\,A(x)\,(\frac{\partial w}{\partial t})\delta(\frac{\partial w}{\partial t})dx + \int_0^L \rho\,I(x)\,(\frac{\partial\theta}{\partial t})\delta(\frac{\partial\theta}{\partial t})\,dx$$

$$- \int_0^L E\,I(x)\,(\frac{\partial\theta}{\partial x})\,\delta(\frac{\partial\theta}{\partial x})\,dx - \int_0^L k'\,GA(x)(\frac{\partial w}{\partial x} - \theta)\delta(\frac{\partial w}{\partial x} - \theta)\,dx$$

$$- \int_0^L F_x(\frac{\partial w}{\partial x})\,\delta(\frac{\partial w}{\partial x})\,dx + (\frac{1}{2})\int_0^L F_z\,A(x)\;\delta w\;dx\}\,dt \quad (2.24)$$

The order of integrations with respect to x and t is interchangeable and the variation and differentiation operators are commutative , so we can perform the following integrations by parts :

$$\int_{t_1}^{t_2} \rho A(x) \left(\frac{\partial w}{\partial t}\right) \delta\left(\frac{\partial w}{\partial t}\right) dt = \int_{t_1}^{t_2} \rho A(x) \left(\frac{\partial w}{\partial t}\right) \frac{\partial}{\partial t} (\delta w)\, dt$$

$$= \rho A(x) \left(\frac{\partial w}{\partial t}\right) \delta w \,\Big|_{t_1}^{t_2} - \int_{t_1}^{t_2} \frac{\partial}{\partial t} \left(\rho A(x) \frac{\partial w}{\partial t}\right) \delta w \; dt$$

$$= - \int_{t_1}^{t_2} \rho A(x) \left(\frac{\partial^2 w}{\partial t^2}\right) \delta w \; dt \tag{2.25}$$

because δw vanishes at $t = t_1$ and t_2 . In a same way , it is obtained that :

$$\int_{t_1}^{t_2} \rho\, I(x) \left(\frac{\partial \theta}{\partial t}\right) \delta\left(\frac{\partial \theta}{\partial t}\right) dt = - \int_{t_1}^{t_2} \rho\, I(x) \left(\frac{\partial^2 \theta}{\partial t^2}\right) \delta \theta \, dt \tag{2.26}$$

On the other hand , integration over the spatial variable yields

$$\int_0^L E\, I(x) \left(\frac{\partial \theta}{\partial x}\right) \delta\left(\frac{\partial \theta}{\partial x}\, dx\right) = \int_0^L E\, I(x) \left(\frac{\partial \theta}{\partial x}\right) \frac{\partial}{\partial x} (\delta \theta)\, dx$$

$$= E\, I(x) \left(\frac{\partial \theta}{\partial t}\right) \delta \theta \,\Big|_0^L - \int_0^L \frac{\partial}{\partial x} \left(E\, I(x) \frac{\partial \theta}{\partial x}\right) \delta \theta \, dx \tag{2.27}$$

and

$$\int_0^L k'\, GA(x) \left(\frac{\partial w}{\partial x} - \theta\right) \delta\left(\frac{\partial w}{\partial x} - \theta\right) dx = \int_0^L k'\, GA(x) \left(\frac{\partial w}{\partial x} - \theta\right) \frac{\partial}{\partial x} (\delta w)\, dx$$

$$- \int_0^L k'\, GA(x) \left(\frac{\partial w}{\partial x} - \theta\right) \delta \theta \, dx = \left\{ k'\, GA(x) \left(\frac{\partial w}{\partial x} - \theta\right)\right\} \delta w \,\Big|_0^L$$

$$- \int_0^L \frac{\partial}{\partial x} \left\{ k'\, GA(x) \left(\frac{\partial w}{\partial x} - \theta\right) \delta w \, dx - \int_0^L k'\, GA(x) \left(\frac{\partial w}{\partial x} - \theta\right) \delta \theta \, dx \tag{2.28}$$

Also ,

$$\int_0^L F_x \left(\frac{\partial w}{\partial x}\right) \delta\left(\frac{\partial w}{\partial x}\right) dx = \int_0^L F_x \left(\frac{\partial w}{\partial x}\right) \frac{\partial}{\partial x} (\delta w)\, dx$$

$$= F_x \left(\frac{\partial w}{\partial x}\right) \delta w \,\Big|_0^L - \int_0^L \frac{\partial}{\partial x} \left(F_x \frac{\partial w}{\partial x}\right) \delta w \, dx \tag{2.29}$$

Using the above equations into equation (2.24) produces

$$\int_{t_1}^{t_2}\{-\int_0^L \rho A(x)\left(\frac{\partial^2 w}{\partial t^2}\right)\delta w\;dx-\int_0^L \rho I(x)\left(\frac{\partial^2 \theta}{\partial t^2}\right)\delta\theta\,dx-E I(x)\left(\frac{\partial \theta}{\partial x}\right)\delta\theta\,\Big|_0^L$$

$$+\int_0^L \frac{\partial}{\partial x}\left(E I(x)\frac{\partial \theta}{\partial x}\right)\delta\theta\,dx-\{k' GA(x)\left(\frac{\partial w}{\partial x}-\theta\right)\}\delta w\,\Big|_0^L+\int_0^L \frac{\partial}{\partial x}\{k' GA(x)\left(\frac{\partial w}{\partial x}-\theta\right)\}\,\delta w\,dx$$

$$+\int_0^L k' GA(x)\left(\frac{\partial w}{\partial x}-\theta\right)\delta\theta\,dx-F_x\left(\frac{\partial w}{\partial x}\right)\delta w\,\Big|_0^L$$

$$+\int_0^L \frac{\partial}{\partial x}\left(F_x\frac{\partial w}{\partial x}\right)\delta w\,dx+\left(\frac{1}{2}\right)\int_0^L F_z A(x)\delta w\,dx\}\,dt=0. \qquad (2.30)$$

After rearranging , equation (2.30) takes the form :

$$\int_{t_1}^{t_2}\{\int_0^L\left(\frac{\partial}{\partial x}\{k' GA(x)\left(\frac{\partial w}{\partial x}-\theta\right)\}-\rho A(x)\left(\frac{\partial^2 w}{\partial t^2}\right)\right.$$

$$\left.+\frac{\partial}{\partial x}\{F_x\left(\frac{\partial w}{\partial x}\right)\}+\left(\frac{1}{2}\right)F_z A(x)\right\}\delta w\;dx$$

$$+\int_0^L\left(\frac{\partial}{\partial x}\left(E I(x)\frac{\partial \theta}{\partial x}\right)+k' GA(x)\left(\frac{\partial w}{\partial x}-\theta\right)\right\}-\rho I(x)\left(\frac{\partial^2 \theta}{\partial t^2}\right)\}\delta\theta\,dx$$

$$-E I(x)\left(\frac{\partial \theta}{\partial x}\right)\delta\theta\,\Big|_0^L-\{k' GA(x)\left(\frac{\partial w}{\partial x}-\theta\right)+F_x\left(\frac{\partial w}{\partial x}\right)\}\delta w\,\Big|_0^L\}\,dt=0 \qquad (2.31)$$

The virtual displacement $\delta\theta$ and δw are arbitrary and independent , so they can be taken equal zero at $x = 0$ and $x = L$ and arbitrary for $0 < x < L$; therefore , we must have :

$$\frac{\partial}{\partial x}\{k' GA(x)\left(\frac{\partial w}{\partial x}-\theta\right)\}-\rho A(x)\left(\frac{\partial^2 w}{\partial t^2}\right)+\frac{\partial}{\partial x}\left(F_x\frac{\partial w}{\partial x}\right)+\left(\frac{1}{2}\right)F_z A(x)=0 \qquad (2.32)$$

$$\frac{\partial}{\partial x}\left(E I(x)\frac{\partial \theta}{\partial x}\right)+k' GA(x)\left(\frac{\partial w}{\partial x}-\theta\right)-\rho I(x)\left(\frac{\partial^2 \theta}{\partial t^2}\right)=0 \qquad (2.33)$$

Now if we substitute the expression of F_z from equation (2.5) into equation (2.32) , we obtain :

$$\frac{\partial}{\partial x}\{k' GA(x)\left(\frac{\partial w}{\partial x}-\theta\right)\}-\rho A(x)\left(\frac{\partial^2 w}{\partial t^2}\right)+\frac{\partial}{\partial x}\{F_x\frac{\partial w}{\partial x}\}+\left(\frac{1}{2}\right)\rho A(x)\,\Omega^2 w\sin^2\psi=0 \qquad (2.34)$$

In addition , if we write

$$E\,I(x)\,(\frac{\partial\theta}{\partial x})\,\delta\theta\,\Big|_0^L = 0 \qquad (2.35)$$

$$\{\,k'\,GA(x)\,(\frac{\partial w}{\partial x} - \theta) + F_x(\frac{\partial w}{\partial x})\}\,\delta w\,\Big|_0^L = 0 \qquad (2.36)$$

We take into account the possibility that either $E\,I(x)\,(\frac{\partial\theta}{\partial x})$ or $\delta\theta$, on the one hand , and either $\{\,k'\,GA(x)\,(\frac{\partial w}{\partial x} - \theta) + F_x(\frac{\partial w}{\partial x})\}$ or δw , on the other , vanishes at any ends $x = 0$ and $x = L$.

Equations (2.33) and (2.34) are the differential equations of motion that must be satisfied over the length of the beam and (2.35) and (2.36) represent the boundary conditions . The four equations together constitute the boundary-value problem . Equation (2.35) requires either the bending moment or the beam rotation variation vanish at each end and (2.36) requires that either the shearing and the axial force or the deflection variation be zero at each end . It is the satisfaction of these boundary conditions that renders the solution of the differential equations (2.33) and (2.34) unique .

CHAPTER THREE

FINITE ELEMENT FORMULATION

The elastic beam configuration can be defined by a properly generated mesh of finite beam elements . In this formulation , beam elements are linearly tapered in two planes . Any combination of taper ratios in the two planes are permitted by the model developed in this study . The beam is divided into elements of equal length $l^i = L/n$, as shown in Fig. 3.1 . The element consists of two nodes , each node has two degrees of freedom of transverse displacement w^i and bending rotation θ^i .

3.1 CENTRIFUGALLY STIFFENED TAPERED BEAM ELEMENT

It is assumed that the axis of the beam is straight , and deformation is confined to shear and bending in the direction of longitudinal axis . The later assumption eliminates torsion due to bending . This implies that the centroid C of the cross-section and shear center coincide [19] . See Fig. 2.2 .

Assuming that the elastic beam is aligned along the x -axis in the undeformed state, one can describe the local coordinate vector of an arbitrary point p^i on element i with respect to the element axes , shown in Fig. 3.1 as

$$\{ w^i \} = [N^i_w] \{ q^i \}$$

$$\{ \theta^i \} = [N^i_\theta] \{ q^i \} \qquad (3.1)$$

where $\{ q^i \}$ is a vector of nodal coordinates of the beam element .

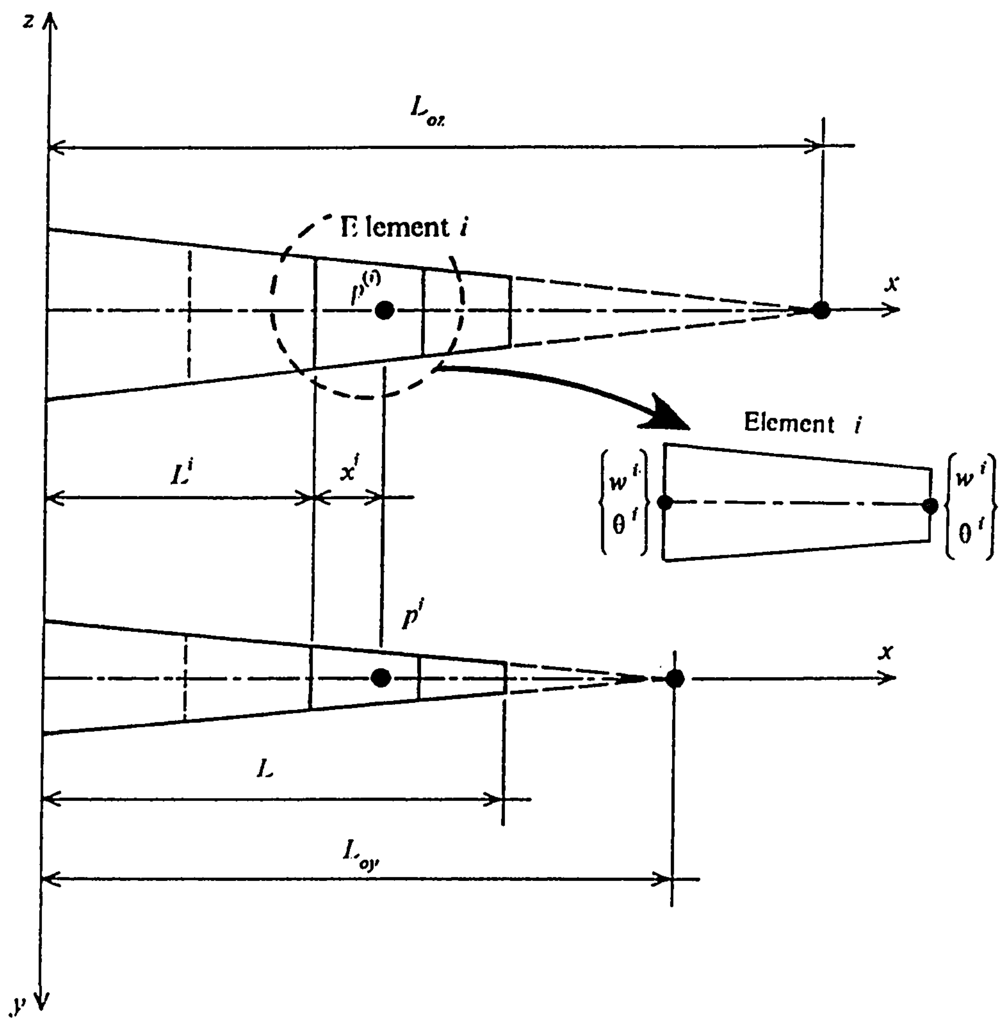

Fig. 3.1 A beam element linearly tapered in two planes .

where deformations are confined to one plane .

The matrices $[N_w^i]_{1x4}$ and $[N_\theta^i]_{1x4}$ are the elemental shape functions (or interpolation functions) with nonzero entries given by [3] and [35] as :

$$N_{w_1}^i = \{ 1 - 3\xi^{i2} + 2\xi^{i3} + (1 - \xi^i) \Phi \} / (1 + \Phi)$$

$$N_{w_2}^i = l^i \{ \xi^i - 2\xi^{i2} + \xi^{i3} + (\xi^i - \xi^{i2}) \Phi / 2 \} / (1 + \Phi)$$

$$N_{w_3}^i = \{ 3\xi^{i2} - 2\xi^{i3} + \xi^i \Phi \} / (1 + \Phi)$$

$$N_{w_4}^i = l^i \{ - \xi^{i2} + \xi^{i3} - (\xi^i - \xi^{i2}) \Phi / 2 \} / (1 + \Phi)$$

$$N_{\theta_1}^i = 6 \{ - \xi^i + \xi^{i2} \} / \{ l^i (1 + \Phi) \}$$

$$N_{\theta_2}^i = \{ 1 - 4\xi^i + 3\xi^{i2} + (1 - \xi^i) \Phi \} / (1 + \Phi)$$

$$N_{\theta_3}^i = 6 \{ \xi^i - \xi^{i2} \} / \{ l^i (1 + \Phi) \}$$

$$N_{\theta_4}^i = \{ - 2\xi^i + 3\xi^{i2} + \xi^i \Phi \} / (1 + \Phi) \qquad (3.2)$$

where

$$\xi^i = x^i / l^i \qquad (3.3)$$

and

$$\Phi = 12 E^i I_x^i / (k^{i\prime} G^i A_x^i l^{i2}) \qquad (3.4)$$

The parameter Φ is known as the shear deformation parameter (the ratio between the bending stiffness and the shear stiffness) , E^i is the modulus of rigidity , I_x^i is the second moment of the cross-sectional area , A_x^i is the cross-sectional area of the beam element , l^i is the element length , G^i is the shear modulus and $k^{i\prime}$ is the shear correction factor depending on the shape of the cross-section . The shear correction factor $k^{i\prime}$ is given by equations (2.9) and (2.10) .

3.2 GEOMETRICAL PROPERTIES OF THE CROSS-SECTIONAL AREA

In order to define the entries of the stiffness and mass matrices one needs to introduce the following parameters :

$$L^i = \sum_{j=1}^{n} l^j \ , \ L_{iy} = L_{oy} - L^i \ , \ L_{iz} = L_{oz} - L^i$$

$$\mu_1 = L_{iy} L_{iz} \ , \ \mu_2 = \frac{1}{2}(L_{iy} + L_{iz}) \tag{3.5}$$

To find the cross-sectional area at any arbitrary location of element i, let :

$$\frac{z_i}{z_o} = \frac{L_{oz} - \{ x^i + (i-1) l^i \}}{L_{oz}} \tag{3.6}$$

and let

$$(i-1) l^i = L^i \tag{3.7}$$

Substitute in the above expression , we obtain :

$$\frac{z_i}{z_o} = \frac{L_{oz} - x^i - L^i}{L_{oz}} \tag{3.8}$$

Similarly ,

$$\frac{y_i}{y_o} = \frac{L_{oy} - x^i - L^i}{L_{oy}} \tag{3.9}$$

Since

$$A_x^i = y_i \ z_i \tag{3.10}$$

Substitute equations (3.8) and (3.9) into equation (3.10) , one can obtain :

$$A_x^i = y_o \frac{L_{oy} - x^i - L^i}{L_{oy}} \ z_o \frac{L_{oz} - x^i - L^i}{L_{oz}} \tag{3.11}$$

After rearranging , equation (3.11) takes the form :

$$A_x^i = \frac{A_o}{L_{oy} L_{oz}} \{ \mu_1 - 2\mu_2 x^i + {x^i}^2 \} \tag{3.12}$$

where

$$A_o = y_o z_o \tag{3.13}$$

is the cross-sectional area of the root of the beam .

Following the same procedure , one can obtain the expression for the second moment of the cross-sectional area

$$I_x^i = \frac{1}{12} y_i z_i^3 \tag{3.14}$$

Substitute equations (3.8) and (3.9) into equation (3.14) , we get

$$I_x^i = \frac{1}{12} y_o \frac{L_{oy} - x^i - L^i}{L_{oy}} z_o^3 \frac{\{ L_{oz} - x^i - L^i \}^3}{L_{oz}^{\ 3}} \tag{3.15}$$

After rearranging , equation (3.15) becomes :

$$I_x^i = \frac{I_o}{L_{oy} L_{oz}^3} \{ \mu_1 L_{iz}^2 - (L_{iz}^3 + 3 \mu_1 L_{iz}) x^i + 6 \mu_2 L_{iz} x^{i^2} - 2 (L_{iz} + \mu_2) x^{i^3} + x^{i\,4} \} \tag{3.16}$$

where

$$I_o = \frac{1}{12} y_o z_o^3 \tag{3.17}$$

is the second moment of the cross-sectional area of the root of the beam .

In equation (3.16) , it is assumed that the flexural motion takes place in the x-z plane ; flapping motion . Similar expression can be obtained for flexural motion in the x-y plane by just interchanging the subscripts y and z . Equation (3.16) can be written in a simpler form as :

$$I_x^i = \frac{I_o}{L_{oy} L_{oz}^3} \{ a_o - a_1 x^i + a_2 x^{i^2} - a_3 x^{i^3} + x^{i\,4} \} \tag{3.18}$$

where

$$a_o = \mu_1 L_{iz}^2 \ , \ a_1 = L_{iz}^3 + 3 \mu_1 L_{iz} \ , \ a_2 = 6 \mu_2 L_{iz} \ , \ a_3 = 2 (L_{iz} + \mu_2) \tag{3.19}$$

3.3 STIFFNESS MATRICES

The strain energy expression of the i th spinning tapered beam element of length l^i is given by :

$$U^i = (\frac{1}{2})\int_0^{l^i} \{E^i I^i_x (\frac{\partial \theta^i}{\partial x^i})^2 + k^i G^i A^i_x (\frac{\partial w^i}{\partial x^i} - \theta^i)^2 + F^i_x (\frac{\partial w^i}{\partial x^i})^2\} dx^i \tag{3.20}$$

where F^i_x is the centrifugal force in the longitudinal direction of the beam elemct . The first term of equation (3.20) represents the flexural strain energy , while the second term represents the shear strain energy and the last one represents the strain energy due to the centrifugal force F^i_x .

Equation (3.20) can be written in matrix form as :

$$[U^i] = \frac{1}{2}\{ q^i \}^T [K^i]\{ q^i \} \tag{3.21}$$

where $[K^i]$ is the composite stiffness matrix given by

$$[K^i] = [k^i_e] + [k^i_s] + [k^i_c] \tag{3.22}$$

where

$$[k^i_e] = \int_0^{l^i} [B^i_e]^T E^i I^i_x [B^i_e] \, dx^i = \textit{elastic stiffness matrix} \tag{3.23}$$

$$[k^i_s] = \int_0^{l^i} [B^i_s]^T k^i G^i A^i_x [B^i_s] \, dx^i = \textit{shear stiffness matrix} \tag{3.24}$$

$$[k^i_c] = \int_0^{l^i} F^i_x [B^i_w]^T [B^i_w] dx^i = \textit{centrifugal stiffness matrix} \tag{3.25}$$

The curvature κ^i and the shear strain γ^i within the element are expressed as

$$\kappa^i = \frac{\partial \theta^i}{\partial x^i} = [B^i_e] \{q^i\} \tag{3.26}$$

$$\gamma^i = \frac{\partial w^i}{\partial x^i} - \theta^i = [B^i_s] \{q^i\} \tag{3.27}$$

where

$$[B^i_w] = \frac{\partial}{\partial x^i}[N^i_w] \tag{3.28}$$

$$[B^i_e] = \frac{\partial}{\partial x^i}[N^i_\theta] \tag{3.29}$$

$$[B^i_s] = \frac{\partial}{\partial x^i}[N^i_w] - [N^i_\theta] = [B^i_w] - [N^i_\theta] \tag{3.30}$$

As can be seen from equation (3.30) , there is a coupling between w^i and θ^i degrees of freedom .

Carrying out the integration of equation (3.23) , the elastic stiffness matrix $[k^i_e]$ is obtained with nonzero entries as presented in Table 3.1

The explicit expression for the element shear stiffness matrix $[k^i_s]$ is obtained by carrying out the integration of equation (3.24) . The shear stiffness matrix $[k^i_s]$ is obtained with nonzero entries as presented in Table 3.2

The centrifugal stiffness matrix is established by evaluating the integral of equation (3.25) . In order to do this , one can define the centrifugal force associated with a differential element located at point p^i of the finite element i as :

$$dF^i_p = \rho^i A^i_x \Omega^2 r^i_p dr^i_p \tag{3.31}$$

where

$$r^i_p \approx L^i + x^i = (i-1)l^i + x^i \tag{3.32}$$

when small deformations are considered . The tensile force acting on a section at p^i due to the centrifugal effect , can be calculated by integrating equation (3.31) over the span between point p^i and the free end of the beam as shown in Fig. 3.2 .

TABLE 3.1 Elastic stiffness matrix of tapered beam element

$$[\,k_e^i\,] = \frac{E^i I_o}{L_{oy} L_{oz}^3 (1 + \Phi)^2}\,[\,k_{ab}^{(e)}\,] \quad ; \; a,b = 1,2,\ldots,4$$

The nonzero entries of the lower triangular part of $[\,k_{ab}^{(e)}\,]$ are given by :

$$k_{11}^{(e)} = -k_{31}^{(e)} = k_{33}^{(e)} = \frac{12}{l^{i3}}\alpha_o - \frac{6}{l^{i2}}\alpha_1 + \frac{24}{5l^i}\alpha_2 - \frac{21}{5}\alpha_3 + \frac{132}{35}l^i$$

$$k_{21}^{(e)} = -k_{32}^{(e)} = \frac{6}{l^{i2}}\alpha_o + \frac{1}{l^i}(\Phi - 2)\alpha_1 + \frac{1}{5}(-5\Phi + 7)\alpha_2 + \frac{3}{10}(3\Phi - 4)l^i\alpha_3$$
$$+ \frac{2}{35}(-14\Phi + 19)l^{i2}$$

$$k_{22}^{(e)} = \frac{1}{l^i}(\Phi^2 + 2\Phi + 4)\alpha_o - \frac{1}{2}(\Phi^2 + 2)\alpha_1 + \frac{1}{15}(5\Phi^2 - 5\Phi + 8)l^i\alpha_2$$
$$- \frac{1}{20}(5\Phi^2 - 8\Phi + 8)l^{i2}\alpha_3 + \frac{1}{35}(7\Phi^2 - 14\Phi + 12)l^{i3}$$

$$k_{41}^{(e)} = -k_{43}^{(e)} = \frac{6}{l^{i2}}\alpha_o - \frac{1}{l^i}(\Phi + 4)\,\alpha_1 + \frac{1}{5}(5\Phi + 17)\,\alpha_2 - \frac{3}{10}(3\Phi + 10)l^i\alpha_3$$
$$+ \frac{2}{35}(14\Phi + 47)l^{i2}$$

$$k_{42}^{(e)} = -\frac{1}{l^i}(\Phi^2 + 2\Phi - 2)\,\alpha_o + \frac{1}{2}(\Phi^2 + 2\Phi - 2)\,\alpha_1 - \frac{1}{15}(5\Phi^2 + 10\Phi - 13)l^i\alpha_2$$
$$+ \frac{1}{20}(5\Phi^2 + 10\Phi - 16)l^{i2}\alpha_3 - \frac{1}{35}(7\Phi^2 + 14\Phi - 26)l^{i3}$$

$$k_{44}^{(e)} = \frac{1}{l^i}(\Phi^2 + 2\Phi + 4)\,\alpha_o - \frac{1}{2}(\Phi^2 + 4\Phi + 6)\,\alpha_1 + \frac{1}{15}(5\Phi^2 + 25\Phi + 38)l^i\alpha_2$$
$$- \frac{1}{20}(5\Phi^2 + 28\Phi + 44)l^{i2}\alpha_3 + \frac{1}{35}(7\Phi^2 + 42\Phi + 68)l^{i3}$$

TABLE 3.2 Shear stiffness matrix of tapered beam element

$$[\,k_s^i\,] = \frac{A_o\, k'^i\, G^i\, \Phi^2}{I_{oy}\, I_{oz}(\,1 + \Phi\,)^2}\,[\,k_{ab}^{(s)}\,] \quad ; a,b = 1\,,2\,,....,4$$

The nonzero entries of the lower triangular part of $[\; k_{ab}^{(s)} \;]$ are given by :

$$k_{11}^{(s)} = -\,k_{31}^{(s)} = k_{33}^{(s)} = \frac{1}{l^i}\,\mu_1 - \mu_2 + \frac{1}{3}\,l^i$$

$$k_{21}^{(s)} = -\,k_{32}^{(s)} = k_{41}^{(s)} = -\,k_{43}^{(s)} = \frac{1}{2}\,\mu_1 - \frac{1}{2}\,l^i\,\mu_2 + \frac{1}{6}\,l^{i2}$$

$$k_{22}^{(s)} = k_{42}^{(s)} = k_{44}^{(s)} = \frac{1}{4}\,l^i\,\mu_1 - \frac{1}{4}\,l^{i2}\mu_2 + \frac{1}{12}\,l^{i3}$$

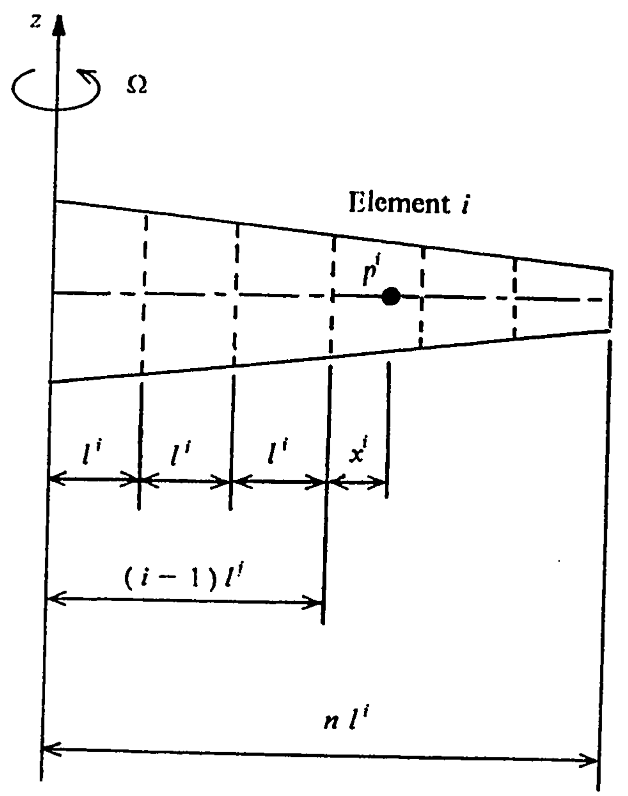

Fig. 3.2 Location of the tapered beam element

The resulting tensile force is then

$$F_p^i = \rho^i \Omega^2 \{ \int_x^{l^i} [(i - 1) l^i + x^i] A_x^i dx^i + \int_{il^i}^{nl^i} x^i A_x^i dx^i \} \tag{3.33}$$

where A_x^i is given by equation (3.12) .

Evaluating the integral in equation (3.33) , one can obtain the following expression :

$$F_p^i = \frac{\rho^i A_o \Omega^2}{L_{oy} L_{oz}} [\beta_o - \beta_1 x^i - \beta_2 x^{i^2} - \beta_3 x^{i^3} - \beta_4 x^{i^4}] \tag{3.34}$$

where

$$\beta_o = \Lambda_o - \Lambda_1 + \Lambda_2$$

$$\Lambda_o = \frac{1}{2} \mu_1 l^{i^2} (n^2 - i^2 + 2i - 1)$$

$$\Lambda_1 = \frac{2}{3} \mu_2 l^{i^3} (n^3 - i^3 + \frac{3}{2} i - \frac{1}{2})$$

$$\Lambda_2 = \frac{1}{4} l^{i^4} (n^4 - i^4 + \frac{4}{3} i - \frac{1}{3})$$

$$\beta_1 = \mu_1 L^i$$

$$\beta_2 = \frac{1}{2} (\mu_1 - 2 \mu_2 L^i)$$

$$\beta_3 = \frac{1}{3} (L^i - 2 \mu_2)$$

$$\beta_4 = \frac{1}{4} \tag{3.35}$$

The axial stresses resulting from the tensile force given by equation (3.34) are incorporated into the integration of equation (3.25) , resulting in the centrifugal stiffness matrix of the rotating beam element given in Table 3.3 .

TABLE 3.3 Centrifugal stiffness matrix of tapered beam element

$$[\,k_c^i\,] = \frac{A_o \rho^i \Omega^2}{L_{oy} L_{oz} (1+\Phi)^2}\,[\,k_{ab}^{(c)}\,] \quad ; \; a,b = 1,2,\ldots,4$$

The nonzero entries of the lower triangular part of $[\,k_{ab}^{(c)}\,]$ are given by :

$$k_{11}^{(c)} = -k_{31}^{(c)} = k_{33}^{(c)} = \frac{1}{5l^i}(5\Phi^2+10\Phi+6)\beta_o - \frac{1}{10}(5\Phi^2+10\Phi+6)\beta_1$$

$$- \frac{1}{105}(35\Phi^2+63\Phi+36)l^i\beta_2 - \frac{1}{140}(35\Phi^2+56\Phi+30)l^{i2}\beta_3 - \frac{1}{35}(7\Phi^2+10\Phi+5)l^{i3}\beta_4$$

$$k_{21}^{(c)} = -k_{32}^{(c)} = \frac{1}{10}\beta_o - \frac{1}{120}(10\Phi^2+16\Phi+12)l^i\beta_1 - \frac{1}{420}(35\Phi^2+49\Phi+30)l^{i2}\beta_2$$

$$- \frac{1}{280}(21\Phi^2+26\Phi+14)l^{i3}\beta_3 - \frac{1}{420}(28\Phi^2+31\Phi+15)l^{i4}\beta_4$$

$$k_{22}^{(c)} = \frac{1}{60}(5\Phi^2+10\Phi+8)l^i\beta_o - \frac{1}{120}(5\Phi^2+6\Phi+4)l^{i2}\beta_1 - \frac{1}{210}(7\Phi^2+7\Phi+4)l^{i3}\beta_2$$

$$- \frac{1}{1680}(49\Phi^2+44\Phi+22)l^{i4}\beta_3 - \frac{1}{420}(11\Phi^2+9\Phi+4)l^{i5}\beta_4$$

$$k_{41}^{(c)} = -k_{43}^{(c)} = \frac{1}{10}\beta_o + \frac{1}{60}(5\Phi^2+8\Phi)l^i\beta_1 + \frac{1}{420}(35\Phi^2+63\Phi+12)l^{i2}\beta_2$$

$$+ \frac{1}{280}(21\Phi^2+40\Phi+10)l^{i3}\beta_3 + \frac{1}{420}(28\Phi^2+55\Phi+15)l^{i4}\beta_4$$

$$k_{42}^{(c)} = -\frac{1}{60}(5\Phi^2+10\Phi+2)l^i\beta_o + \frac{1}{120}(5\Phi^2+10\Phi+2)l^{i2}\beta_1 + \frac{1}{210}(7\Phi^2+14\Phi+3)l^{i3}\beta_2$$

$$+ \frac{1}{1680}(49\Phi^2+98\Phi+22)l^{i4}\beta_3 + \frac{1}{420}(11\Phi^2+22\Phi+5)l^{i5}\beta_4$$

$$k_{44}^{(c)} = \frac{1}{60}(5\Phi^2+10\Phi+8)l^i\beta_o - \frac{1}{120}(5\Phi^2+14\Phi+12)l^{i2}\beta_1 - \frac{1}{210}(7\Phi^2+21\Phi+18)l^{i3}\beta_2$$

$$- \frac{1}{1680}(49\Phi^2+152\Phi+130)l^{i4}\beta_3 - \frac{1}{420}(11\Phi^2+35\Phi+30)l^{i5}\beta_4$$

3.4 INERTIA PROPERTIES

The contribution of the kinetic energy expression of the non-spinning i th tapered beam element of length l^i due to translational and rotational deformation is given by :

$$T^i = \left(\frac{1}{2}\right)\int_0^{l^i} \rho^i A_x^i \left(\frac{\partial w^i}{\partial t^i}\right)^2 dx^i + \left(\frac{1}{2}\right)\int_0^{l^i} \rho^i I_x^i \left(\frac{\partial \theta^i}{\partial t^i}\right)^2 dx^i \tag{3.36}$$

The first term in equation (3.36) represents the translational kinetic energy , while the second one is the rotational kinetic energy .

Equation (3.36) can be written in matrix form as follows :

$$[T^i] = \frac{1}{2}\{\dot{q}^i\}^T [M^i]\{\dot{q}^i\} \tag{3.37}$$

where $[M^i]$ is the composite mass matrix given by

$$[M^i] = [M_t^i] + [M_r^i] \tag{3.38}$$

where $[M^i]$ is known as the consistent mass matrix because it is formulated from the same shape functions $[N_w^i]$ and $[N_\theta^i]$ that are used to formulate the stiffness matrix .

where

$$[M_t^i] = \int_0^{l^i} [N_w^i]^T \rho^i A_x^i [N_w^i]\, dx^i = \textit{translational mass matrix} \tag{3.39}$$

$$[M_r^i] = \int_0^{l^i} [N_\theta^i]^T \rho^i I_x^i [N_\theta^i]\, dx^i = \textit{rotary inertia mass matrix} \tag{3.40}$$

The explicit expressions for the element translational mass matrix $[M_t^i]$ and the element rotary inertia mass matrix $[M_r^i]$ are obtained by carrying out the integration of equations (3.39) and (3.40) respectively . The translational and rotary inertia mass matrices $[M_t^i]$ and $[M_r^i]$ are obtained with nonzero entries as presented in Tables 3.4 and 3.5 respectively .

TABLE 3.4 Translational mass matrix of tapered beam element

$$[\,M_t^t\,] = \frac{A_o\rho^t}{I_{oy}\,I_{oz}(\,1 + \Phi\,)^2}\,[\,M_{ab}^{(t)}\,] \quad ; \; a,b = 1\,,2\,,....,4$$

The nonzero entries of the lower triangular part of $[\,M_{ab}^{(t)}\,]$ are given by :

$$M_{11}^{(t)} = \frac{1}{210}(70\Phi^2 + 147\Phi + 78)\,\mu_1 l' - \frac{1}{210}(35\Phi^2 + 70\Phi + 36)\,\mu_2 l'^2 + \frac{1}{630}(21\Phi^2 + 39\Phi + 19)\,l'^3$$

$$M_{21}^{(t)} = \frac{1}{840}(35\Phi^2 + 77\Phi + 44)\,\mu_1 l'^2 - \frac{1}{420}(14\Phi^2 + 27\Phi + 14)\,\mu_2 l'^3 + \frac{1}{2520}(21\Phi^2 + 36\Phi + 17)\,l'^4$$

$$M_{22}^{(t)} = \frac{1}{840}(7\Phi^2 + 14\Phi + 8)\,\mu_1 l'^3 - \frac{1}{840}(7\Phi^2 + 12\Phi + 6)\,\mu_2 l'^4 + \frac{1}{2520}(6\Phi^2 + 9\Phi + 4)\,l'^5$$

$$M_{31}^{(t)} = \frac{1}{210}(35\Phi^2 + 63\Phi + 27)\,\mu_1 l' - \frac{1}{210}(35\Phi^2 + 63\Phi + 27)\,\mu_2 l'^2 + \frac{1}{1260}(63\Phi^2 + 111\Phi + 46)\,l'^3$$

$$M_{32}^{(t)} = \frac{1}{840}(35\Phi^2 + 63\Phi + 26)\,\mu_1 l'^2 - \frac{1}{420}(21\Phi^2 + 36\Phi + 14)\,\mu_2 l'^3 + \frac{1}{2520}(42\Phi^2 + 69\Phi + 25)\,l'^4$$

$$M_{33}^{(t)} = \frac{1}{210}(70\Phi^2 + 147\Phi + 78)\,\mu_1 l' - \frac{1}{210}(105\Phi^2 + 224\Phi + 120)\,\mu_2 l'^2 + \frac{1}{630}(126\Phi^2 + 270\Phi + 145)\,l'^3$$

$$M_{41}^{(t)} = -\frac{1}{840}(35\Phi^2 + 63\Phi + 26)\,\mu_1 l'^2 + \frac{1}{420}(14\Phi^2 + 27\Phi + 12)\,\mu_2 l'^3 - \frac{1}{2520}(21\Phi^2 + 42\Phi + 19)\,l'^4$$

$$M_{42}^{(t)} = -\frac{1}{840}(7\Phi^2 + 14\Phi + 6)\,\mu_1 l'^3 + \frac{1}{840}(7\Phi^2 + 14\Phi + 6)\,\mu_2 l'^4 - \frac{1}{2520}(6\Phi^2 + 12\Phi + 5)\,l'^5$$

$$M_{43}^{(t)} = -\frac{1}{840}(35\Phi^2 + 77\Phi + 44)\,\mu_1 l'^2 + \frac{1}{420}(21\Phi^2 + 5\Phi + 30)\,\mu_2 l'^3 - \frac{1}{2520}(42\Phi^2 + 105\Phi + 65)\,l'^4$$

$$M_{44}^{(t)} = \frac{1}{840}(7\Phi^2 + 14\Phi + 8)\,\mu_1 l'^3 - \frac{1}{840}(7\Phi^2 + 16\Phi + 10)\,\mu_2 l'^4 + \frac{1}{2520}(6\Phi^2 + 15\Phi + 10)\,l'^5$$

TABLE 3.5 Rotary inertia mass matrix of tapered beam element

$$[M_r^i] = \frac{\rho^i A_o l^i}{I_{ey} L_{oz}^3 (1+\Phi)^2} \left(\frac{r_g}{l^i}\right)^2 [M_{ab}^{(r)}] \quad ; \; a,b = 1, 2, \ldots, 4$$

The nonzero entries of the lower triangular part of $[M_{ab}^{(r)}]$ are given by :

$$M_{11}^{(r)} = -M_{31}^{(r)} = M_{33}^{(r)} = \frac{6}{5}\alpha_o - \frac{3}{5}l^i\alpha_1 + \frac{12}{35}l^{i2}\alpha_2 - \frac{3}{14}l^{i3}\alpha_3 + \frac{1}{7}l^{i4}$$

$$M_{21}^{(r)} = -M_{32}^{(r)} = -\frac{1}{10}(5\Phi-1)l^i\alpha_o + \frac{1}{10}(2\Phi-1)l^{i2}\alpha_1 - \frac{1}{70}(7\Phi-5)l^{i3}\alpha_2$$
$$+ \frac{1}{140}(8\Phi-7)l^{i4}\alpha_3 - \frac{1}{28}(\Phi-1)l^{i5}$$

$$M_{22}^{(r)} = \frac{1}{30}(10\Phi^2+5\Phi+4)l^{i2}\alpha_o - \frac{1}{60}(5\Phi^2-2\Phi+2)l^{i3}\alpha_1 + \frac{1}{210}(7\Phi^2-7\Phi+4)l^{i4}\alpha_2$$
$$- \frac{1}{840}(14\Phi^2-20\Phi+11)l^{i5}\alpha_3 + \frac{1}{420}(4\Phi^2-7\Phi+4)l^{i6}$$

$$M_{41}^{(r)} = -M_{43}^{(r)} = -\frac{1}{10}(5\Phi-1)l^i\alpha_o + \frac{3}{10}\Phi l^{i2}\alpha_1 - \frac{1}{35}(7\Phi+1)l^{i3}\alpha_2$$
$$+ \frac{1}{28}(4\Phi+1)l^{i4}\alpha_3 - \frac{1}{28}(3\Phi+1)l^{i5}$$

$$M_{42}^{(r)} = \frac{1}{30}(5\Phi^2-5\Phi-1)l^{i2}\alpha_o - \frac{1}{60}(5\Phi^2-5\Phi-1)l^{i3}\alpha_1 + \frac{1}{140}(7\Phi^2-7\Phi-2)l^{i4}\alpha_2$$
$$- \frac{1}{840}(28\Phi^2-28\Phi-11)l^{i5}\alpha_3 + \frac{1}{84}(2\Phi^2-2\Phi-1)l^{i6}$$

$$M_{44}^{(r)} = \frac{1}{30}(10\Phi^2+5\Phi+4)l^{i2}\alpha_o - \frac{1}{20}(5\Phi^2+4\Phi+2)l^{i3}\alpha_1 + \frac{1}{35}(7\Phi^2+7\Phi+3)l^{i4}\alpha_2$$
$$- \frac{1}{168}(28\Phi^2+32\Phi+13)l^{i5}\alpha_3 + \frac{1}{28}(4\Phi^2+5\Phi+2)l^{i6}$$

3.5 GENERALIZED EIGENVALUE PROBLEM

The potential energy V^i per unit volume of the beam element is given by [3] :

$$V^i = -\left(\frac{1}{2}\right)\int_0^{l^i} F_z\, w\, A_x^i\, dx^i \tag{3.41}$$

Or , in matrix form :

$$V^i = -\frac{1}{2}\{q^i\}^T\, \Omega^2 \sin^2\Psi\, [\, M_t\,]\, \{q^i\} \tag{3.42}$$

The sum of the individual element energies over the entire beam using equations (3.21) , (3.37) and (3.42) gives the Lagrangian function , i.e;

$$L = \sum_{j=1}^{n} (\, T^i - U^i - V^i\,) \tag{3.43}$$

Substitute equations (3.21) , (3.37) and (3.42) into Lagrange's equation ,

$$\frac{\partial}{\partial t}\left(\frac{\partial L}{\partial \dot{q}^i}\right) - \frac{\partial L}{\partial q^i} = 0 \tag{3.44}$$

we obtain the following governing differential equation of the assembled structure for the free vibrations of the rotating tapered beam :

$$(\, [\, K\,] - \Omega^2 \sin^2\Psi\, [\, M_t\,]\,)\, \{q\} + [\, M\,]\, \{\, \ddot{q}\, \} = \{0\} \tag{3.45}$$

where $\{q\}$ is a vector of all nodal coordinates of the beam and $[\, K\,]$ and $[\, M\,]$ are the global stiffness and mass matrices of the whole beam obtained by the standard finite element assembly procedure . The term $\Omega^2 \sin^2\Psi\, [\, M_t\,]\, \{q\}$ accounts for the centripetal acceleration contribution that causes a softening effect on the lead-lag frequencies . For the assumed configuration , however , the gyroscopic terms have no contribution to the eigenvalue calculations , [31] .

On assuming the solution of equation (3.44) in the form

$$\{\, q\, \} = \{\, \overline{q}\, \}\, e^{i\omega t} \tag{3.46}$$

we obtain the following generalized eigenvalue problem :

$$([K] - \Omega^2 \sin^2\Psi [M_t] - \omega^2 [M]) \{ \bar{q} \} = \{ 0 \} \qquad (3.47)$$

where $\{ \bar{q} \}$ is a vector of displacement amplitudes of vibration and ω is the frequency of harmonic vibrations . The solution of equation (3.47) gives the natural frequencies and the corresponding mode shapes .

CHAPTER FOUR

RESULTS AND DISCUSSIONS

A linearly tapered rotating beam based on both Euler-Bernoulli and Timoshenko theories with its spin axis aligned along the inertial Z-axis is considered . The out-of-plane transverse vibration can be represented by equation (3.45) when the plane in which the beam is bending makes an angle $\Psi = 0$, with the direction of rotation . Therefore , the free vibration of the flapping motion can be expressed as

$$[M]\{\ddot{q}\} + [K]\{q\} = 0 \tag{4.1}$$

where $[M]$ and $[K]$ are the assembled mass and stiffness matrices , respectively , of the whole beam . The vector $\{q\}$ represents all nodal coordinates of the beam .

The eigenvalue problem associated with equation (4.1) is given by :

$$([K] - \lambda [M])\{\bar{q}\} = 0 \tag{4.2}$$

where $\{\bar{q}\}$ is a vector of displacement amplitudes of vibrations and λ is the frequency parameter given by :

$$\lambda = \omega \sqrt{\rho A_o L^4 / EI_o} \tag{4.3}$$

Solutions of equation (4.2) are obtained by means of a finite element program that evaluates the spinning effect at the element level developed by Khulief [25 , 31] and modified by the author for the Timoshenko case . In this program the element matrices developed in this thesis and presented in Tables 3.1 to 3.5 , are generated . The finite element assembly procedure is then invoked to assemble the mass and stiffness matrices of equation (4.2) . The generalized eigenvalue problem is then solved by means of EISPACK routines [37] .

In this analysis , both fixed and hinged end conditions are considered for a wide range of rotational speed parameter and taper ratios . The explicit expressions for the rotational speed parameter and taper ratios are given by :

$$\eta = \Omega L^2 / \sqrt{E I_o / \rho A_o} \tag{4.4}$$

and

$$\nu_y = L / L_{oy} , \quad \textit{in x-y plane} . \tag{4.5}$$

$$\nu_z = L / L_{oz} , \quad \textit{in x-z plane} . \tag{4.6}$$

A variety of results ranging up to the tenth frequency are tabulated for general use in Tables 4.1 - 4.31 . These results cover a range of situations including uniform , tapered , rotating and non-rotating beams for both fixed and hinged end conditions . The results are presented in both tabular and graphical forms . For Euler-Bernoulli beams the results were obtained with twelve finite beam elements , while for Timoshenko case , they were obtained with twenty five finite beam elements . In both cases , a consistent mass formulation has been employed .

Comparisons are made , whenever possible , with exact solutions and numerical results available in the literature . The case of hinged-free Timoshenko beam has not been solved by the investigators in this field and no results for such work could be cited in the literature .

The first six bending frequencies of transverse vibrations for rotating and non-rotating , Euler-Bernoulli and Timoshenko beams are examined and plotted in Figs. 4.1

to 4.8 for the clamped-free end conditions and in Figs. 4.17 to 4.25 for the hinged-free end conditions at a wide range of rotational speed parameter and taper ratios . The effect of rotation on the frequency ratios (λ_T / λ_E) for both cantilever and hinged-free beams for several taper ratios is shown respectively in Tables 4.15 to 4.18 and in Tables 4.31 to 4.34 . This effect is also shown graphically in Figs. 4.9 to 4.10 and in Figs. 4.26 to 4.27, respectively for the end conditions mentioned above . The corresponding mode shapes are also shown in Figs. 4.11 - 4.16 for cantilever beam and in Figs. 4.28 - 4.29 for the the hinged-free beam . For the presented results , values of the taper ratio in the range $0.0 \leq \nu \leq 1.0$ are considered , where , $\nu_y = \nu_z = \nu$, for all the analysis unless otherwise stated . A more detail of these results will follow throughout the discussion .

The case of uniform beam corresponds to the value of $\nu = 0.0$, while $\nu = 1.0$ define the case of a thetrahedron or wedge . Values of speed ratio η are taken in the range $0.0 \leq \eta \leq 12.0$ as shown in tabular and graphical forms .

4.1 EULER-BERNOULLI BEAM

As can be seen , the presented results either in tabular or graphical forms indicate that Euler-Bernoulli frequencies are higher than Timoshenko frequencies . Neglecting the effect of shear strain on the beam deflection leads to the the assumption of infinite shear modulus , ($G = \infty$) . This assumption increases the rigidity of the beam theoretically , therefore the classical beam frequencies are higher than Timoshenko frequencies . Since the effects of shear and rotary inertia are a function of the wave length of the vibrations , they are more marked in the higher modes , therefore the effect increases as the mode order increases . The properties of Euler-Bernoulli beam were non-dimensionalized by setting $\lambda = \omega \sqrt{\rho A_o L^4 / EI_o}$, where E is the modulus of elasticity , I is the second moment of the cross-sectional area , ρ is the mass density , A is the cross-sectional area and L is the beam length .

4.1.1 CANTILEVER EULER-BERNOULLI BEAM

Tables 4.1 through 4.6 present the first ten natural frequencies for out-of-plane vibrations of a rotating cantilever beam for different values of rotational speed parameter and taper ratios . The present results show an excellent agreement with the results obtained by Downs , [5] , who used a new discretization technique for the evaluation of the natural frequencies of the non-rotating tapered cantilever beam with unequal breadth and taper .

As an example , the percentage errors between the present work and the the exact solution , [27] , in the first three frequencies were respectively 0.00 , 0.00 , 0.01 for the uniform non-rotating cantilever beam , and were 0.00 , 0.00 , 0.00 and 0.00 , 0.00 , 0.00 for the same beam rotating at η = 1.0 and η = 10.0 , respectively . For the case of non-rotating tapered cantilever beam , where ν = 0.3 , and ν = 0.6 , the percentage errors in the first three frequencies , respectively , were 0.00 , 0.00 , 0.01 and 0.00 , 0.00 and 0.00 when compared to Downs [5] .

Tables 4.1 through 4.7 show that for a fixed taper ratio , the first ten frequencies increase with increasing speed ratio . This can be seen in Figs. 4.1 - 4.4 for the first six frequencies . It is also shown that as the taper ratio increases , the first frequency increases slightly for $0.0 \le \eta \le 3.0$ as shown in Figs. 4.5 and 4.6 . It decreases for $0.0 \le \nu \le 0.5$ and increases for $0.5 \le \nu \le 0.9$ at the speed ratio of η = 5.0 as shown in Fig. 4.7 . And finally , it is decreasing when $0.0 \le \nu \le 0.6$ and is increasing when $0.6 \le \nu \le 0.9$ at η = 10.0 as shown in Fig. 4.8 . Figure 4.5 shows that for a non-rotating beam , The second frequency is decreasing for taper ratios ranging from 0.0 to

0.8 and increasing for $0.8 \leq \nu \leq 0.9$. The same trend can be seen in Figs. 4.6 - 4.8 when η is equal to 2.0 , 5.0 and 10.0 reaching minimum frequencies at taper ratios 0.75 , 0.70 and 0.65 , respectively . The third frequency decreases for η = 0.0 and η = 2.0 , and follows the same trend as the second one when η becomes larger . Figures 4.5 - 4.7 show that the fourth , fifth and sixth frequencies decrease with increasing taper ratio and increasing speed ratio in the range $0.0 \leq \eta \leq 5.0$, while Fig. 4.8 shows that the fifth and sixth frequencies are still decreasing when the fourth one changes his behavior by decreasing in $0.0 \leq \nu \leq 0.8$ and increasing for $0.8 \leq \nu \leq 0.9$.

4.1.2 HINGED FREE EULER-BERNOULLI BEAM

Tables 4.19 - 4.24 show the first ten frequencies of Euler-Bernoulli hinged free beam for a wide range of taper and speed ratios . The results are obtained using twelve finite element beam (same as for the cantilever beam) . Such beams are known to constitute a semidefinite stiffness matrix (i.e; they include rigid body mode and a value of zero is to be found for the first frequency for a non-rotating beam) . The rigid body modes are not shown neither in the tables nor in the figures for this case because they are known to take the value of the speed ratio η .

As a comparison between the present model and the exact solution , given by Wright et al. [27] , the percentage errors in the first three frequencies , were 0.00 , 0.01 and 0.00 for the non-rotating uniform hinged-free beam . For the rotating uniform hinged-free beam , where η = 5.0 , the percentage errors in the first three frequencies , respectively , were 0.00 , 0.01 and 0.03 , and when η = 10.0 the errors were 0.00 % , 0.00 % and 0.02 % for the first three frequencies , respectively .

As for the cantilever beam , Tables 4.19 - 4.24 show that for a fixed taper ratio , the first ten frequencies increase with increasing the speed ratio . This can also be shown in Figs. 4.17 through 4.21 for the first six modes .

The variation of the frequencies versus taper ratios at constant speed ratios are shown in Figs. 4.22 - 4.25 . The same trend can be seen as described before for the case of cantilever beam .

4.2 TIMOSHENKO BEAM

In addition to the constant parameter $\sqrt{\rho A_o L^4 / E I_o}$, in Timoshenko beam theory , there are two further parameters expressing the slenderness ratio and cross-sectional properties of the beam . The first , related to the slenderness ratio , can be expressed as r_g / L where $r_g = \sqrt{I_o / A_o}$ is the radius of gyration of the cross-section , and L is the length of the whole beam . The second independent variable is the product $G k'$. Since G / E may be taken as a material constant (which varies little between materials) , k' may be regarded as the second variable . The values of k' are governed by purely geometric considerations and are given by equations (2.15) and (2.16) .

Since , most of the investigations on this problem [3 , 5] lack sufficient information to adequately reproduce the same results at least for the non-rotating tapered Timoshenko beam (because results for rotating tapered Timoshenko are not available in the literature) , a computer program was developed to scan over the best dimensions of the beam in order to reproduce the results given by Downs [5] who suggested values of Poisson's ratio = 0.3 , ratio of radius of gyration at cantilever root to the beam length = 0.08 and a shear correction factor of 0.85 which is a case of thick beam . These informations are not sufficient if one needs to reproduce the same results because the dimensions of the cross-sectional area of the beam are not given . Since $r_g / L = 0.08$ gives $z_o = \sqrt{12}\,(0.08\, L)$, where z_o is the thickness at the root of the beam , this means that z_o is a function of L. In order to reproduce the results presented by Downs [5] , the following beam dimensions are used : $L = 1\ m$, $z_o = 0.277128\ m$, and $y_o = z_o / 3 = 0.092376\ m$. where z_o and y_o are the thickness and the width at the root of the beam respectively .

If the shear deformation parameter Φ and the rotary inertia mass matrix $[M_r^i]$ are excluded , the present model reduces to the classical Bernoulli-Euler tapered beam model used by Khulief [31] . It is interesting to observe that if the untruncated lengths L_{oy} and L_{oz} tend to infinity , the taper ratios become zero , resulting in the case of a uniform beam presented by Yokoyama [3] .

4.2.1 CANTILEVER TIMOSHENKO BEAM

Tables 4.7 - 4.14 show the frequency ratios of a cantilever Timoshenko beam at a wide range of rotational speed parameter and taper ratios . The same observation can be drawn concerning the increase of frequencies for increasing speed ratio at a fixed taper ratio as can be seen in Figs. 4.1 - 4.4 . This trend is valid for both Euler-Bernoulli and Timoshenko cases .

The results presented for the case of non-rotating cantilever Timoshenko beam were compared to Downs [5] . For the case of uniform beam , the errors in the first three frequencies were 0.18 % , 0.02 % and 0.06 % respectively . For a tapered beam of 0.6 taper ratio the percentage errors in the first three frequencies , respectively , were 0.13 , 0.12 and 0.05 . For a tapered beam of 1.0 taper ratio , the percentage errors in the first eight frequencies , respectively , were 0.05 , 0.53 , 1.21 , 1.94 , 2.59 , 3.05 , 2.82 and 0.71 . This implies that the third through the seventh frequencies for the case of 1.0 taper ratio , experience a relatively larger error which may be caused by the discretization of the beam and the sharp end of the cantilever . Downs [5] , who used twelve unequal subdivisions in his discretization for the this case (ν = 1.0) instead of eight subdivisions for the other taper ratios . concluded that subdivision of the tapered beam for dynamic discretization requires considerable care , particularly for taper ratios close to one in order to minimize the errors inherent in the discretization process . He mentioned also that a similar problem was encountered by Housner and Keightley, when applying the Myklestad-Prohl technique followed by Stodola iteration to both wedge and cone . Their subdivision of the cantilever into hundred equal length segments proved insufficient to produce results of acceptable accuracy , even for the second mode and consequently the outer ten percent of the beam was further subdivided into thirty equal segments .

As mentioned earlier , there is no available results in the literature for the rotating tapered Timoshenko beams .

Figures 4.5 - 4.6 show that the first three frequencies follow the same trend described for the Euler-Bernoulli cantilever beam for the different values of taper ratios at the specified speed ratios . The fourth and fifth frequencies are both decreasing for speed ratios such that $0.0 \le \eta \le 2.0$. For $\eta = 5.0$, these two frequencies are decreasing in $0.0 \le \nu \le 0.8$ and increasing in $0.8 \le \nu \le 0.9$, while for $\eta = 10.0$, we can see that the fourth frequency is decreasing in $0.0 \le \nu \le 0.7$ and increasing in $0.7 \le \nu \le 0.9$, but the fifth one is increasing for $0.0 \le \nu \le 0.1$ and $0.75 \le \nu \le 0.9$, and decreasing in $0.1 \le \nu \le 0.75$. To end up with the variation of the different frequencies in function of taper ratios , let us describe the behaviour of the sixth and last frequency . For non-rotating beam , the sixth frequency increases in $0.0 \le \nu \le 0.4$ and decreases in $0.4 \le \nu \le 0.9$. For speed ratio greater than zero , say $\eta = 2.0$, this frequency increases in $0.0 \le \nu \le 0.3$ and decreases in $0.3 \le \nu \le 0.9$, and for $\eta = 5.0$, it increases in

$0.0 \le \nu \le 0.35$ and $0.8 \le \nu \le 0.9$, and decreases in $0.35 \le \nu \le 0.8$. Finally, for $\eta = 10.0$, the sixth frequency increases in $0.0 \le \nu \le 0.4$ and $0.7 \le \nu \le 0.9$, and decreases in $0.4 \le \nu \le 0.7$.

The effect of rotation on the frequency ratios (λ_T / λ_E) of the cantilever beam is shown in Tables 4.15 - 4.18 and is represented graphically in Figs. 4.9 and 4.10 , from which we can conclude that these ratios increase for the first , third and fifth frequencies by increasing the speed and taper ratios while in the first frequency this ratio is increasing for $0.0 \le \nu \le 0.5$, and is decreasing for $0.5 \le \nu \le 0.7$, as shown in Figs. 4.9 - 4.10 . From these figures it is confirmed that Timoshenko frequencies are lower than Euler-Bernoulli frequencies , which means that (λ_T / λ_E) $\le 1.$ for any value of η and ν.

In Figs. 4.11 - 4.16 , the first three mode shapes for Euler-Bernoulli , Timoshenko , rotating and non-rotating beam at different taper and speed ratios are shown . It is to be noted here that the amplitude of Timoshenko mode shapes are greater than that of Euler-Bernoulli resulting in the effect of the rotary inertia and shear deformation incorporated for the Timoshenko beam . As a second remark , it is clear that as the taper and speed ratio increases , the relative amplitudes of the total deflection decreases for both Euler and Timoshenko beams and , the amplitudes of modes 2 and 3 for rotating beam are higher than that of non-rotating one .

4.2.1 HINGED-FREE TIMOSHENKO BEAM

Up to the knowledge of the author , and as mentioned earlier , there is no available results in the literature for this case . Figures 4.17 - 4.21 show that the first six frequencies increase when the speed ratio increases . This agrees with what we mentioned before and is valid for all types of beams studied in this research . In Figs. 4.22 - 4.25 , the description done before for the behavior of the different frequencies as a function of the taper ratio at constant speed ratio is almost the same except for the fifth frequency which is increasing in $0.0 \leq \nu \leq 0.4$ and decreasing in $0.4 \leq \nu \leq 0.9$ for non rotating beam and is increasing in $0.0 \leq \nu \leq 0.2$ and $0.7 \leq \nu \leq 0.9$ and decreasing in $0.2 \leq \nu \leq 0.7$ at $\eta = 10.0$.

Figures 4.26 - 4.27 show the effect of rotation on the frequency ratios (λ_T / λ_E) of the hinged-free Timoshenko beam which is also shown in Tables 4.31- 4.34 . For taper ratios of 0.0 and 0.2 , these ratios of the first , second and third frequencies follow the same trend described for the cantilever beam , while for the fourth frequency , these are increasing in $0.0 \leq \eta \leq 6.0$ and decreasing in $6.0 \leq \eta \leq 12.0$ for uniform hinged-free beam and these are increasing in $0.0 \leq \eta \leq 10.0$ and decreasing in $10.0 \leq \eta \leq 12.0$ for a tapered hinged-free beam of 0.2 taper ratio . In the same way , we can describe the behavior of these frequency ratios of the fifth frequency as well as the other frequency ratios for the different values of the taper ratios as shown in Figs. 4-26 - 4.27 . It is also confirmed here that Timoshenko frequencies are lower than Euler-Bernoulli frequencies as expected . The mode shapes of the hinged-free beam are shown in Figs. 4.28 and 4.29 for $\nu = 0.7$, and all that can be said here is similar to the precedent case concerning the amplitudes of the vibration .

As a concluding remark , the results reveal an interesting observation , that is concerning the existence of a critical taper ratio where the frequencies of a rotating beam reverse the direction of change . The centrifugal effect is more dominant than the softening effect resulting from the decrease of the cross-sectional area .

TABLE 4.1 Frequency parameter λ of uniform Euler-Bernoulli cantilever beam , ($\nu_y = \nu_z = 0.0$) .

Speed ratio η	Frequency									
	λ_1	λ_2	λ_3	λ_4	λ_5	λ_6	λ_7	λ_8	λ_9	λ_{10}
0	3.51602	22.0348	61.7049	120.959	200.110	299.369	419.135	560.027	722.815	908.338
	3.51602*	22.0345*	61.6972*	120.902*	199.860*	298.566*	416.991*	555.165*	–	–
1	3.68165	22.1814	61.8494	121.108	200.262	299.522	419.291	560.183	723.008	908.494
	3.6817**	22.1810**	61.8418**	121.051**	200.012**	–	–	–	–	–
3	4.79728	23.3206	62.9925	122.292	201.472	300.750	420.529	561.428	724.255	909.741
	4.7973**	23.3203**	62.9850**	122.236**	201.223**	–	–	–	–	–
5	6.44955	25.4464	65.2124	124.662	203.868	303.188	422.994	563.909	726.743	912.228
	6.4495**	25.4461**	65.2050**	124.566**	203.622**	–	–	–	–	–
7	8.29967	28.3345	68.3931	128.026	207.403	306.805	426.662	567.608	730.457	915.945
	8.2996**	28.3341**	68.3931**	127.972**	207.161**	–	–	–	–	–
10	11.2024	33.6410	74.6566	134.936	214.697	314.334	434.342	575.380	738.281	923.788
	11.2023**	33.6404**	74.6493**	134.884**	214.461**	–	–	–	–	–

* *Reference [5]*
** *Reference [27]*

TABLE 4.2 Frequency parameter λ of a tapered Euler-Bernoulli cantilever beam, ($\nu_y = \nu_z = 0.1$) .

Speed ratio η	***Frequency***									
	λ_1	λ_2	λ_3	λ_4	λ_5	λ_6	λ_7	λ_8	λ_9	λ_{10}
0	*3.67370*	*21.5506*	*59.1958*	*115.451*	*190.593*	*284.819*	*398.506*	*532.230*	*686.738*	*862.683*
1	*3.82016*	*21.6842*	*59.3264*	*115.585*	*190.529*	*284.957*	*398.645*	*532.370*	*686.878*	*862.822*
3	*4.82876*	*22.7093*	*60.3601*	*116.653*	*191.819*	*286.061*	*399.758*	*533.487*	*687.997*	*863.939*
5	*6.36500*	*24.6347*	*62.3713*	*118.757*	*193.977*	*288.255*	*401.974*	*535.716*	*690.230*	*866.167*
7	*8.11516*	*27.2665*	*65.2613*	*121.835*	*197.166*	*291.511*	*405.272*	*539.039*	*693.564*	*869.497*
10	*10.8905*	*32.1372*	*70.9765*	*128.101*	*203.754*	*298.298*	*412.184*	*546.026*	*700.590*	*876.527*

TABLE 4.3 Frequency parameter λ of a tapered Euler-Bernoulli cantilever beam , ($\nu_y = \nu_z = 0.3$) .

Speed ratio η	Frequency									
	λ_1	λ_2	λ_3	λ_4	λ_5	λ_6	λ_7	λ_8	λ_9	λ_{10}
0	4.06693	20.5558	54.0218	104.023	170.788	254.498	355.481	474.224	611.321	767.129
	4.06693*	20.5555*	54.0152*	103.975*	170.577*	253.820*	353.706*	470.237*	–	–
1	4.17159	20.6543	54.1212	104.125	170.891	254.603	355.587	474.330	611.426	767.234
3	4.92744	21.4257	54.9095	104.937	171.717	255.437	356.426	475.172	612.267	768.070
5	6.15973	22.8898	56.4508	106.541	173.356	257.097	358.099	476.851	613.946	769.738
7	7.63240	24.9228	58.6817	108.897	175.783	259.566	360.593	479.358	616.454	772.234
10	10.0454	28.7608	63.1433	113.726	180.819	264.727	365.829	484.637	621.747	777.508

* *Reference [5]*

TABLE 4.4 Frequency parameter λ of a tapered Euler-Bernoulli cantilever beam, ($\nu_y = \nu_z = 0.5$) .

Speed ratio η	***Frequency***									
	λ_1	λ_2	λ_3	λ_4	λ_5	λ_6	λ_7	λ_8	λ_9	λ_{10}
0	*4.62515*	*19.5480*	*48.5853*	*91.8573*	*149.580*	*221.929*	*309.183*	*411.727*	*529.986*	*664.557*
1	*4.68691*	*19.6120*	*48.6520*	*91.9256*	*149.649*	*221.998*	*309.253*	*411.796*	*530.055*	*664.625*
3	*5.15406*	*20.1167*	*49.1813*	*92.4699*	*150.200*	*222.553*	*309.808*	*412.351*	*530.606*	*665.167*
5	*5.97855*	*21.0888*	*50.2224*	*93.5483*	*151.296*	*223.657*	*310.916*	*413.459*	*531.706*	*666.251*
7	*7.03383*	*22.4654*	*51.7425*	*95.1408*	*152.923*	*255.302*	*312.570*	*415.114*	*533.352*	*667.872*
10	*8.86166*	*25.1326*	*54.8248*	*98.4317*	*156.319*	*228.754*	*316.052*	*418.607*	*536.830*	*671.302*

TABLE 4.5 Frequency parameter λ of a tapered Euler-Bernoulli cantilever beam, ($\nu_y = \nu_z = 0.6$) .

Speed ratio η	Frequency									
	λ_1	λ_2	λ_3	λ_4	λ_5	λ_6	λ_7	λ_8	λ_9	λ_{10}
0	5.00904	19.0653	45.7448	85.3870	138.216	204.409	284.220	377.998	486.241	610.737
	5.00903*	19.0649*	45.7384*	85.3438*	138.035*	203.845*	282.789*	374.879*	–	–
1	5.05433	19.1191	45.8001	85.4427	138.272	204.464	284.276	378.053	486.296	610.790
3	5.40261	19.5437	46.2392	85.8867	138.717	204.909	284.720	378.495	486.732	611.211
5	6.03755	20.3641	47.1044	86.7675	139.602	205.796	285.607	379.379	487.603	612.503
7	6.87760	21.5312	48.3714	88.0709	140.919	207.118	286.930	380.700	488.906	613.312
10	8.37841	23.8059	50.9518	90.7734	143.673	209.897	289.722	383.490	491.663	615.979

* *Reference* [5]

TABLE 4.6 Frequency parameter λ of a tapered Euler-Bernoulli cantilever beam, ($\nu_y = \nu_z = 0.8$) .

Speed ratio η	Frequency									
	λ_1	λ_2	λ_3	λ_4	λ_5	λ_6	λ_7	λ_8	λ_9	λ_{10}
0	6.19640	18.3860	39.8404	71.2834	112.997	165.198	228.223	302.841	496.616	612.073
	6.19639*	18.3855*	39.8336*	71.2418*	112.828*	164.668*	226.796*	299.231*	–	–
1	6.27433	18.5423	39.9696	71.3893	113.094	165.295	228.325	302.947	496.704	612.180
3	6.81794	19.7255	40.9928	72.2315	113.863	166.065	229.139	303.797	497.407	613.039
5	7.64147	21.7856	42.9789	73.8894	115.382	167.591	230.753	305.488	498.810	614.748
7	8.56115	24.3123	45.7999	76.3117	117.613	169.842	233.140	308.000	500.907	617.288
10	10.0199	28.3545	51.1781	81.2166	122.180	174.488	238.083	313.238	505.334	622.596

* *Reference* [5]

TABLE 4.7 Frequency parameter λ of uniform Timoshenko cantilever beam, ($\nu_y = \nu_z = 0.0$) .

Speed ratio η	Frequency									
	λ_1	λ_2	λ_3	λ_4	λ_5	λ_6	λ_7	λ_8	λ_9	λ_{10}
0	3.31813	16.2603	36.6842	58.3679	80.5852	94.8401	107.661	115.757	135.202	141.743
	3.32405*	16.2890*	36.7078*	58.2788*	80.2127*	94.4520*	106.836*	114.732*	–	–
1	3.48267	16.4271	36.8912	58.6247	80.8735	94.9659	107.885	115.965	135.500	141.983
3	4.57699	17.7013	38.4913	60.6116	83.0827	95.8714	109.615	117.618	137.659	144.018
5	6.17093	19.9919	41.4367	64.2661	87.0129	97.3354	112.685	120.915	140.957	148.604
7	7.93995	22.9707	45.3605	69.0927	91.7523	99.2384	116.469	125.647	144.835	155.496
10	10.7127	28.1829	52.3501	77.3610	97.6814	103.772	123.389	133.206	153.428	165.895

* *Reference [5]*

TABLE 4.8 Frequency parameter λ of a tapered Timoshenko cantilever beam , ($\nu_y = \nu_z = 0.1$) .

Speed ratio η	Frequency									
	λ_1	λ_2	λ_3	λ_4	λ_5	λ_6	λ_7	λ_8	λ_9	λ_{10}
0	3.46988	16.2452	36.2132	57.8703	80.4629	98.0284	108.788	117.963	135.659	143.683
1	3.61395	16.3919	36.3952	58.0974	80.7274	98.1703	108.966	118.134	135.929	143.872
3	4.59707	17.5186	37.8085	59.8643	82.7797	99.1586	110.431	119.443	138.086	145.394
5	6.07535	19.5660	40.4371	63.1593	86.5686	100.555	113.414	121.853	141.636	148.566
7	7.74650	22.2623	43.9871	67.6083	91.5512	101.898	117.455	125.313	145.762	153.815
10	10.3918	27.0474	50.4315	75.5794	99.5234	104.154	123.811	132.286	152.692	164.006

TABLE 4.9 Frequency parameter λ of a tapered Timoshenko cantilever beam , ($\nu_y = \nu_z = 0.3$) .

Speed ratio η	Frequency									
	λ_1	λ_2	λ_3	λ_4	λ_5	λ_6	λ_7	λ_8	λ_9	λ_{10}
0	3.84693	16.1490	35.0759	56.3837	79.1207	101.422	114.444	123.106	139.024	147.859
	3.85346*	16.1766*	35.1026*	56.3081*	78.7486*	100.592*	113.912*	121.735*	–	–
1	3.94602	16.2510	35.2041	56.5447	79.3130	101.620	114.476	123.295	139.139	148.044
3	4.66047	17.0429	36.2080	57.8079	80.8224	103.143	114.763	124.725	140.074	149.466
5	5.82180	18.5162	38.1116	60.2135	83.6975	105.830	115.514	127.167	142.053	151.986
7	7.20637	20.5115	40.7499	63.5644	87.6975	108.810	117.295	129.918	145.305	155.096
10	9.47336	24.1675	45.7102	69.8901	95.1934	111.566	123.333	133.503	152.443	160.311

* *Reference [5]*

TABLE 4.10 Frequency parameter λ of a tapered Timoshenko cantilever beam, ($\nu_y = \nu_z = 0.5$).

Speed ratio η	Frequency									
	λ_1	λ_2	λ_3	λ_4	λ_5	λ_6	λ_7	λ_8	λ_9	λ_{10}
0	4.37932	15.9802	33.6222	54.1575	76.4846	99.6495	121.892	125.618	148.239	152.557
1	4.43224	16.0371	33.6966	54.2523	76.5987	99.7807	121.970	125.697	148.404	152.573
3	4.83368	16.4836	34.2837	55.0003	77.4997	100.816	122.493	126.416	149.708	152.699
5	5.54543	17.3359	35.4159	56.4462	79.2429	102.811	123.134	128.171	152.204	152.948
7	6.45962	18.5282	37.0220	58.5042	81.7262	105.630	123.649	131.058	153.309	155.708
10	8.04652	20.8008	40.1394	62.5162	86.5688	110.983	124.404	136.875	154.221	162.160

TABLE 4.11 Frequency parameter λ of a tapered Timoshenko cantilever beam , ($\nu_y = \nu_z = 0.6$) .

Speed ratio η	Frequency									
	λ_1	λ_2	λ_3	λ_4	λ_5	λ_6	λ_7	λ_8	λ_9	λ_{10}
0	4.74359	15.8912	32.7523	52.6984	74.6089	97.6555	121.041	129.374	146.751	161.354
	4.74979*	15.9107*	32.7692*	52.6316*	74.2587*	96.8403*	119.904*	128.763*	–	–
1	4.77924	15.9351	32.8084	52.7691	74.6932	97.7529	121.141	129.392	146.876	161.371
3	5.05595	16.2813	33.2523	53.3270	75.3607	98.5232	121.923	129.545	147.859	161.494
5	5.56341	16.9494	34.1150	54.4123	76.6599	100.021	123.370	129.917	149.765	161.717
7	6.23916	17.8981	35.3522	55.9718	78.5218	102.169	125.184	130.717	152.476	162.028
10	7.45277	19.7428	37.7931	59.0577	82.2248	106.390	127.400	133.675	157.550	162.863

* *Reference* [5]

TABLE 4.12 Frequency parameter λ of a tapered Timoshenko cantilever beam, ($\nu_y = \nu_z = 0.8$) .

Speed ratio η	Frequency									
	λ_1	λ_2	λ_3	λ_4	λ_5	λ_6	λ_7	λ_8	λ_9	λ_{10}
0	5.85906	15.9240	30.7504	48.8498	69.2348	91.2239	114.289	135.835	141.624	163.831
	5.86287*	15.9230*	30.7258*	48.7398*	68.9018*	90.4981*	113.738*	134.722*	–	–
1	5.93170	16.1037	30.9244	49.0133	69.3955	91.3874	114.458	135.924	141.726	164.018
3	6.44975	17.3890	32.2646	50.2976	70.6633	92.6775	115.785	136.541	142.615	165.493
5	7.16499	19.3775	34.6780	52.7425	73.1064	95.1681	118.341	137.378	144.698	168.319
7	7.93730	21.5511	37.7318	56.1099	76.5595	98.7040	121.942	138.121	148.143	172.210
10	9.16699	24.7950	42.7470	62.2441	83.1747	105.557	128.709	139.257	155.418	178.149

* *Reference [5]*

TABLE 4.13 Frequency parameter λ of a tapered Timoshenko cantilever beam , ($\nu_y = \nu_z = 0.9$) .

Speed ratio η	Frequency									
	λ_1	λ_2	λ_3	λ_4	λ_5	λ_6	λ_7	λ_8	λ_9	λ_{10}
0	6.78804	16.4756	29.9571	46.5242	65.4589	86.1994	108.284	131.083	143.503	156.703
	6.78850*	16.4421*	29.8463*	46.2748*	64.9540*	85.2855*	107.568*	132.014*	–	–
1	7.01255	17.1963	30.7930	47.3019	66.1652	86.8559	108.911	131.666	143.589	157.295
3	7.96327	20.6385	35.8012	52.7332	71.3869	91.7571	113.574	135.851	144.332	161.765
5	8.88925	23.8895	41.3316	60.1502	79.7048	100.045	121.463	141.140	147.318	169.470
7	9.79003	26.7398	46.1722	67.0898	88.4907	109.751	130.846	143.367	155.202	178.174
10	11.1714	30.6728	52.6834	76.3667	100.573	124.129	141.951	148.915	169.839	188.844

* *Reference [5]*

TABLE 4.14 Frequency parameter λ of a tapered Timoshenko cantilever beam , ($\nu_y = \nu_z = 1.0$) .

Speed ratio η	Frequency									
	λ_1	λ_2	λ_3	λ_4	λ_5	λ_6	λ_7	λ_8	λ_9	λ_{10}
0	8.13783	18.6734	32.0262	47.6662	65.1654	84.1119	104.074	124.604	144.076	150.150
	8.13372*	18.5758*	31.6431*	46.7586*	63.5173*	81.6222*	101.216*	123.450*	–	–
1	8.58208	20.7325	36.0074	53.5160	72.6896	93.0410	113.926	134.115	147.441	154.816
3	9.83865	25.5527	44.4461	65.5841	88.3050	112.153	136.321	148.402	162.565	179.205
5	10.9766	29.4397	50.9603	74.7839	100.097	126.336	146.941	155.704	180.752	190.291
7	12.0577	32.8498	56.5741	82.6829	110.171	137.982	149.006	169.218	191.593	197.384
10	13.6711	37.5533	64.2035	93.3589	123.602	147.058	157.466	187.830	198.258	200.342

* *Reference* [5]

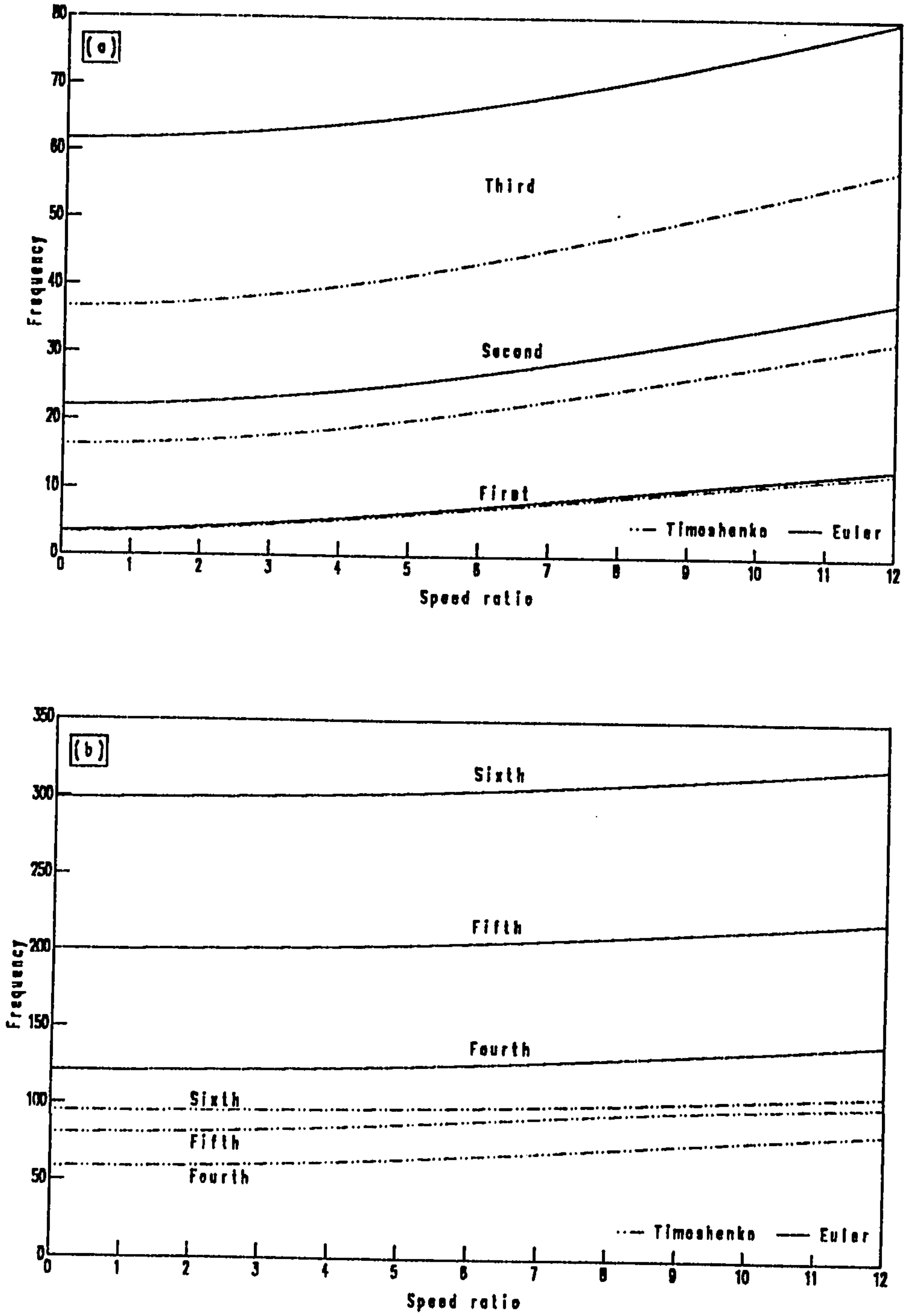

Fig. 4.1 The first six bending frequencies of uniform cantilever beam ; ($v_y = v_z = 0.0$) ;
a) First , second and third , b) Fourth , fifth and sixth .

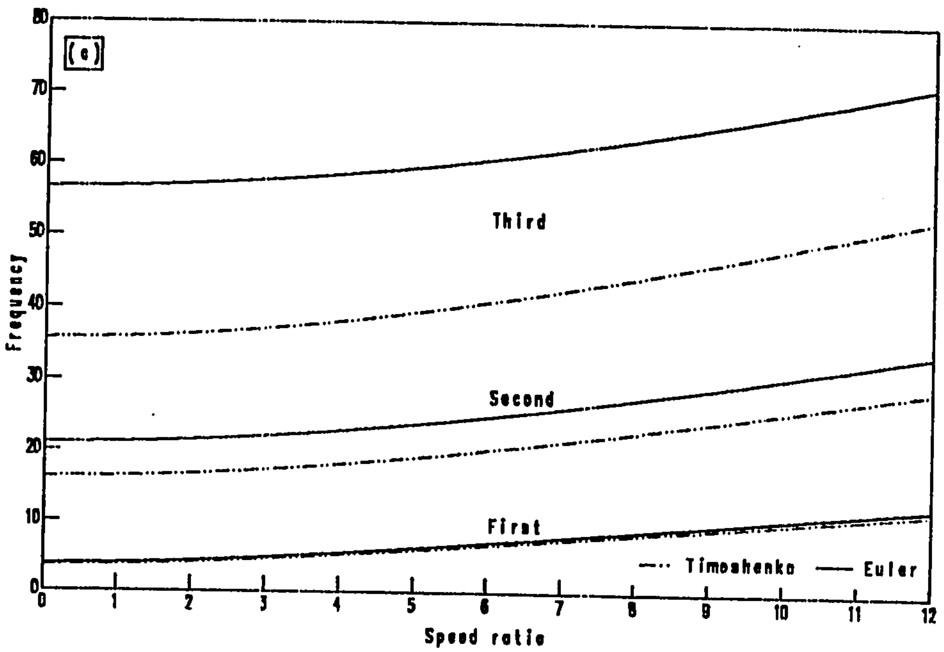

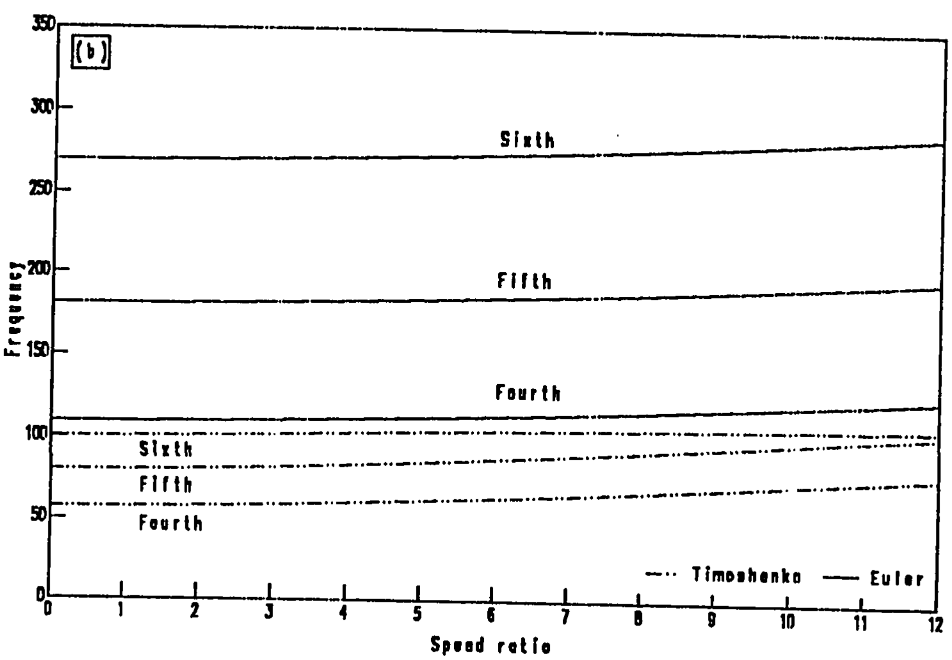

Fig. 4.2 The first six bending frequencies of a tapered cantilever beam ; ($\nu_y = \nu_z = 0.2$) ;
a) First , second and third , b) Fourth , fifth and sixth .

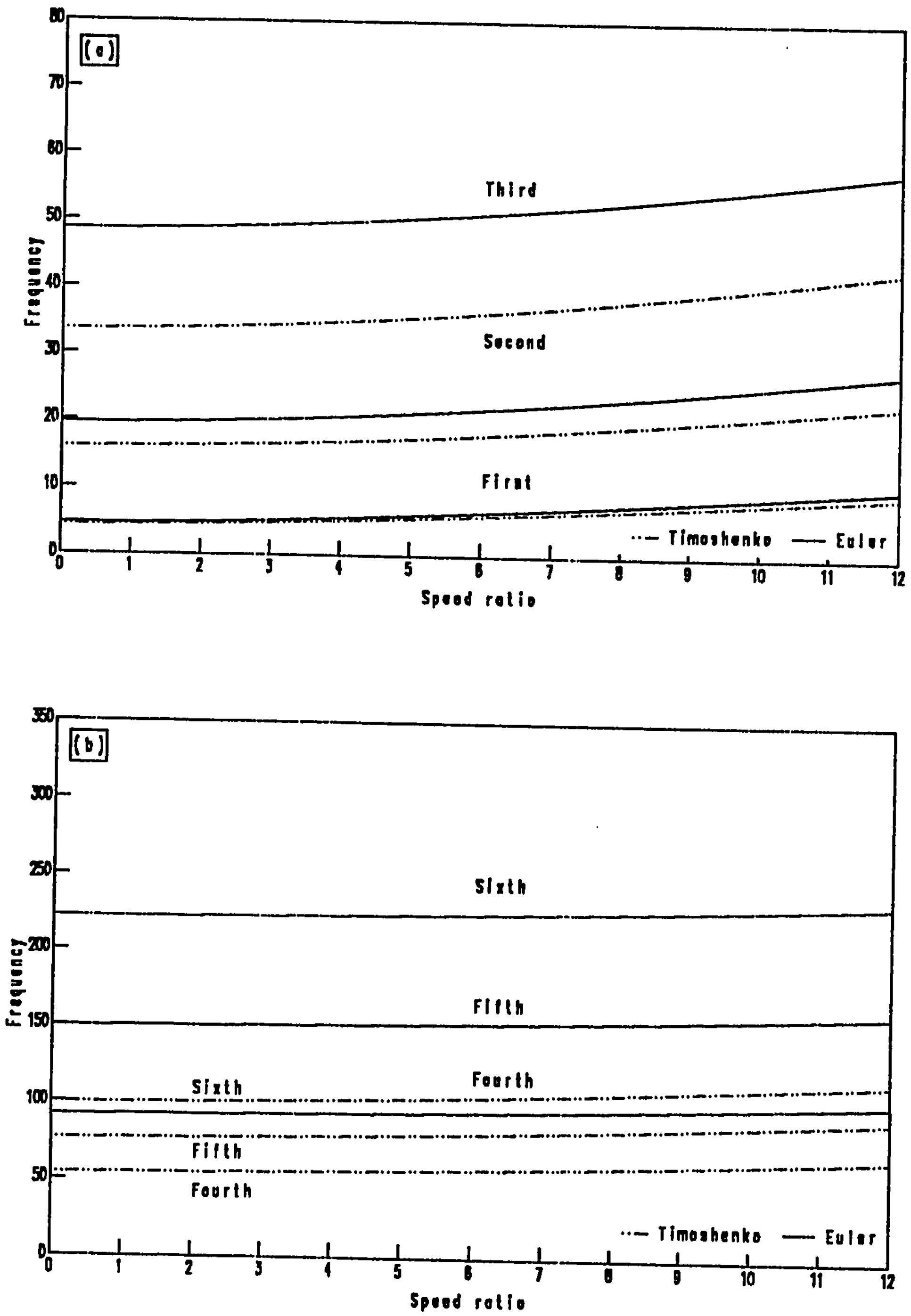

Fig. 4.3 The first six bending frequencies of a tapered cantilever beam ; ($v_y = v_z = 0.5$) ;
a) First , second and third , b) Fourth , fifth and sixth .

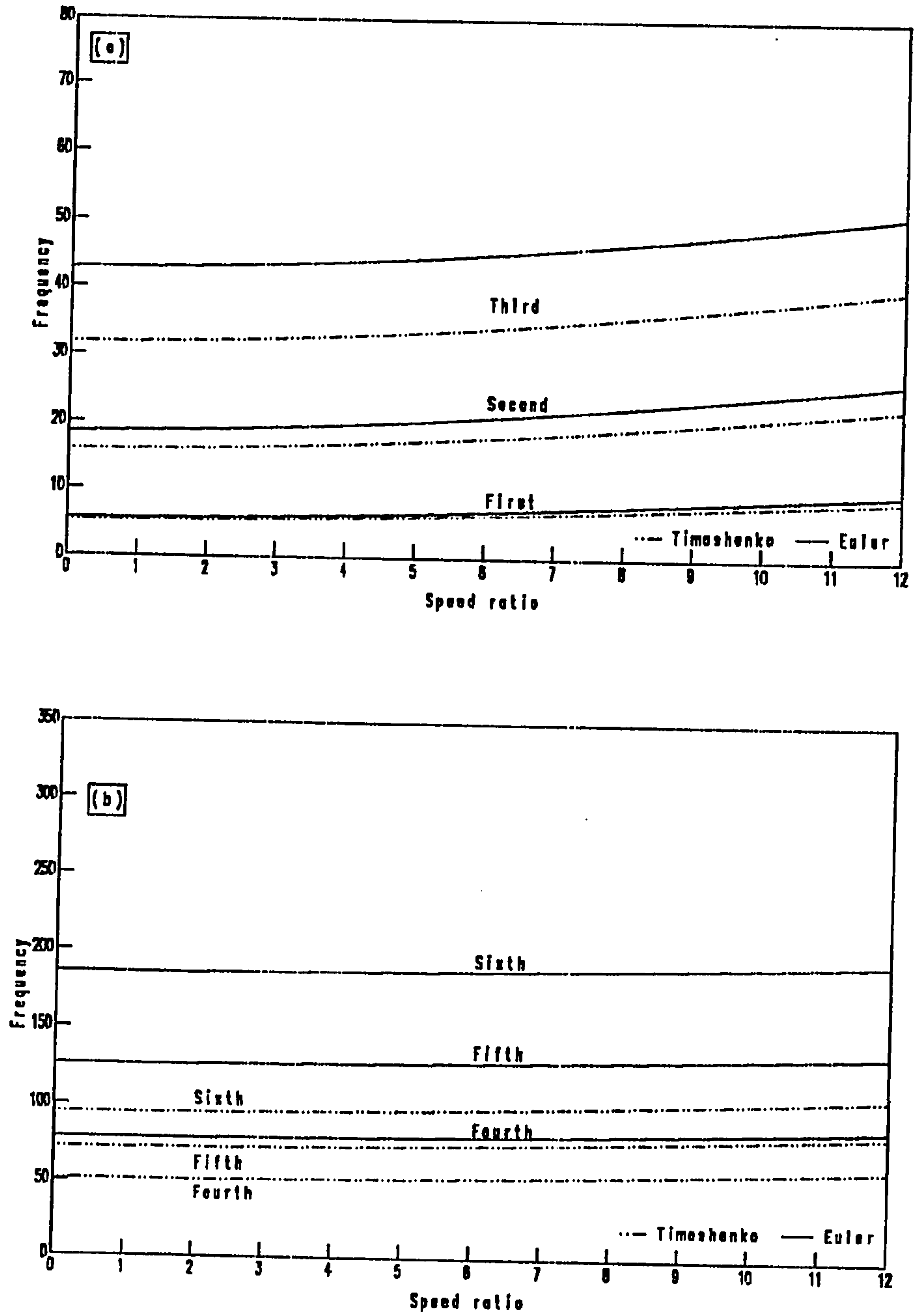

Fig. 4.4 The first six bending frequencies of a tapered cantilever beam ; ($\nu_y = \nu_z = 0.7$) ;
a) First , second and third , b) Fourth , fifth and sixth .

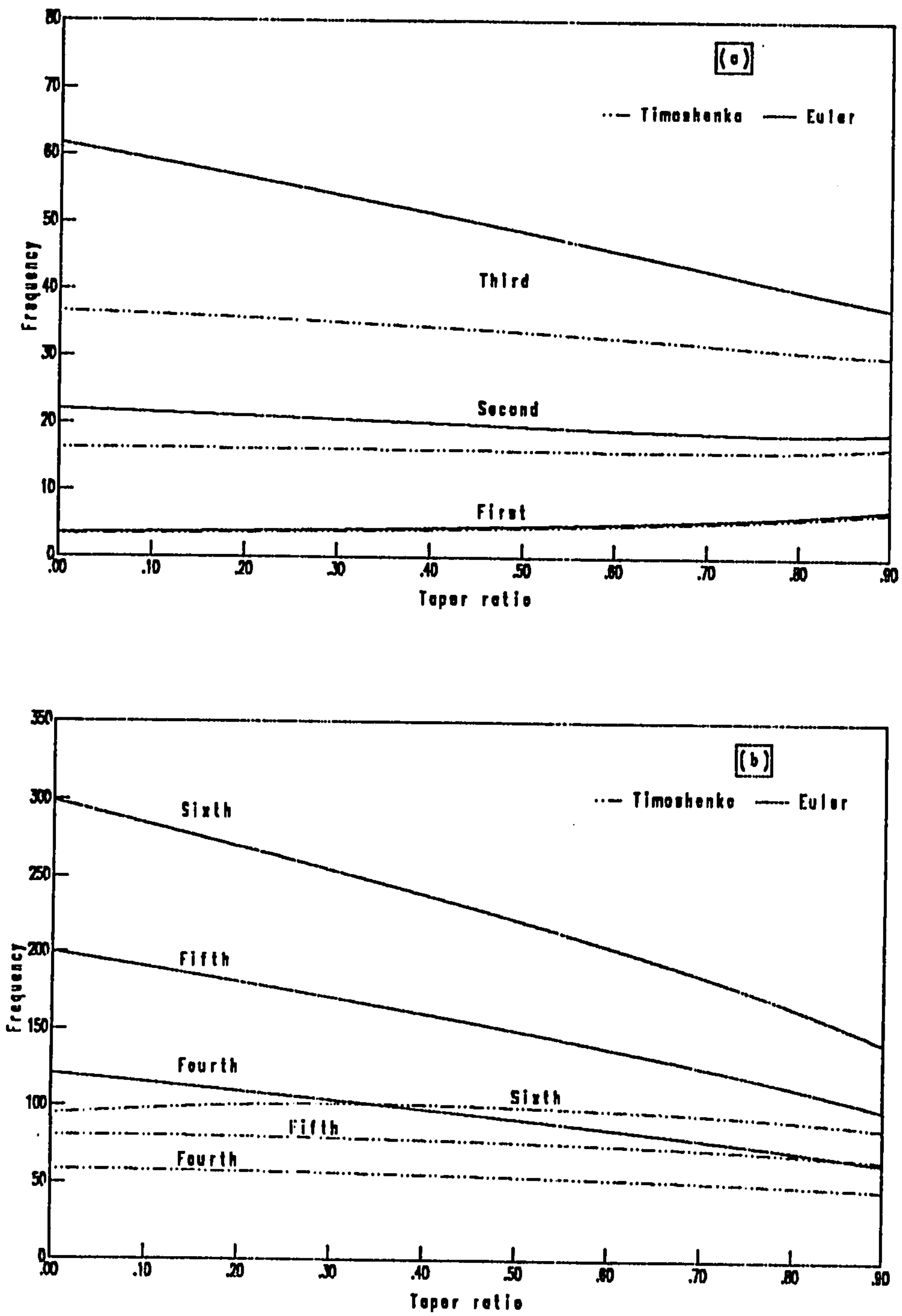

Fig. 4.5 The first six bending frequencies of non-rotating cantilever beam ; (η = 0.0) ; a) First , second and third , b) Fourth , fifth and sixth .

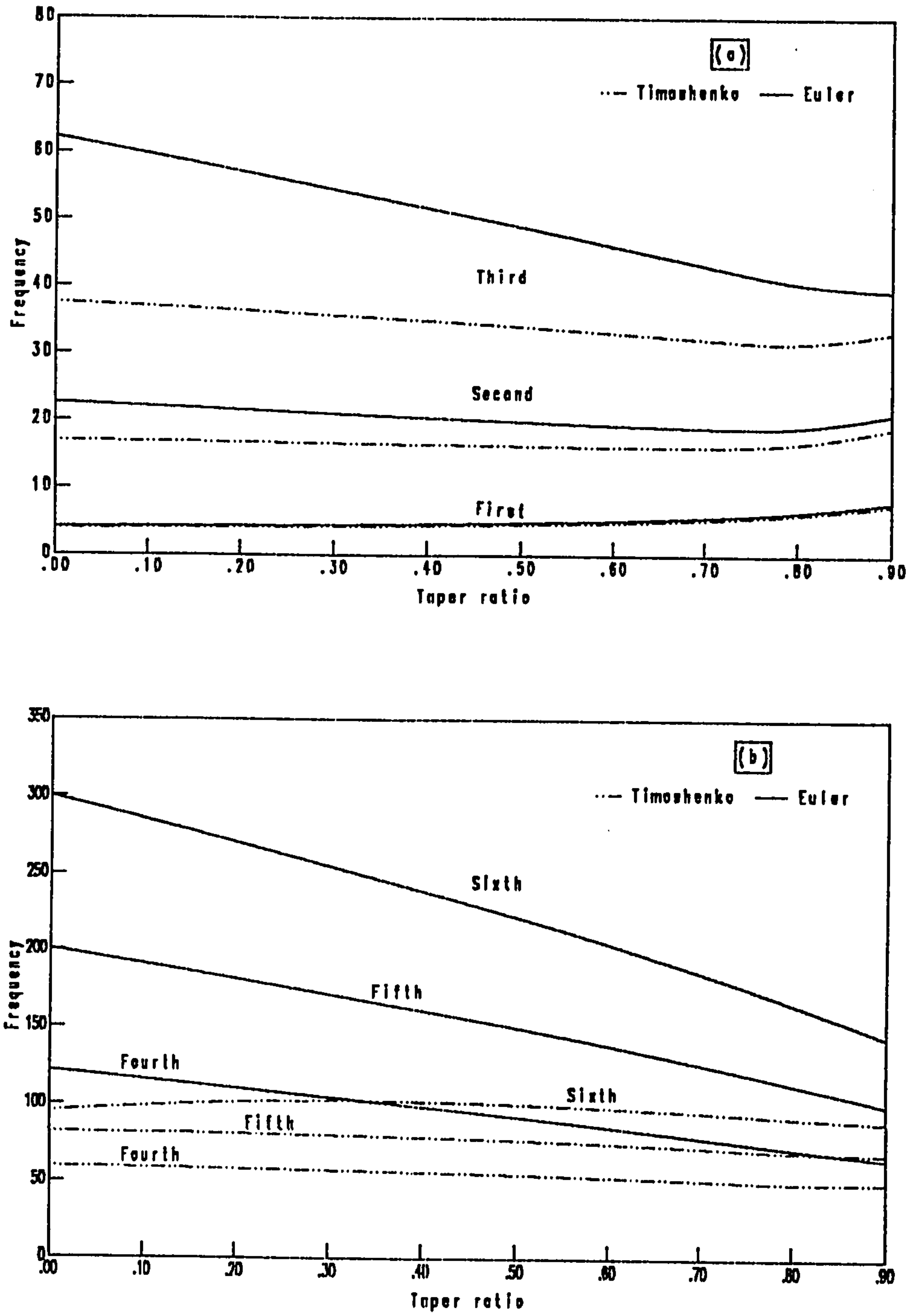

Fig. 4.6 The first six bending frequencies of rotating cantilever beam ; (η = 2.0) ; a) First , second and third , b) Fourth , fifth and sixth .

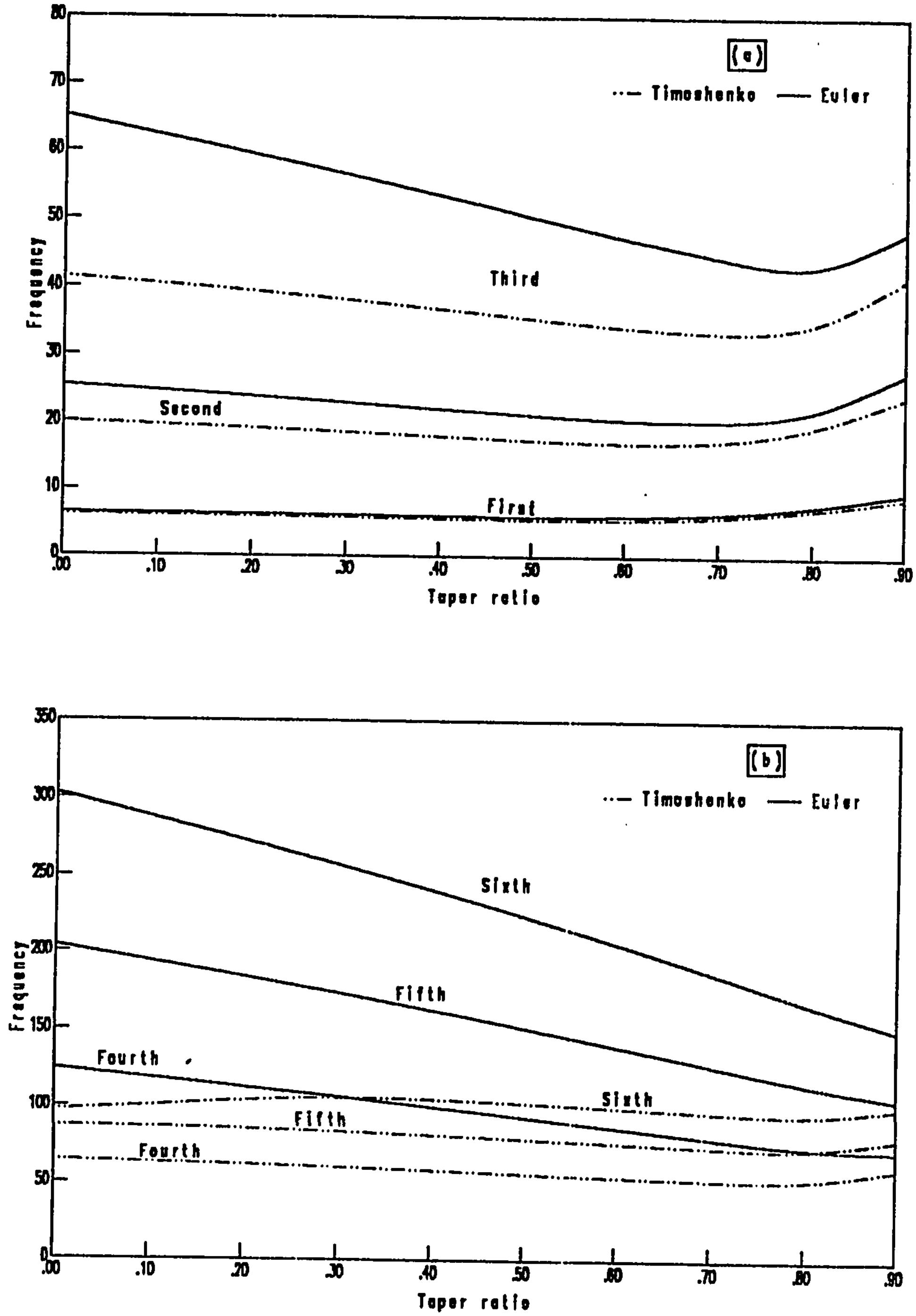

Fig. 4.7 The first six bending frequencies of rotating cantilever beam ; (η = 5.0) ;
a) First , second and third , b) Fourth , fifth and sixth .

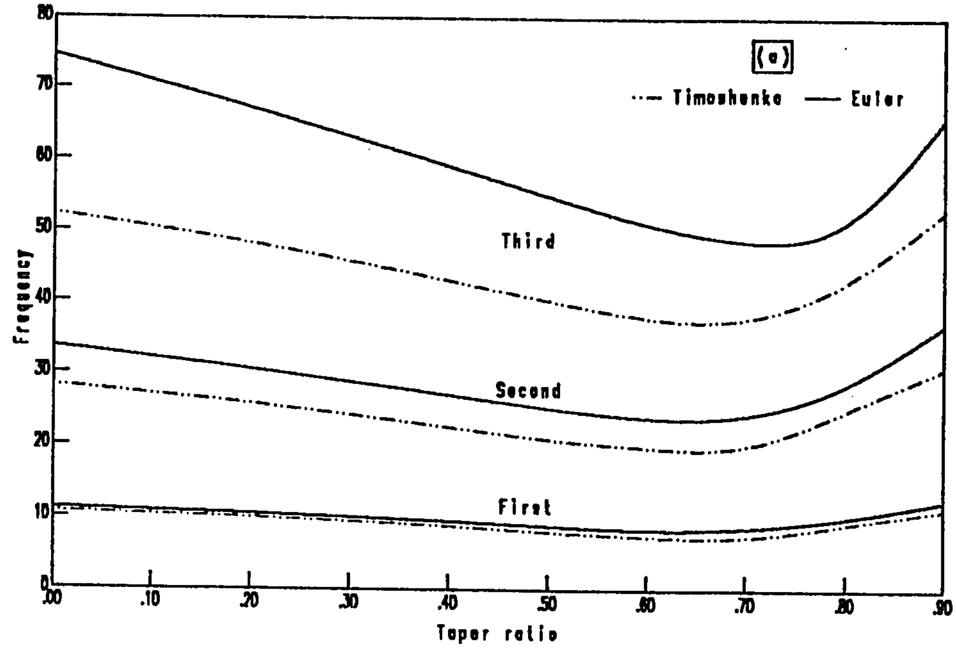

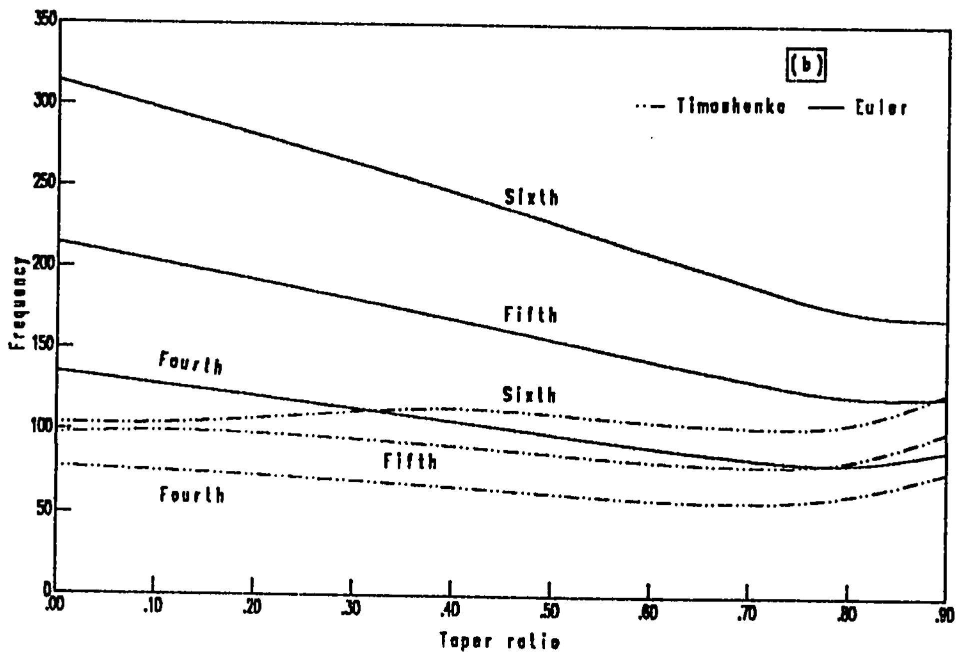

Fig. 4.8 The first six bending frequencies of rotating cantilever beam ; (η = 10.0) ;
a) First , second and third , b) Fourth , fifth and sixth .

TABLE 4.15 *Effect of rotation on the frequency ratios (λ_T / λ_E) of uniform cantilever beam ($\nu_y = \nu_z = 0.0$).*

Speed ratio η	Frequency ratios				
	Mode 1	Mode 2	Mode 3	Mode 4	Mode 5
0	0.94372	0.73794	0.59451	0.48254	0.40270
1	0.94595	0.74058	0.59647	0.48407	0.40384
2	0.95043	0.74803	0.60215	0.48854	0.40715
3	0.95408	0.75904	0.61104	0.49563	0.41237
4	0.95606	0.77206	0.62241	0.50487	0.41911
5	0.95680	0.78565	0.63541	0.51568	0.42681
6	0.95686	0.79874	0.64925	0.52748	0.43482
7	0.95668	0.81069	0.66323	0.53967	0.44238
8	0.95643	0.82121	0.67680	0.55171	0.44864
9	0.95628	0.83021	0.68955	0.56307	0.45287
10	0.95628	0.83775	0.70121	0.57332	0.45497
11	0.95640	0.84397	0.71161	0.58199	0.45552
12	0.95664	0.84902	0.72067	0.58869	0.45534

λ_T : *Timoshenko frequency .*
λ_E : *Euler-Bernoulli frequency .*

TABLE 4.16 Effect of rotation on the frequency ratios (λ_T / λ_E) of a tapered cantilever beam ($\nu_y = \nu_z = 0.2$).

Speed ratio η	Frequency ratios				
	Mode 1	Mode 2	Mode 3	Mode 4	Mode 5
0	0.94525	0.76971	0.62996	0.52098	0.44216
1	0.94600	0.77141	0.63143	0.52219	0.44314
2	0.94768	0.77625	0.63569	0.52576	0.44603
3	0.94927	0.78355	0.64245	0.53148	0.45071
4	0.95331	0.79242	0.65124	0.53908	0.45695
5	0.95078	0.80199	0.66152	0.54818	0.46451
6	0.95087	0.81155	0.67273	0.55843	0.47306
7	0.95076	0.82061	0.68437	0.56939	0.48231
8	0.95058	0.82886	0.69603	0.58076	0.49193
9	0.95042	0.83619	0.70736	0.59217	0.50161
10	0.95031	0.84261	0.71813	0.60337	0.51105
11	0.95028	0.84812	0.72815	0.61411	0.51993
12	0.95033	0.85283	0.73734	0.62418	0.52791

λ_T : *Timoshenko frequency .*
λ_E : *Euler-Bernoulli frequency .*

TABLE 4.17 *Effect of rotation on the frequency ratios (λ_T / λ_E) of a tapered cantilever beam ($\nu_y = \nu_z = 0.5$).*

Speed ratio η	*Frequency ratios*				
	Mode 1	*Mode 2*	*Mode 3*	*Mode 4*	*Mode 5*
0	*0.94685*	*0.81740*	*0.69202*	*0.58958*	*0.51133*
1	*0.94566*	*0.81772*	*0.69260*	*0.59017*	*0.51185*
2	*0.94242*	*0.81838*	*0.69432*	*0.59193*	*0.51342*
3	*0.93784*	*0.81939*	*0.69708*	*0.59479*	*0.51597*
4	*0.93269*	*0.82066*	*0.70076*	*0.59865*	*0.51945*
5	*0.92755*	*0.82204*	*0.70518*	*0.60339*	*0.52376*
6	*0.92273*	*0.82343*	*0.71015*	*0.60886*	*0.52879*
7	*0.91836*	*0.82474*	*0.71550*	*0.61492*	*0.53443*
8	*0.91447*	*0.82590*	*0.72105*	*0.62141*	*0.54055*
9	*0.91104*	*0.82687*	*0.72663*	*0.62818*	*0.54704*
10	*0.90800*	*0.82764*	*0.73214*	*0.63512*	*0.55379*
11	*0.90536*	*0.82821*	*0.73745*	*0.64209*	*0.56070*
12	*0.90303*	*0.82859*	*0.74251*	*0.64901*	*0.56766*

λ_T : *Timoshenko frequency .*
λ_E : *Euler-Bernoulli frequency .*

TABLE 4.18 *Effect of rotation on the frequency ratios (λ_T / λ_E) of a tapered cantilever beam ($\nu_y = \nu_z = 0.7$).*

Speed ratio η	Frequency ratios				
	Mode 1	Mode 2	Mode 3	Mode 4	Mode 5
0	0.94673	0.84970	0.74227	0.64848	0.57281
1	0.94578	0.84993	0.74272	0.64892	0.57319
2	0.94307	0.85060	0.74404	0.65022	0.57433
3	0.93903	0.85159	0.74617	0.65234	0.57619
4	0.93412	0.85280	0.74904	0.65523	0.57875
5	0.92882	0.85406	0.75253	0.65883	0.58196
6	0.92348	0.85528	0.75649	0.66305	0.58576
7	0.91836	0.85635	0.76081	0.66780	0.59008
8	0.91401	0.85724	0.76535	0.67298	0.59487
9	0.90888	0.85792	0.76997	0.67850	0.60004
10	0.90468	0.85842	0.77458	0.68426	0.60553
11	0.90079	0.85875	0.77908	0.69017	0.61127
12	0.89721	0.85896	0.78341	0.69615	0.61719

λ_T : *Timoshenko frequency .*
λ_E : *Euler-Bernoulli frequency .*

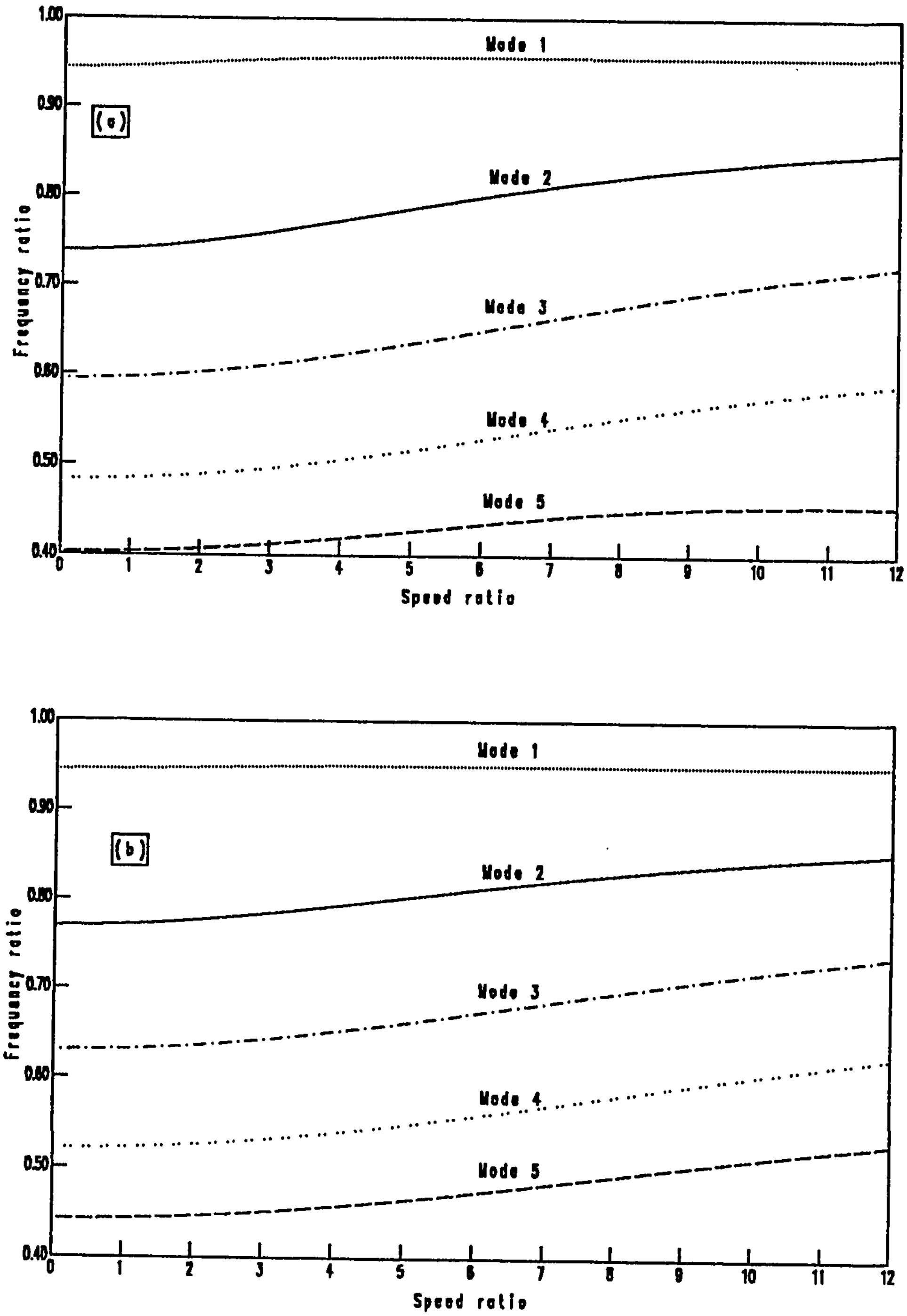

Fig. 4.9 Effect of rotation on the frequency ratios of a cantilever beam ; a) Uniform beam ($\nu_y = \nu_z = 0.0$) ; b) Tapered beam ($\nu_y = \nu_z = 0.2$) .

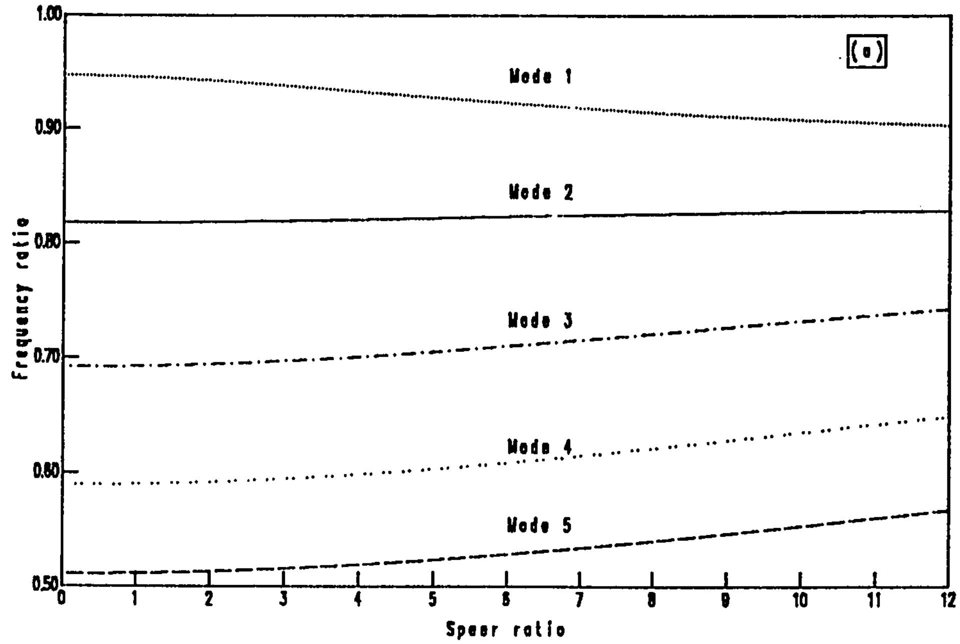

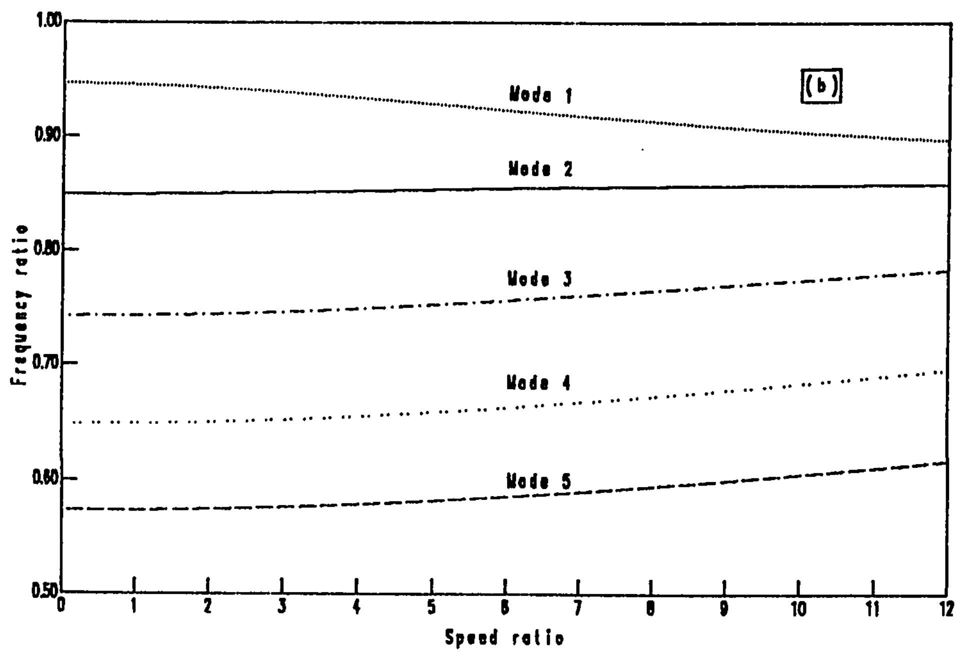

Fig. 4.10 Effect of rotation on the frequency ratios of a tapered cantilever beam ; a) ($\nu_y = \nu_z = 0.5$) ; b) ($\nu_y = \nu_z = 0.7$).

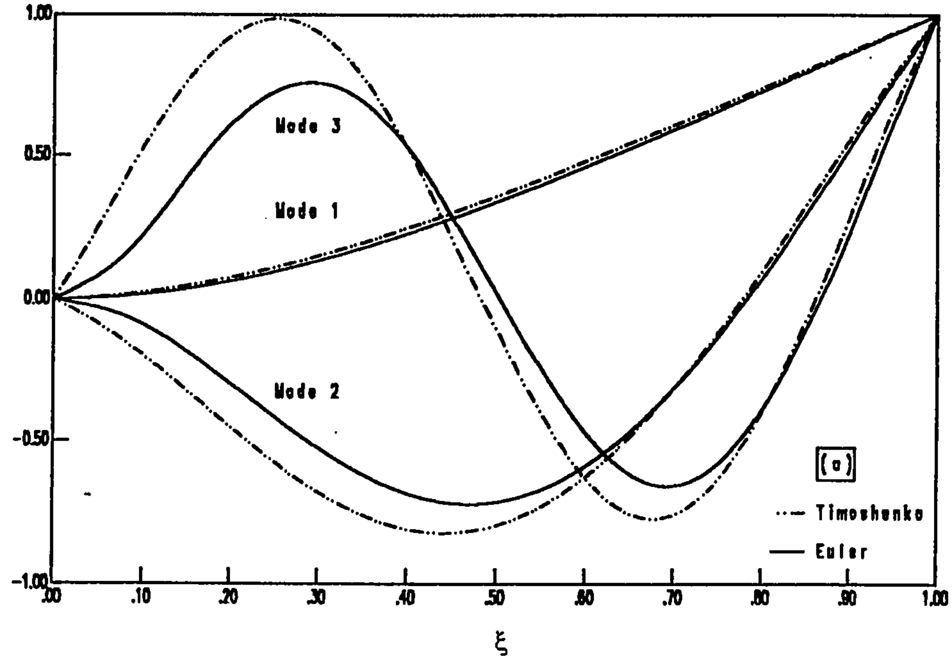

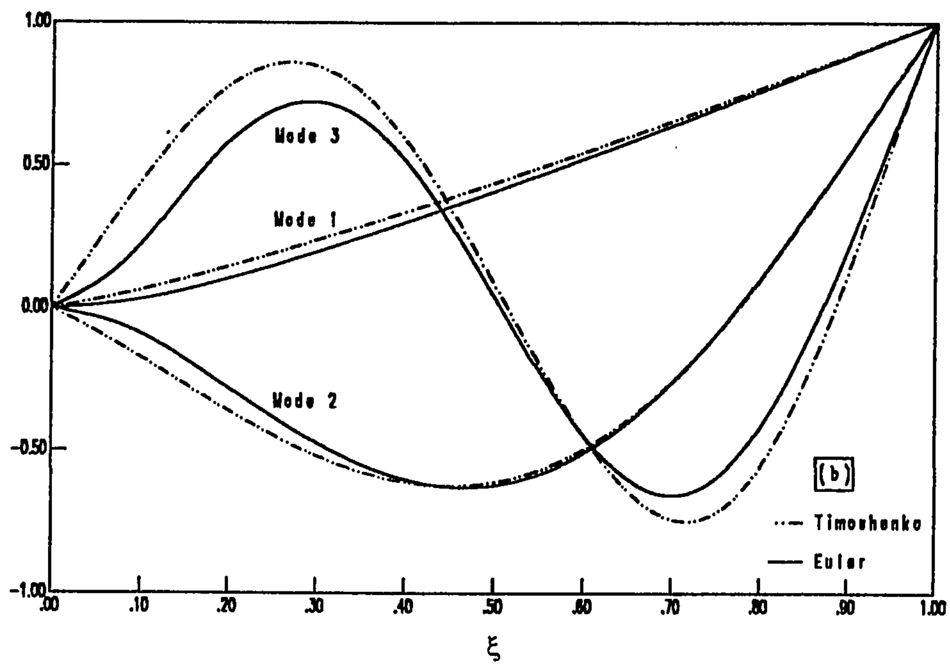

Fig 4.11 The first three flexural mode shapes of uniform cantilever beam ; ($\nu_y = \nu_z = 0.0$) ; a) $\eta = 0.$, b) $\eta = 10.0$.

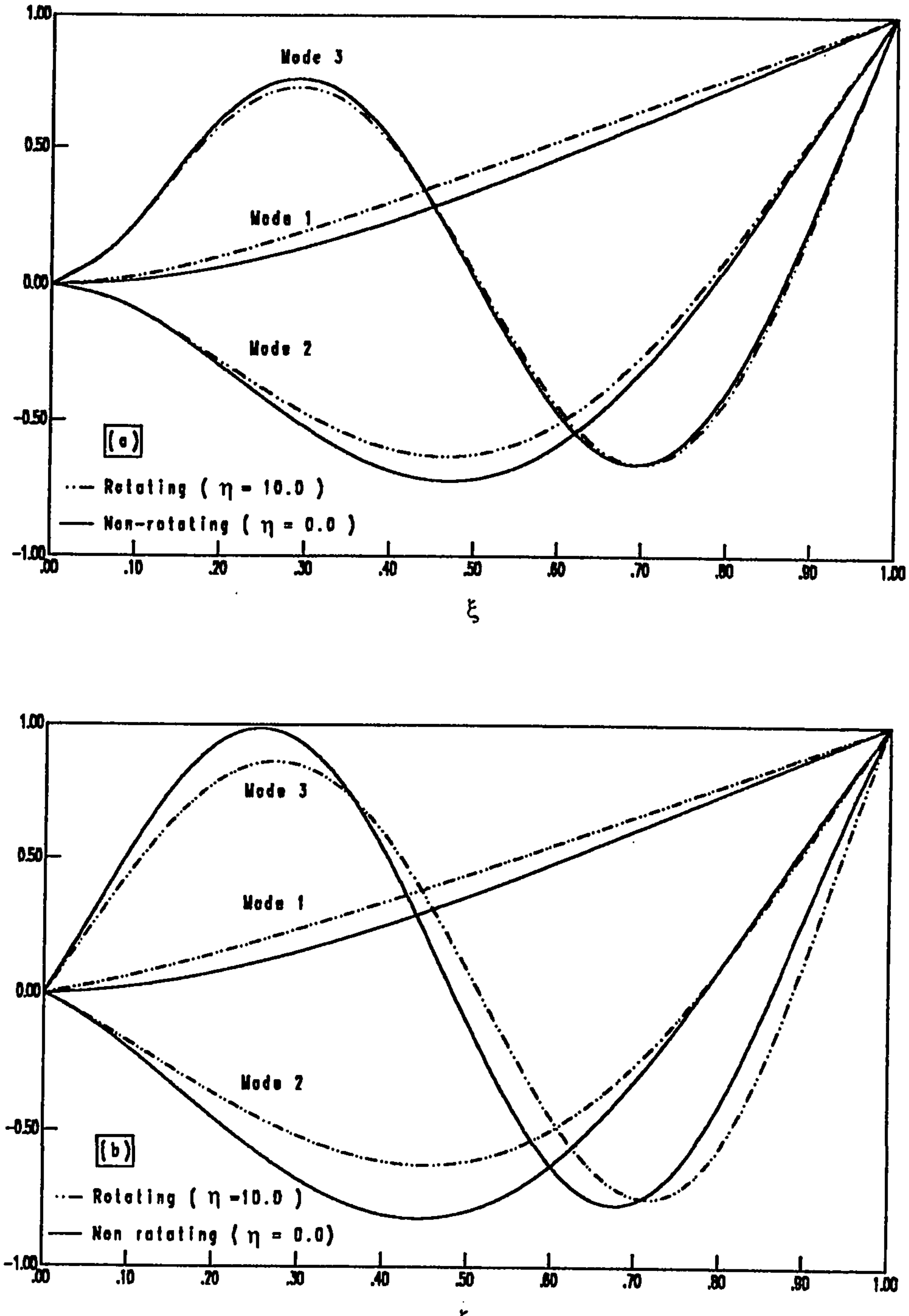

Fig. 4.12 The first three flexural mode shapes of uniform cantilever beam ; ($\nu_y = \nu_z = 0.0$) ; a) Euler beam , b) Timoshenko beam .

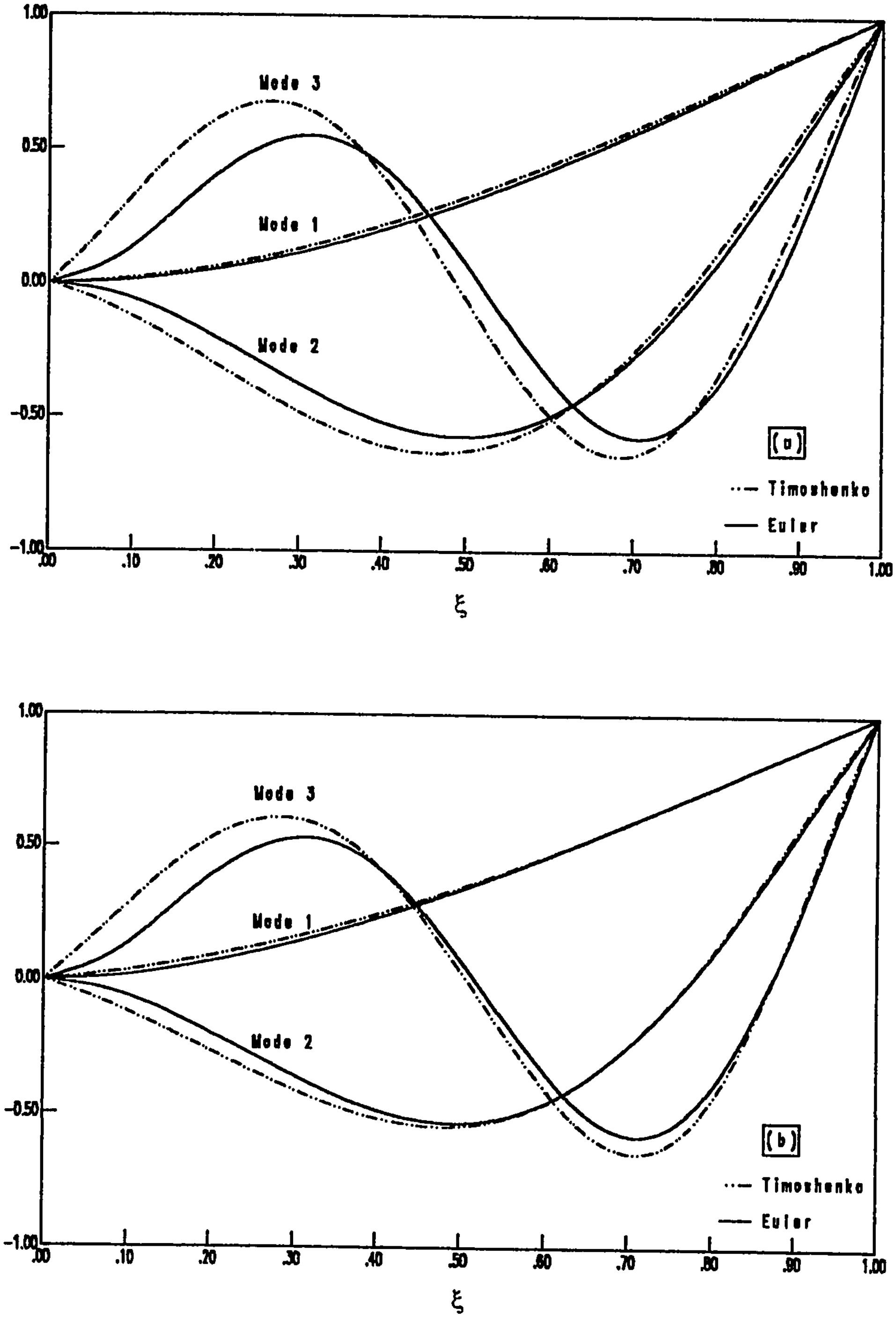

Fig 4.13 The first three flexural mode shapes of a tapered cantilever beam ; ($\nu_y = \nu_z = 0.3$) ; a) $\eta = 0.$, b) $\eta = 10.0$.

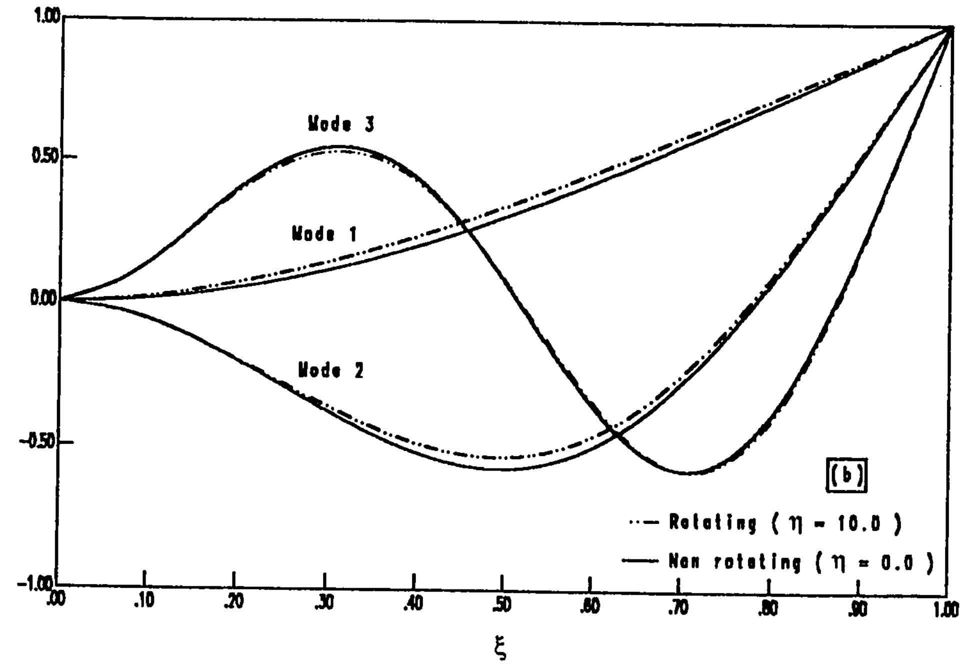

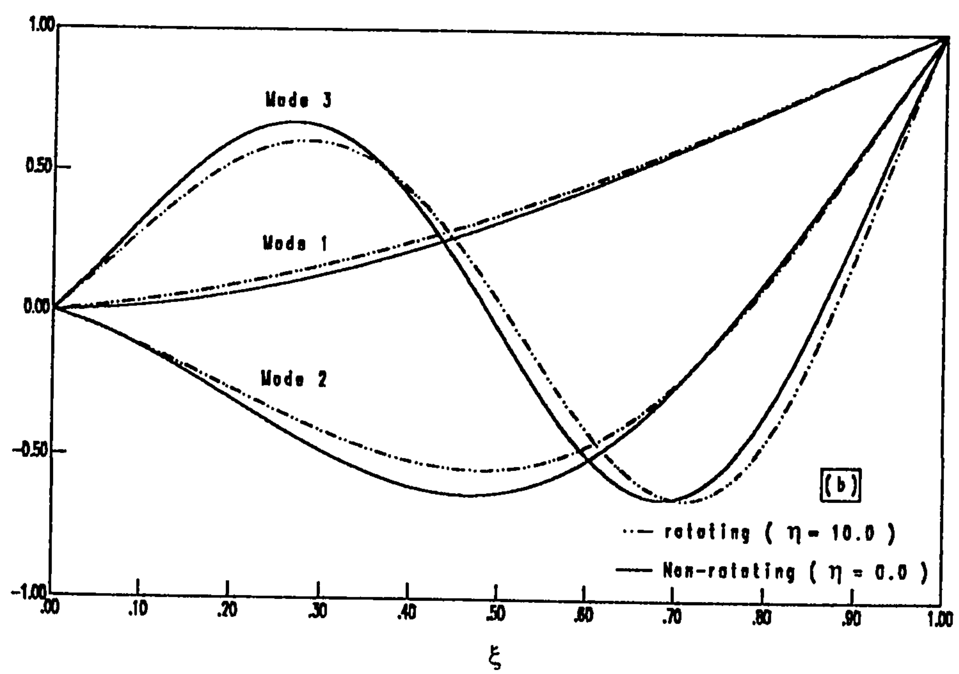

Fig. 4.14 The first three flexural mode shapes of a tapered cantilever beam . ($\nu_y = \nu_z = 0.3$) ; a) Euler beam , b) Timoshenko beam .

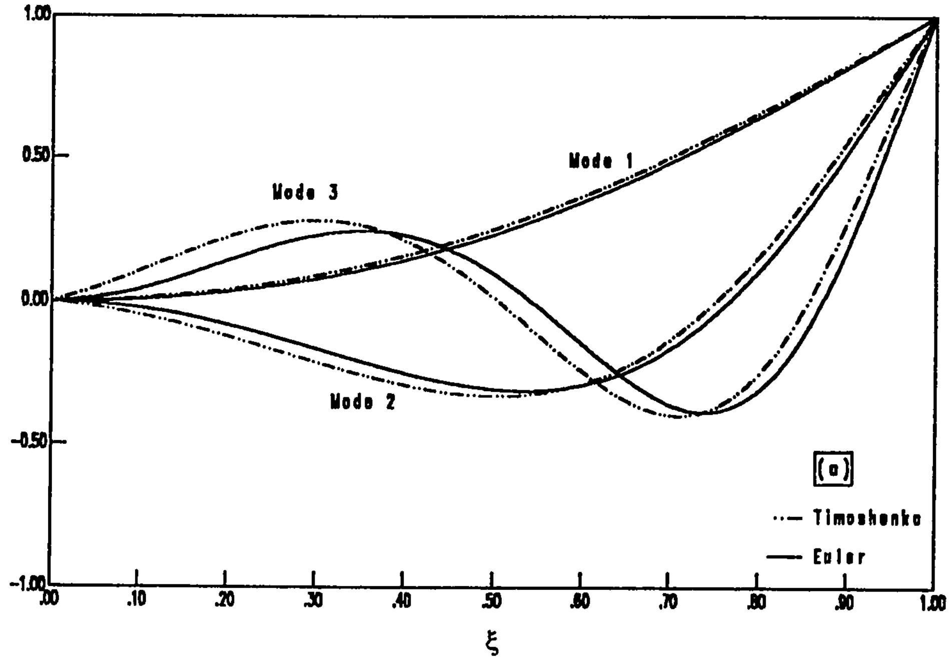

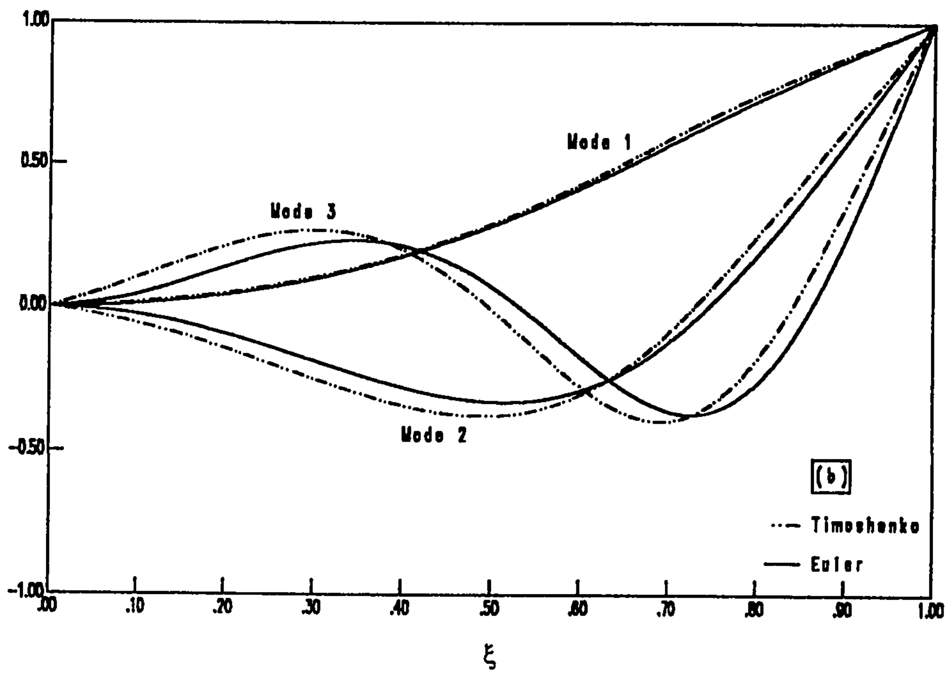

Fig 4.15 The first three flexural mode shapes of a tapered cantilever beam . ($\nu_y = \nu_z = 0.7$) ; a) $\eta = 0$, b) $\eta = 10.0$.

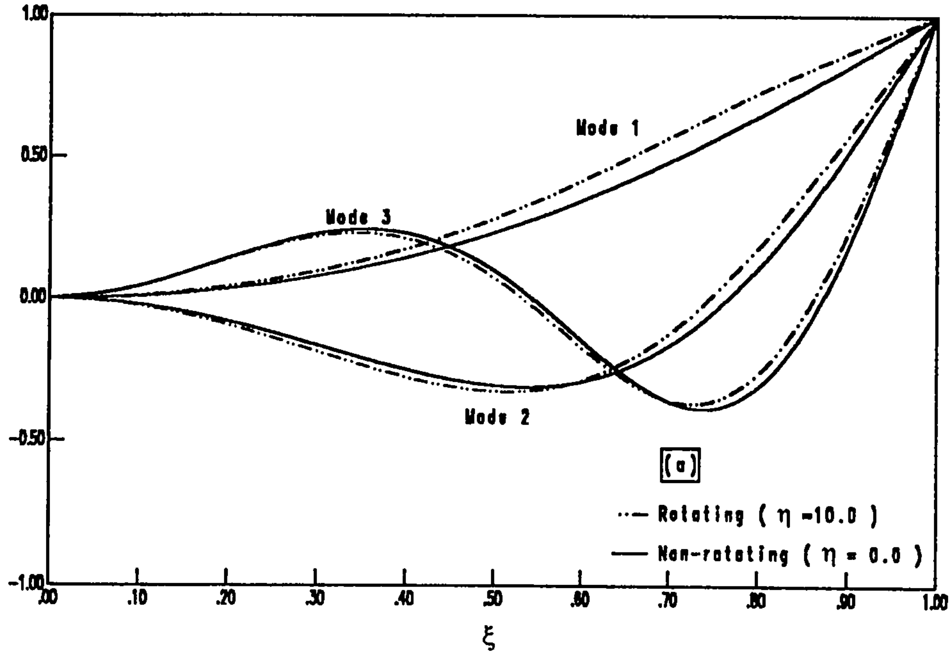

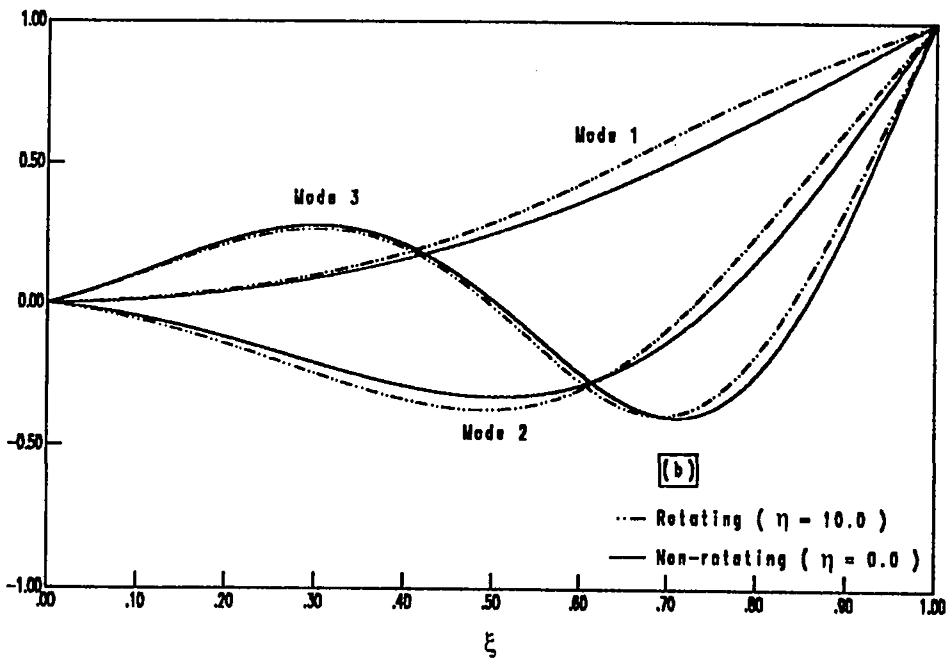

Fig. 4.16 The first three flexural mode shapes of a tapered cantilever beam ($\nu_y = \nu_z = 0.7$) ; a) Euler beam , b) Timoshenko beam .

TABLE 4.19 Frequency parameter λ of uniform Euler-Bernoulli hinged-free beam , ($\nu_y = \nu_z = 0.0$) .
(Rigid body mode not included)

Speed ratio η	Frequency									
	λ_1	λ_2	λ_3	λ_4	λ_5	λ_6	λ_7	λ_8	λ_9	λ_{10}
0	*15.4183*	*49.9689*	*104.284*	*178.448*	*272.649*	*387.237*	*522.780*	*680.077*	*860.071*	*1063.22*
	15.4182**	49.9649**	104.248**	178.270**	–	–	–	–	–	–
1	*15.6244*	*50.1477*	*104.457*	*178.618*	*272.817*	*387.405*	*522.946*	*680.242*	*860.235*	*1063.38*
	15.6242**	50.1437**	104.420**	178.440**	–	–	–	–	–	–
3	*17.1808*	*51.5537*	*105.825*	*179.971*	*274.161*	*388.742*	*524.276*	*681.563*	*861.544*	*1064.67*
	17.1807**	51.5498**	105.789**	179.794**	–	–	–	–	–	–
5	*19.9198*	*54.2457*	*108.504*	*182.643*	*276.827*	*391.400*	*526.924*	*684.196*	*864.155*	*1067.25*
	19.9197**	54.2419**	108.469**	182.469**	–	–	–	–	–	–
7	*23.4134*	*58.0258*	*112.389*	*186.572*	*280.774*	*395.351*	*530.869*	*688.125*	*868.056*	*1071.10*
	23.4133**	58.0223**	112.356**	186.401**	–	–	–	–	–	–
10	*29.4440*	*65.2587*	*120.178*	*194.625*	*288.906*	*403.604*	*539.145*	*696.393*	*876.281*	*1079.23*
	29.4439**	65.2554**	120.146**	194.462**	288.406**	–	–	–	–	–

** *Reference [27]*

TABLE 4.20 Frequency parameter λ of a tapered Euler-Bernoulli hinged-free beam, ($\nu_y = \nu_z = 0.1$).
(Rigid body mode not included)

Speed ratio η	Frequency									
	λ_1	λ_2	λ_3	λ_4	λ_5	λ_6	λ_7	λ_8	λ_9	λ_{10}
0	14.9624	47.7577	99.3259	169.734	259.161	367.935	496.584	645.841	816.521	1008.72
1	15.1488	47.9194	99.4814	169.887	259.312	368.085	496.733	645.989	816.668	1008.86
3	16.5624	49.1927	100.716	171.104	260.520	369.286	497.927	647.174	817.841	1010.02
5	19.0679	51.6368	103.135	173.511	262.917	371.674	500.304	649.537	820.183	1012.32
7	22.2836	55.0814	106.651	177.054	266.469	375.225	503.847	653.063	823.681	1015.77
10	27.8701	61.7055	113.722	184.331	273.847	382.651	511.286	660.489	831.062	1023.06

TABLE 4.21 Frequency parameter λ of a tapered Euler-Bernoulli hinged-free beam, ($\nu_y = \nu_z = 0.3$) .
(Rigid body mode not included)

Speed ratio η	Frequency									
	λ_1	λ_2	λ_3	λ_4	λ_5	λ_6	λ_7	λ_8	λ_9	λ_{10}
0	14.0489	43.2560	89.1046	151.670	231.122	327.747	441.994	574.448	725.618	895.158
1	14.1907	43.3802	89.2233	151.787	231.236	327.861	442.107	574.560	725.729	895.267
3	15.2769	44.3603	90.1671	152.713	232.152	328.769	443.007	575.452	726.610	896.137
5	17.2389	46.2540	92.0233	154.548	233.972	330.576	444.802	577.232	728.370	897.873
7	19.8076	48.9478	94.7337	157.256	236.673	333.267	447.480	579.892	731.000	900.472
10	24.3486	54.1956	100.229	162.848	242.304	338.908	453.113	585.499	736.555	905.969

TABLE 4.22 Frequency parameter λ of uniform Euler-Bernoulli hinged-free beam , ($\nu_y = \nu_z = 0.5$) .
(Rigid body mode not included)

Speed ratio η	Frequency									
	λ_1	λ_2	λ_3	λ_4	λ_5	λ_6	λ_7	λ_8	λ_9	λ_{10}
0	13.1895	38.6370	78.3437	132.451	201.127	284.625	383.304	497.592	627.955	777.221
1	13.2836	38.7220	78.4247	132.529	201.204	284.701	383.379	497.665	628.027	777.293
3	14.0146	39.3949	79.0687	133.156	201.820	285.307	383.978	498.255	628.605	777.867
5	15.3735	40.7056	80.3403	134.401	203.044	286.516	385.172	499.433	629.758	779.104
7	17.2087	42.5915	82.2081	136.245	204.866	288.319	386.956	501.194	631.483	780.731
10	20.5493	46.3270	86.0317	140.075	208.681	292.110	390.718	504.913	635.130	784.366

TABLE 4.23 Frequency parameter λ of a tapered Euler-Bernoulli hinged-free beam, ($\nu_y = \nu_z = 0.7$) .
(Rigid body mode not included)

Speed ratio η	Frequency									
	λ_1	λ_2	λ_3	λ_4	λ_5	λ_6	λ_7	λ_8	λ_9	λ_{10}
0	12.5939	33.9351	66.7850	111.390	167.936	236.651	317.878	412.374	522.817	656.588
1	12.6774	34.0111	66.8521	111.453	167.996	236.710	317.937	412.431	522.871	656.638
3	13.3260	34.6128	67.3836	111.950	168.476	237.182	318.407	412.892	523.298	657.040
5	14.5337	35.7842	68.4426	112.939	169.430	238.122	319.344	413.813	524.151	657.843
7	16.1683	37.4678	69.9974	114.406	170.851	239.525	320.744	415.189	525.429	659.045
10	19.1503	40.7949	73.1917	117.463	173.832	242.478	323.697	418.101	528.134	661.593

TABLE 4.24 Frequency parameter λ of a tapered Euler-Bernoulli hinged-free beam , ($\nu_y = \nu_z = 0.9$) .
(Rigid body mode not included)

Speed ratio η	Frequency									
	λ_1	λ_2	λ_3	λ_4	λ_5	λ_6	λ_7	λ_8	λ_9	λ_{10}
0	13.2460	29.8827	54.2733	86.9888	128.399	179.071	240.048	312.361	392.438	475.229
1	13.7882	30.4832	54.6892	87.3108	128.731	179.457	240.455	312.737	392.820	475.577
3	16.8464	34.8107	57.8989	89.8024	131.338	182.487	243.676	315.725	395.834	478.360
5	20.2645	41.3236	63.7047	94.3726	136.268	188.258	249.939	321.623	401.680	483.920
7	23.4484	47.9730	71.0377	100.362	143.025	196.247	258.846	330.266	410.026	492.202
10	27.9976	57.0492	82.8004	110.643	155.341	211.035	275.811	347.744	426.354	509.290

TABLE 4.25 Frequency parameter λ of uniform Timoshenko hinged-free beam, ($\nu_y = \nu_z = 0.0$) .
(Rigid body mode not included)

Speed ratio	Frequency									
η	λ_1	λ_2	λ_3	λ_4	λ_5	λ_6	λ_7	λ_8	λ_9	λ_{10}
0	13.1068	33.9697	57.0638	79.7005	91.7336	100.135	111.941	124.842	138.254	153.680
1	13.3225	34.1957	57.3239	79.9850	91.7771	100.340	112.163	125.045	138.595	153.901
3	14.9253	35.9333	59.3827	82.1460	92.1093	101.870	113.923	126.609	141.293	155.505
5	17.6589	39.0948	63.1587	85.8286	92.8337	104.439	117.251	129.585	146.265	158.371
7	21.0383	43.2470	68.1547	89.4225	94.6935	107.603	121.433	134.191	151.941	163.295
10	26.6942	50.5225	76.7964	91.6442	100.519	113.670	127.592	144.346	158.553	176.428

TABLE 4.26 Frequency parameter λ of a tapered Timoshenko hinged-free beam , ($\nu_y = \nu_z = 0.1$) .
(Rigid body mode not included)

Speed ratio η	Frequency									
	λ_1	λ_2	λ_3	λ_4	λ_5	λ_6	λ_7	λ_8	λ_9	λ_{10}
0	12.9024	33.3396	56.3835	79.6057	94.1266	101.363	113.589	126.284	139.032	154.755
1	13.0947	33.5393	56.6180	79.8172	94.1469	101.592	113.740	126.492	139.289	154.994
3	14.5328	35.0828	58.4409	81.9256	94.2898	103.315	114.953	128.062	141.354	156.738
5	17.0151	37.9211	61.8361	85.6704	94.5541	106.165	117.448	130.815	145.443	159.578
7	20.1188	41.7000	66.4173	90.2779	95.2013	109.238	121.253	134.452	151.004	163.340
10	23.5672	46.0946	71.7851	93.2882	98.0190	112.168	125.784	139.188	156.536	169.030

TABLE 4.27 Frequency parameter λ of a tapered Timoshenko hinged-free beam , ($\nu_y = \nu_z = 0.3$) .
(Rigid body mode not included)

Speed ratio η	Frequency									
	λ_1	λ_2	λ_3	λ_4	λ_5	λ_6	λ_7	λ_8	λ_9	λ_{10}
0	12.4349	31.8644	54.5181	78.1426	98.4941	101.787	121.459	128.141	144.084	156.045
1	12.5736	32.0073	54.6843	78.3375	98.4964	102.006	121.563	128.297	144.203	156.239
3	13.6273	33.1213	55.9872	79.8671	98.5132	103.720	122.271	129.610	145.336	157.779
5	15.4991	35.2124	58.4631	82.7784	98.5442	106.950	123.253	132.385	147.315	160.754
7	17.9038	38.0707	61.9016	86.8203	98.5975	111.309	124.294	136.332	150.032	164.731
10	22.0715	43.3472	68.3675	94.2578	98.8619	118.394	126.771	142.646	155.963	171.096

TABLE 4.28 Frequency parameter λ of a tapered Timoshenko hinged-free beam, ($\nu_y = \nu_z = 0.5$) .
(Rigid body mode not included)

Speed ratio η	Frequency									
	λ_1	λ_2	λ_3	λ_4	λ_5	λ_6	λ_7	λ_8	λ_9	λ_{10}
0	11.9430	30.0683	51.8880	75.2421	99.2025	102.012	123.718	137.640	148.239	164.835
1	12.0250	30.1536	51.9862	75.3574	99.3303	102.020	123.872	137.646	148.405	164.877
3	12.6597	30.8245	52.7605	76.2674	100.305	102.120	125.086	137.693	149.712	165.192
5	13.8317	32.1081	54.2546	78.0272	101.549	102.958	127.431	137.779	152.219	165.733
7	15.3984	33.9078	56.3750	80.5319	101.836	105.639	130.751	137.908	155.692	166.473
10	18.2098	37.3396	60.4889	85.4070	101.975	111.301	136.743	138.607	161.592	168.546

TABLE 4.29 Frequency parameter λ of a tapered Timoshenko hinged-free beam , ($\nu_y = \nu_z = 0.7$) .
(Rigid body mode not included)

Speed ratio η	Frequency									
	λ_1	λ_2	λ_3	λ_4	λ_5	λ_6	λ_7	λ_8	λ_9	λ_{10}
0	11.6294	27.9492	48.2562	70.6368	94.1234	104.851	118.595	143.405	151.661	168.831
1	11.7041	28.0250	48.3319	70.7175	94.2119	104.854	118.695	143.517	151.668	168.965
3	12.2838	28.6220	48.9313	71.3588	94.9140	104.877	119.491	144.408	151.684	169.952
5	13.3597	29.7714	50.1028	72.6162	96.2867	104.927	121.055	146.151	151.728	171.906
7	14.8080	31.3965	51.7964	74.4436	98.2659	105.020	123.332	148.663	151.822	174.746
10	17.4280	34.5288	55.1742	78.1203	102.044	105.428	127.930	151.684	154.067	180.447

TABLE 4.30 Frequency parameter λ of a tapered Timoshenko hinged-free beam , ($\nu_y = \nu_z = 0.9$) .
(Rigid body mode not included)

Speed ratio η	Frequency									
	λ_1	λ_2	λ_3	λ_4	λ_5	λ_6	λ_7	λ_8	λ_9	λ_{10}
0	12.4176	26.1615	43.5329	63.4283	84.9849	106.337	109.001	131.634	156.122	165.021
1	13.0666	27.0793	44.3854	64.1795	85.6652	106.585	109.406	132.262	156.751	165.025
3	16.0395	32.2951	50.1985	69.6895	90.7253	107.273	113.585	136.940	161.431	165.066
5	18.9260	37.8594	57.8673	78.3151	99.1680	107.615	121.568	144.870	165.028	169.527
7	21.6019	42.7605	64.9495	87.2790	106.833	110.072	131.370	154.440	165.109	179.263
10	25.4863	49.4114	74.3839	99.4150	107.786	124.338	147.091	165.153	169.883	195.092

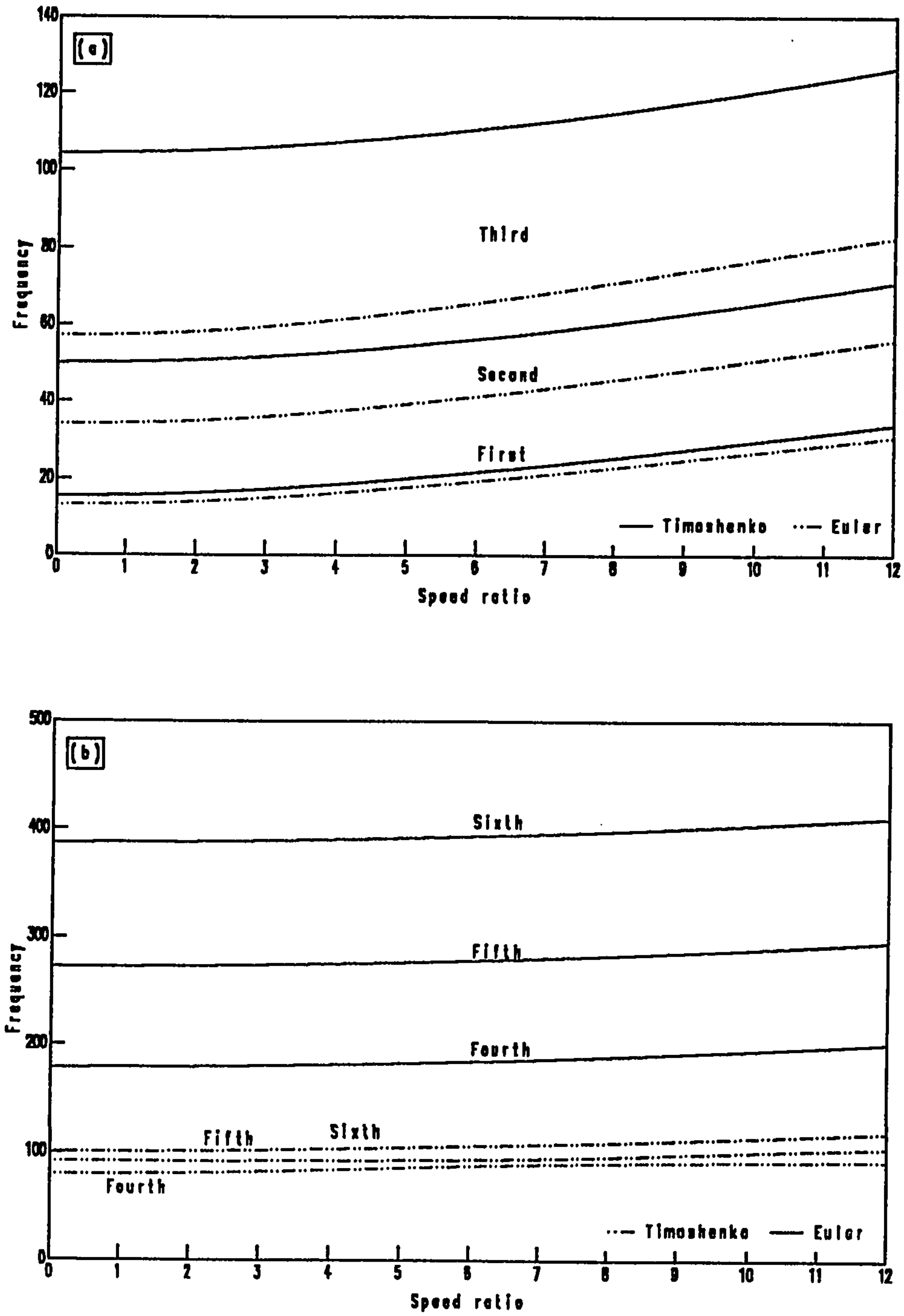

Fig. 4.17 The first six bending frequencies of uniform hinged-free beam ; ($\nu_y = \nu_z = 0.0$) ; a) First , second and third , b) Fourth , fifth and sixth .

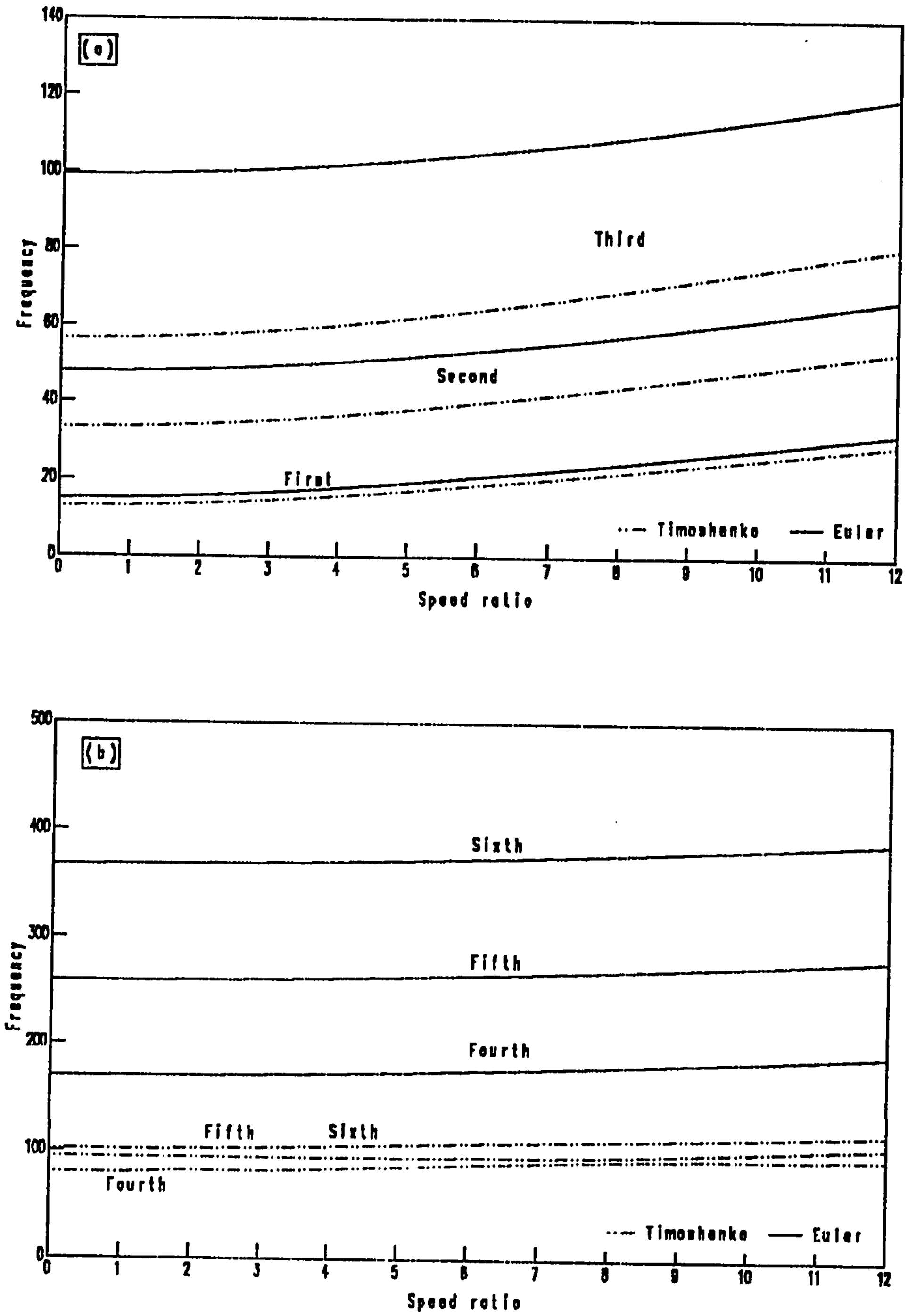

Fig. 4.18 The first six bending frequencies of a tapered hinged-free beam ; ($\nu_y = \nu_z = 0.1$) ; a) First , second and third , b) Fourth , fifth and sixth .

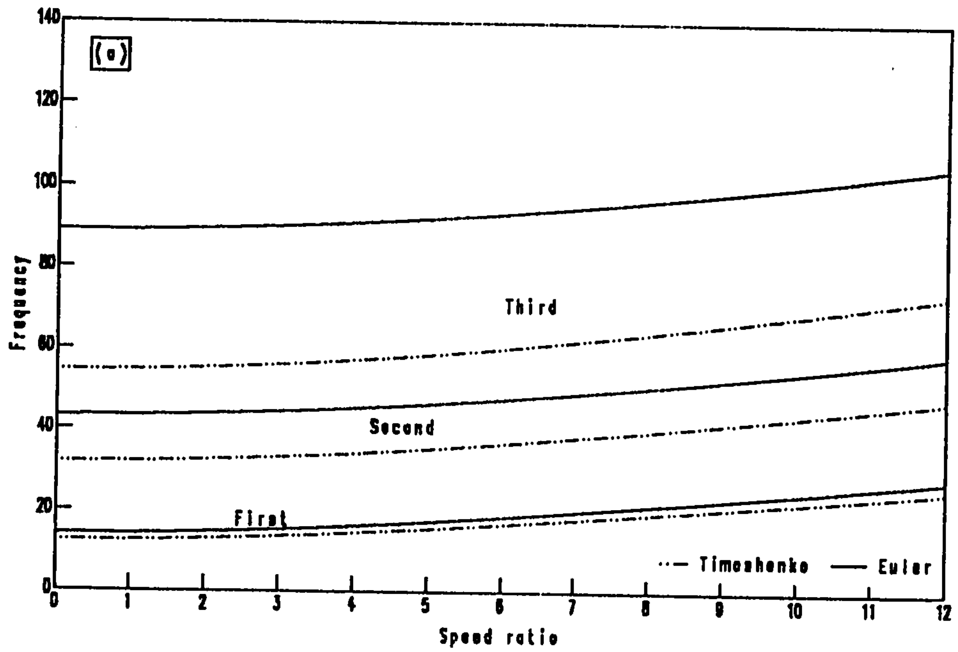

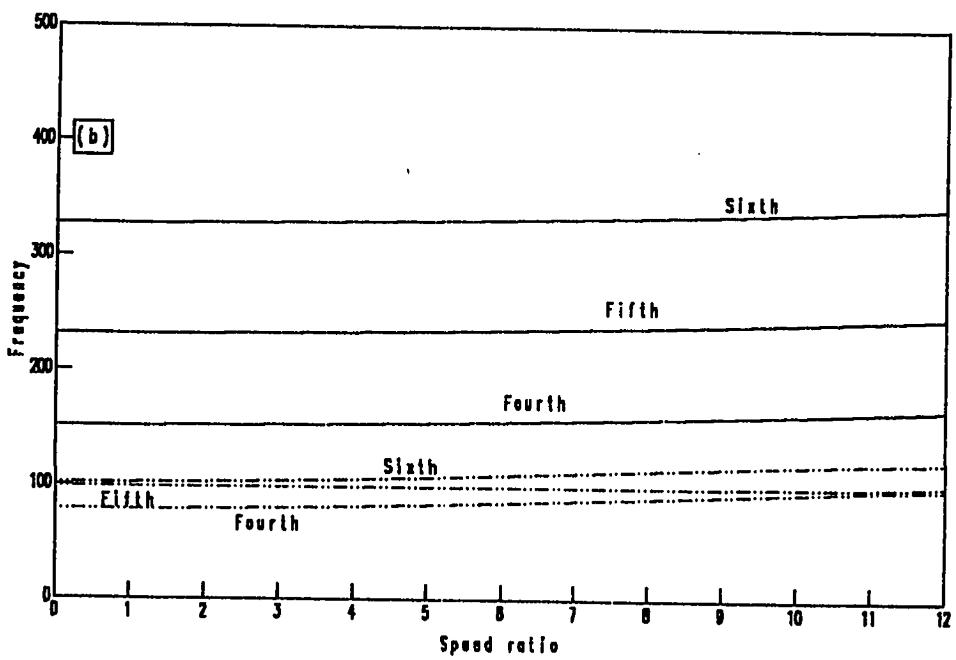

Fig. 4.19 The first six bending frequencies of a tapered hinged-free beam ; ($\nu_y = \nu_z = 0.3$) ; a) First , second and third , b) Fourth , fifth and sixth .

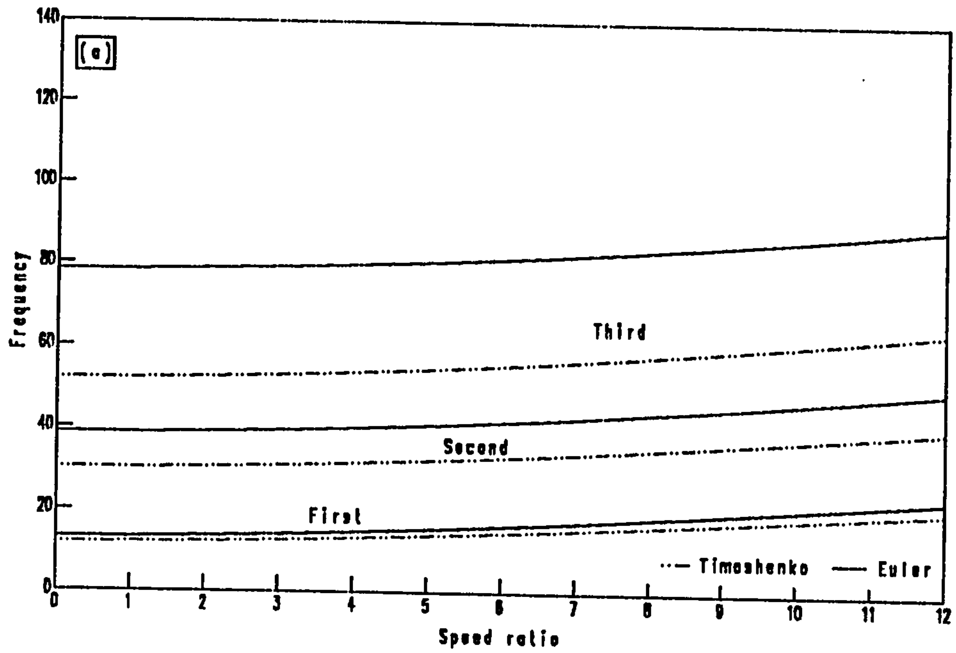

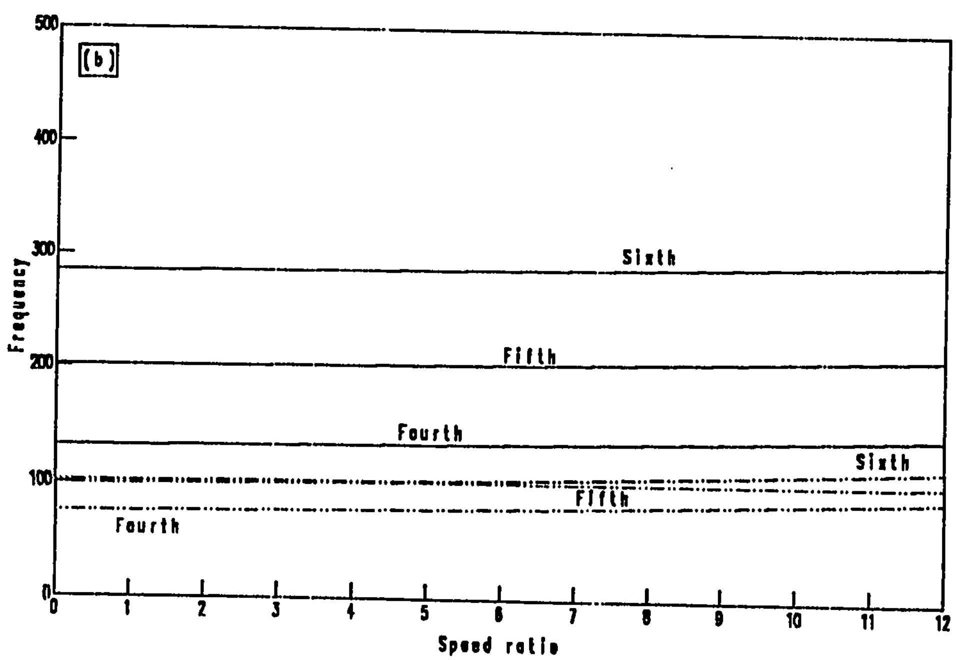

Fig. 4.20 The first six bending frequencies of a tapered hinged-free beam ; ($\nu_y = \nu_z = 0.5$) : a) First , second and third , b) Fourth , fifth and sixth .

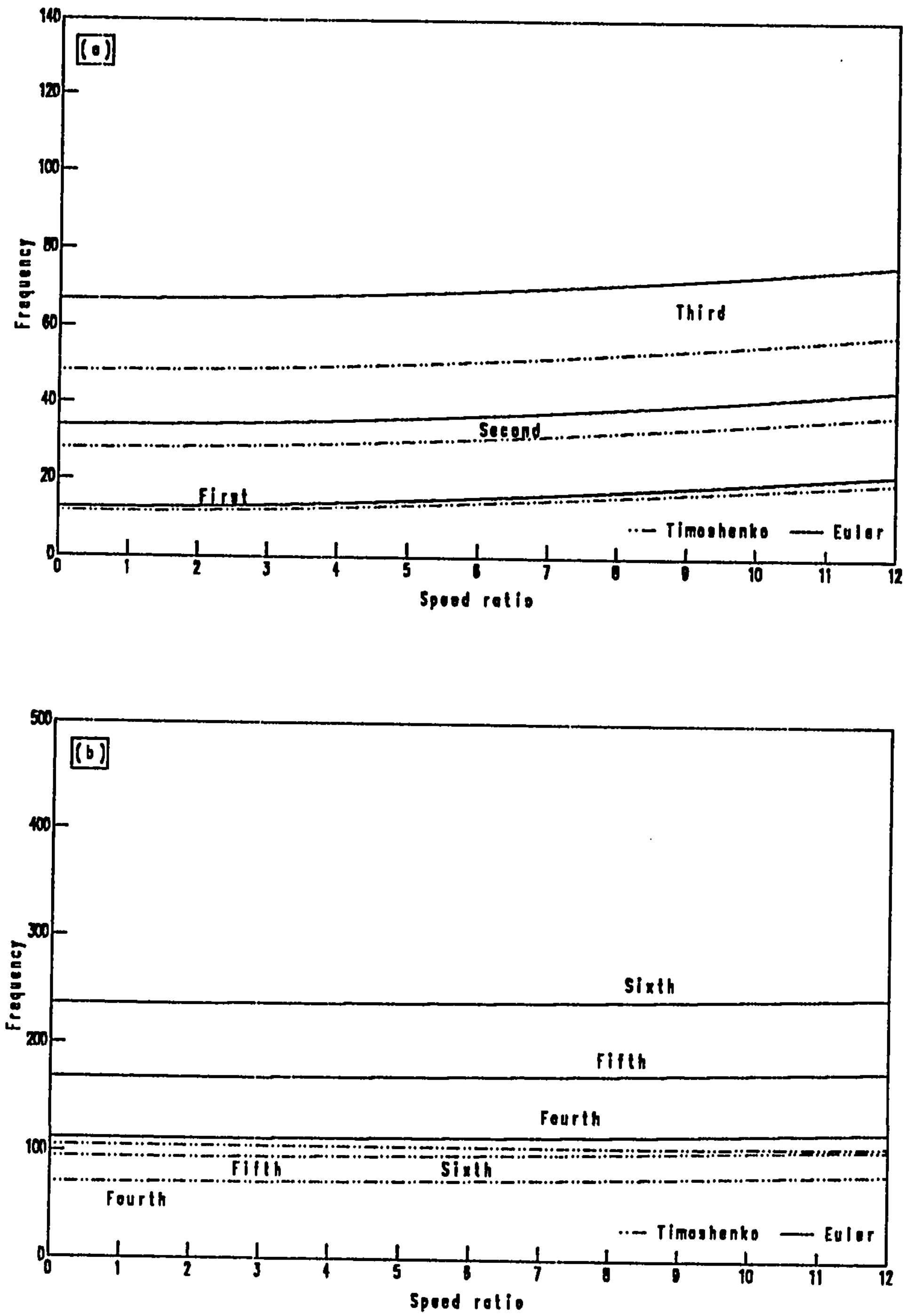

Fig. 4.21 The first six bending frequencies of a tapered hinged-free beam ; ($\nu_y = \nu_z = 0.7$) : a) First , second and third , b) Fourth , fifth and sixth .

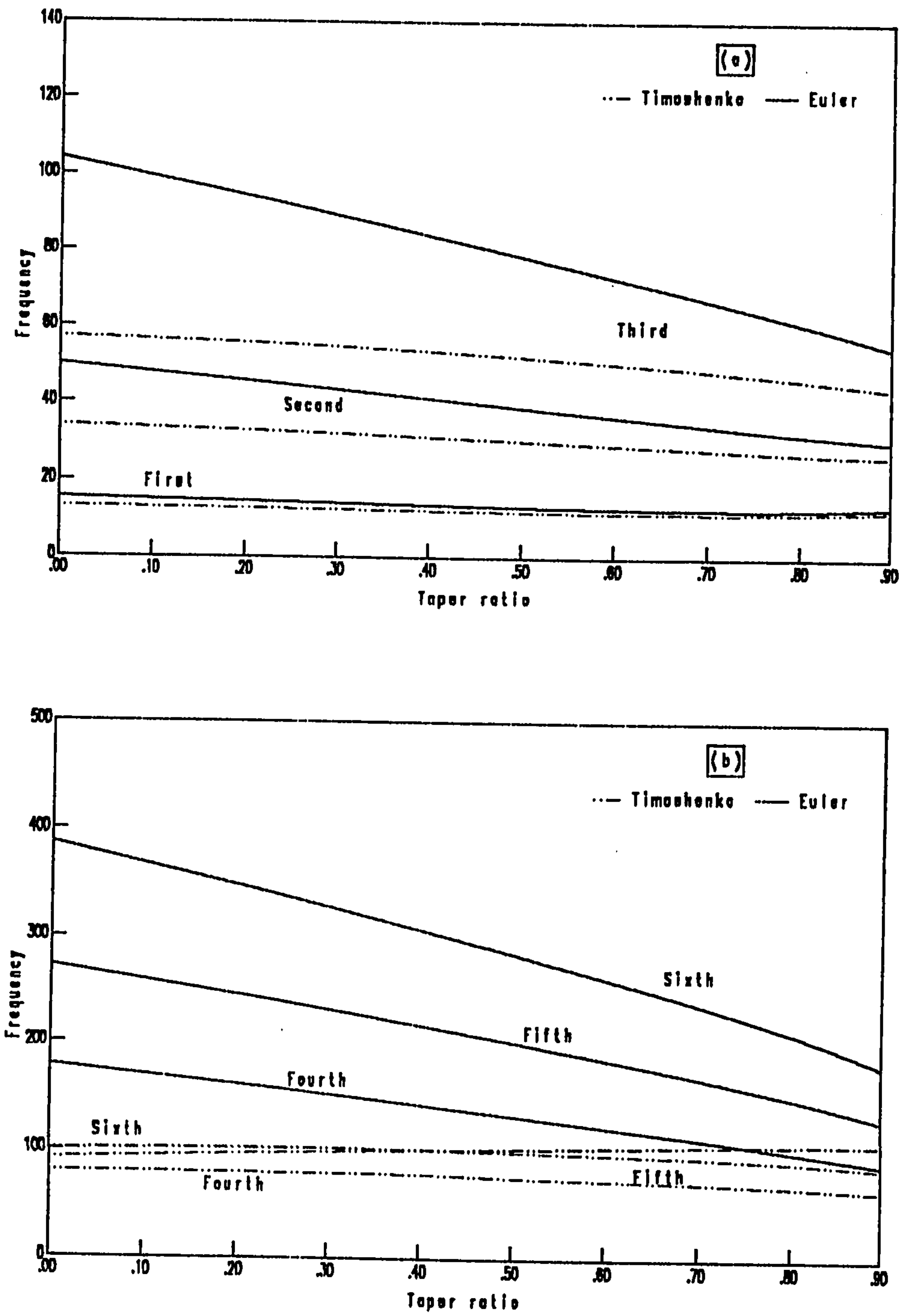

Fig. 4.22 The first six bending frequencies of non-rotating hinged free beam ($\eta = 0.0$);
a) First , second and third , b) Fourth , fifth and sixth .

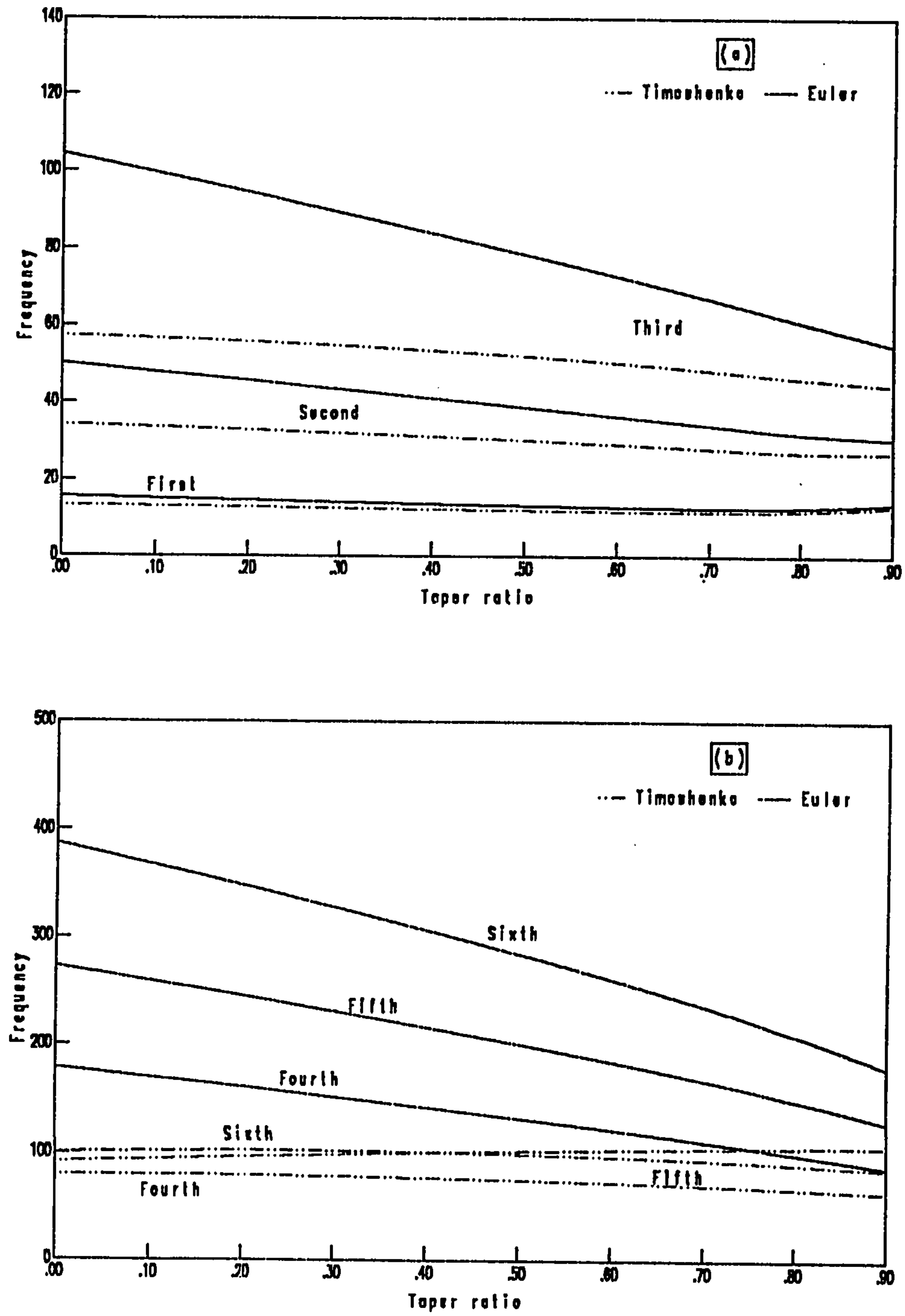

Fig. 4.23 The first six bending frequencies of rotating hinged free beam ($\eta = 1.0$) ;
a) First , second and third , b) Fourth , fifth and sixth .

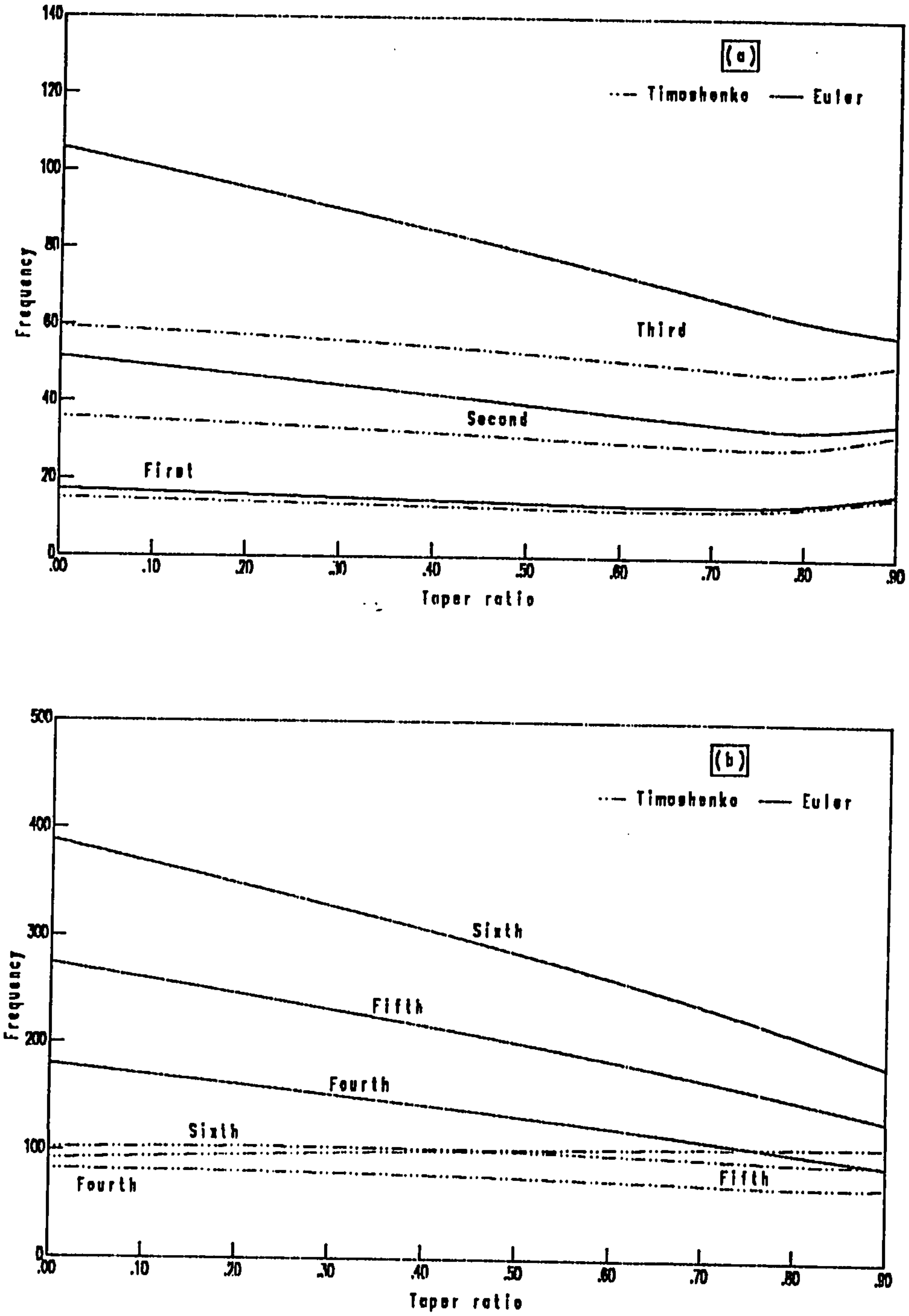

Fig. 4.24 The first six bending frequencies of rotating hinged free beam (η = 3.0); a) First , second and third , b) Fourth , fifth and sixth .

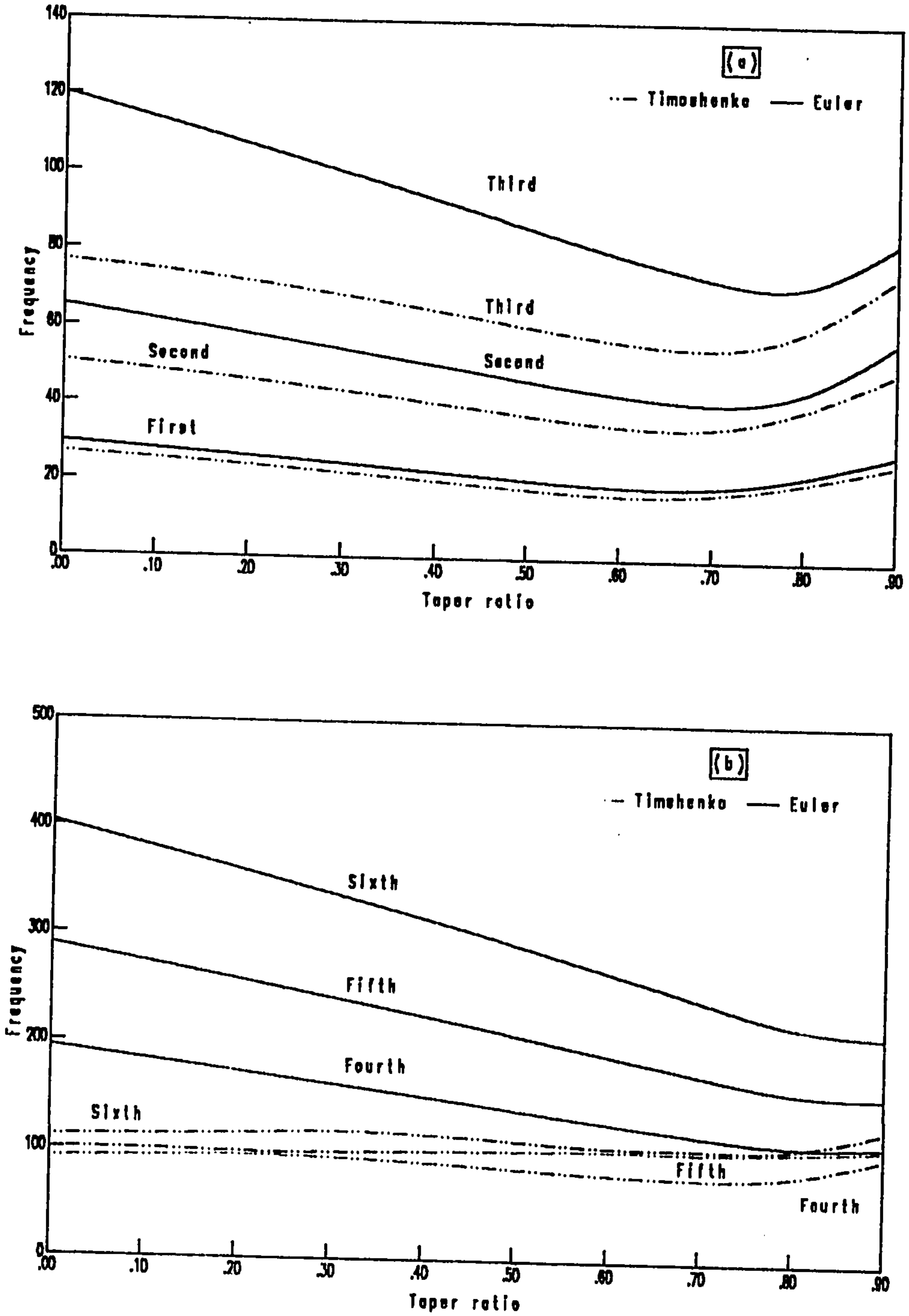

Fig. 4.25 The first six bending frequencies of rotating hinged free beam (η = 10.0); a) First , second and third , b) Fourth , fifth and sixth .

TABLE 4.31 *Effect of rotation on the frequency ratios (λ_T / λ_E) of uniform hinged-free beam ($\nu_y = \nu_z = 0.0$).*

Speed ratio η	Frequency ratios				
	Mode 1	Mode 2	Mode 3	Mode 4	Mode 5
0	0.85008	0.67944	0.54719	0.44663	0.33645
1	0.85267	0.68189	0.54883	0.44779	0.33641
2	0.85957	0.68787	0.55361	0.45118	0.33625
3	0.86872	0.69701	0.56114	0.45644	0.33596
4	0.87812	0.70829	0.57085	0.46298	0.33561
5	0.88649	0.72069	0.58208	0.46992	0.33534
6	0.89333	0.73327	0.59415	0.47596	0.33564
7	0.89856	0.74531	0.60642	0.47929	0.33726
8	0.90236	0.75631	0.61830	0.47892	0.34046
9	0.90496	0.76598	0.62932	0.47568	0.34433
10	0.90661	0.77418	0.63902	0.47087	0.34786
11	0.90747	0.78089	0.64699	0.46527	0.35056
12	0.90771	0.78613	0.65278	0.45940	0.35237

λ_T : *Timoshenko frequency .*
λ_E : *Euler-Bernoulli frequency .*

TABLE 4.32 *Effect of rotation on the frequency ratios (λ_T / λ_E) of a tapered hinged-free beam ($\nu_y = \nu_z = 0.2$).*

Speed ratio η	Frequency ratios				
	Mode 1	Mode 2	Mode 3	Mode 4	Mode 5
0	0.87401	0.71703	0.58912	0.49162	0.39309
1	0.87553	0.71854	0.59039	0.49266	0.39291
2	0.87964	0.72291	0.59413	0.49572	0.39236
3	0.88524	0.72969	0.60008	0.50064	0.39143
4	0.89117	0.73826	0.60791	0.50717	0.39012
5	0.89663	0.74789	0.61717	0.51498	0.38845
6	0.90119	0.75796	0.62743	0.52371	0.38647
7	0.90475	0.76789	0.63824	0.53291	0.38425
8	0.90739	0.77732	0.64922	0.54192	0.38202
9	0.90924	0.78596	0.66003	0.54916	0.38064
10	0.91046	0.79368	0.67040	0.55026	0.38288
11	0.91173	0.80042	0.68013	0.54499	0.38874
12	0.91149	0.80616	0.68906	0.53757	0.39518

λ_T : *Timoshenko frequency .*
λ_E : *Euler-Bernoulli frequency .*

TABLE 4.33 ***Effect of rotation on the frequency ratios (λ_T / λ_E) of a tapered hinged-free beam ($\nu_y = \nu_z = 0.5$).***

Speed ratio η	Frequency ratios				
	Mode 1	Mode 2	Mode 3	Mode 4	Mode 5
0	0.90549	0.77823	0.66231	0.56807	0.49323
1	0.90525	0.77872	0.66288	0.56861	0.49368
2	0.90452	0.78017	0.66456	0.57018	0.49498
3	0.90332	0.78245	0.66727	0.57277	0.49700
4	0.90171	0.78539	0.67091	0.57626	0.49924
5	0.89971	0.78879	0.67531	0.58055	0.49807
6	0.89694	0.79243	0.68032	0.58554	0.49662
7	0.89480	0.79612	0.68576	0.59108	0.49708
8	0.89202	0.79968	0.69147	0.59705	0.49462
9	0.88911	0.80301	0.69729	0.60329	0.49178
10	0.88615	0.80600	0.70310	0.60972	0.48866
11	0.88317	0.80861	0.70877	0.61620	0.48528
12	0.88024	0.81082	0.71423	0.62261	0.48167

λ_T : *Timoshenko frequency .*
λ_E : *Euler-Bernoulli frequency .*

TABLE 4.34 *Effect of rotation on the frequency ratios (λ_T / λ_E) of a tapered hinged-free beam ($\nu_y = \nu_z = 0.7$).*

Speed ratio η	Frequency ratios				
	Mode 1	Mode 2	Mode 3	Mode 4	Mode 5
0	0.92342	0.82361	0.72256	0.63414	0.56047
1	0.92322	0.82399	0.72296	0.63450	0.56079
2	0.92267	0.82513	0.72417	0.63560	0.56177
3	0.92179	0.82692	0.72613	0.63742	0.56337
4	0.92062	0.82925	0.72878	0.63988	0.56556
5	0.91922	0.83197	0.73204	0.64297	0.56829
6	0.91762	0.83493	0.73581	0.64659	0.57152
7	0.91586	0.83795	0.73997	0.65069	0.57515
8	0.91400	0.84095	0.74444	0.65519	0.57909
9	0.91206	0.84378	0.74908	0.66001	0.58316
10	0.91006	0.84640	0.75383	0.66506	0.58703
11	0.90805	0.84874	0.75857	0.67029	0.58981
12	0.90605	0.85076	0.76325	0.67560	0.59002

λ_T : *Timoshenko frequency .*
λ_E : *Euler-Bernoulli frequency .*

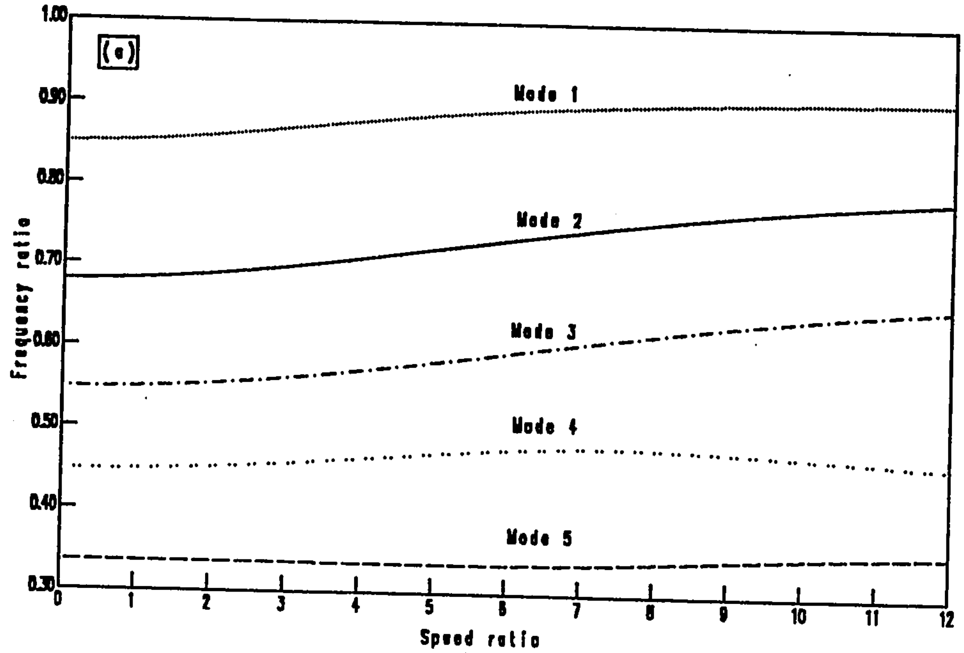

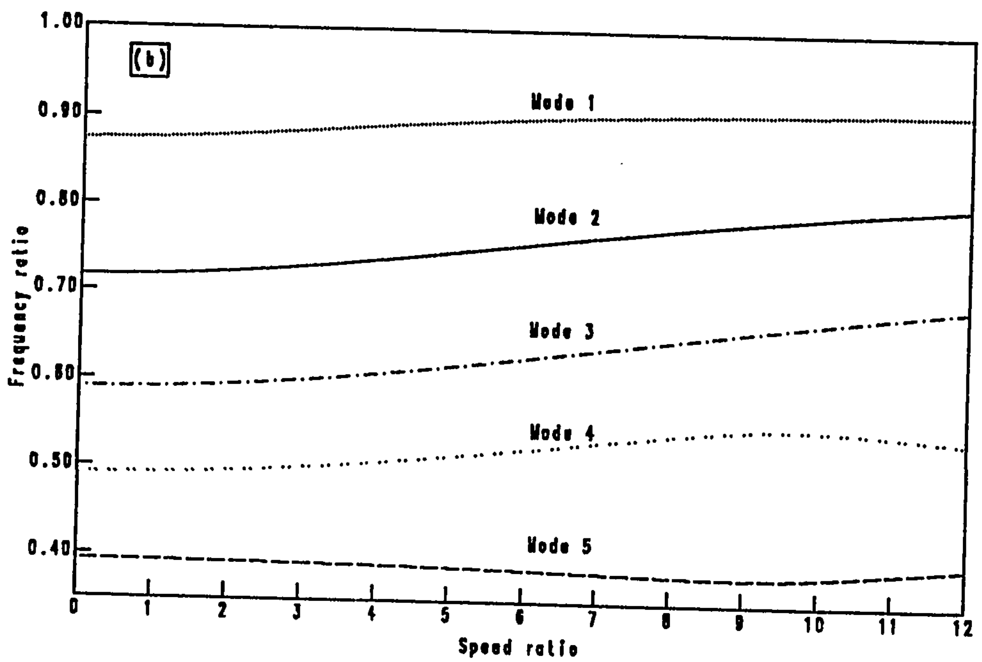

Fig. 4.26 Effect of rotation on the frequency ratios of hinged-free beam ; a) Uniform beam ($v_y = v_z = 0.0$) ; b) Tapered beam ($v_y = v_z = 0.2$).

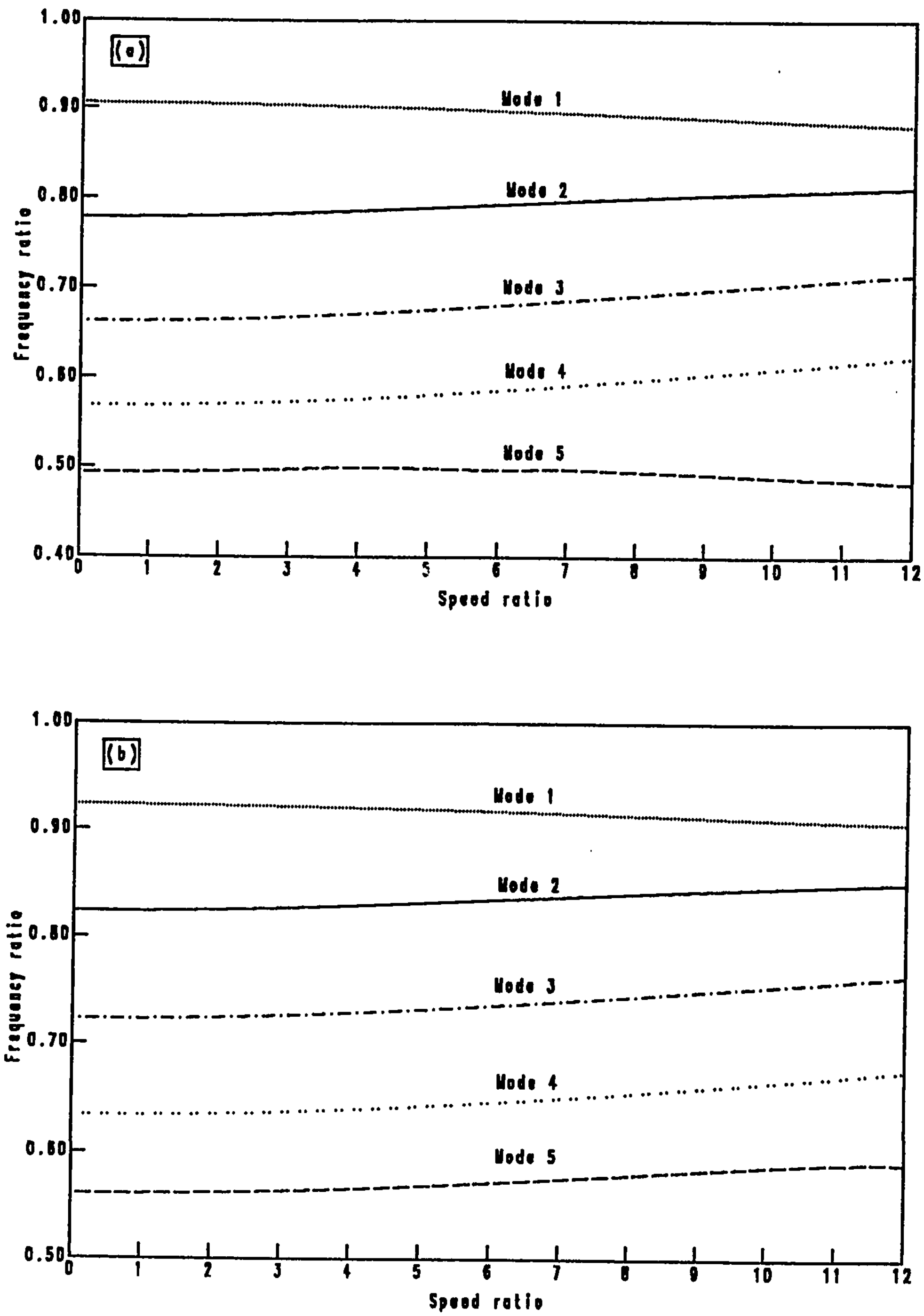

Fig. 4.27 Effect of rotation on the frequency ratios of a tapered hinged-free beam ; a) ($\nu_y = \nu_z = 0.5$) ; b) ($\nu_y = \nu_z = 0.7$) .

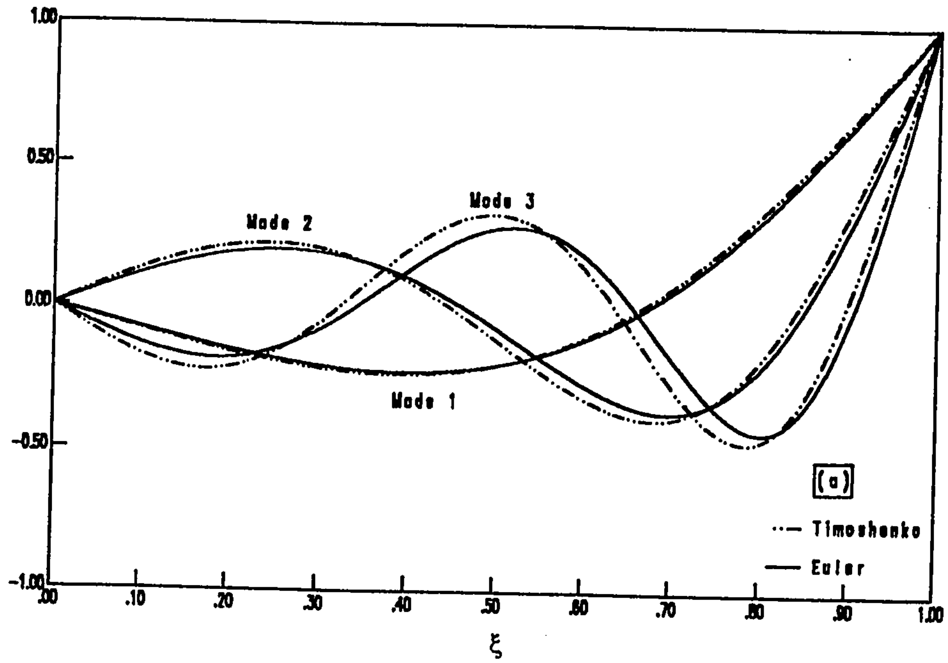

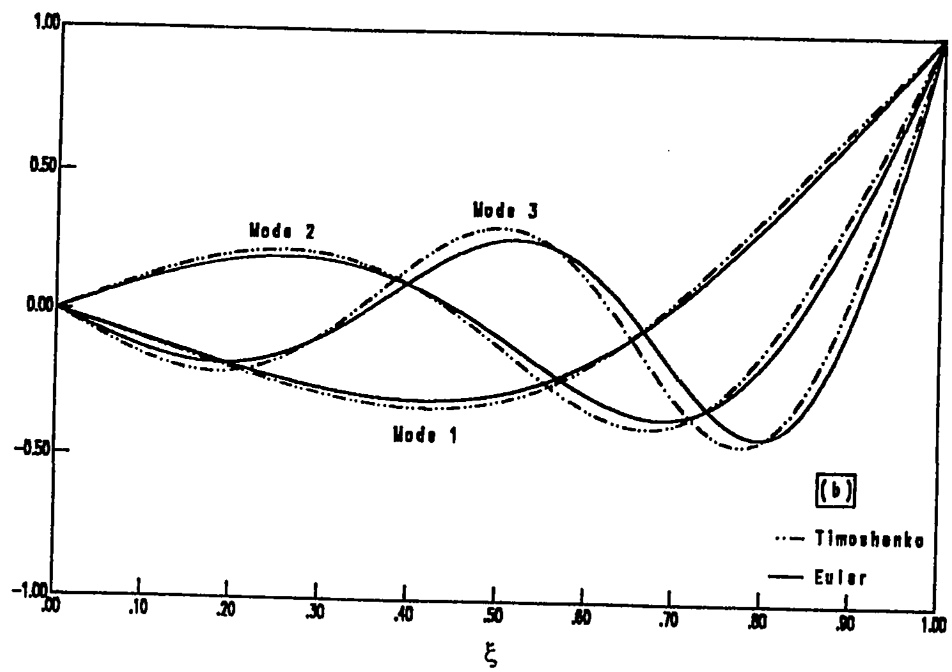

Fig 4.28 The first three flexural mode shapes of a tapered hinged free beam ; ($\nu_y = \nu_z = 0.7$) ; a) $\eta = 0$, b) $\eta = 10.0$.

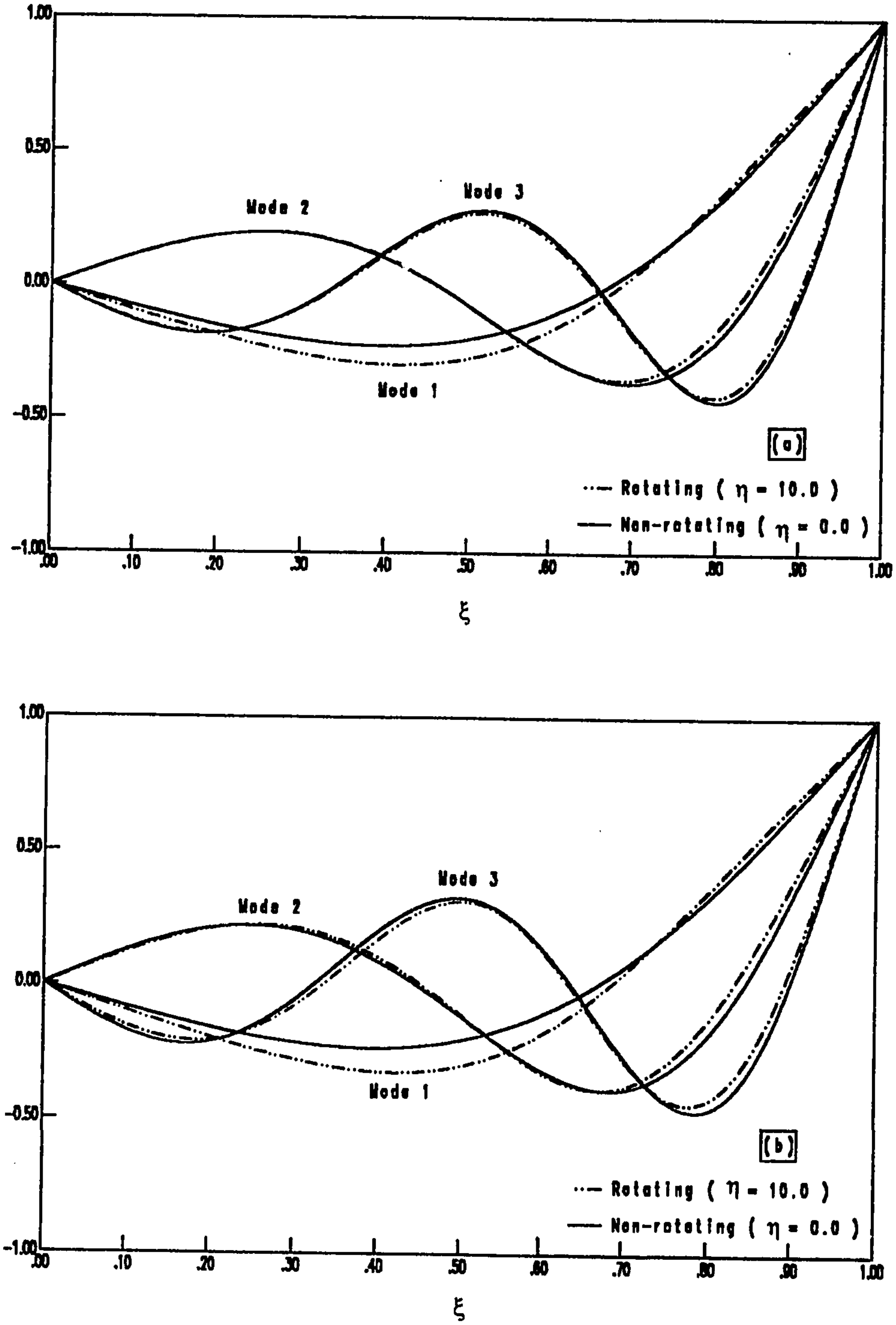

Fig. 4.29 The first three flexural mode shapes of a tapered hinged free beam ; ($\nu_y = \nu_z = 0.7$) ; a) Euler beam , b) Timoshenko beam .

CHAPTER FIVE

CONCLUSIONS

The finite element procedure developed for the free vibration characteristics of rotating and non-rotating tapered beams based on both Euler-Bernoulli and Timoshenko theories has been found to give accurate results . The effects of breadth and depth taper ratios , spin rate , shear deformation and rotary inertia of both cantilever and hinged free beam have been investigated . The results obtained give high accuracy when compared to other numerical results presented by other investigators .

The explicit mass and stiffness matrices of a linearly tapered beam in two planes have been developed in order to provide a means for incorporating as well as investigating the effect of the secondary contributions of shear deformation and rotary inertia in vibration analysis of a rotating and non-rotating tapered beams for both fixed and hinged end conditions . This thesis present for the first time explicit expressions for the rotating tapered Timoshenko beam .

The finite element model presented herein to solve for the natural frequencies of both tapered Euler-Bernoulli and Timoshenko beams has the following capabilities :

1) - It can be used for any type of linearly tapered beam in two planes .

2) - It is applicable to circular or rectangular , hollow or solid cross-sectional area .

3) - It can handle all types of boundary conditions .

4) - It is efficient , accurate and of fast convergence .

The conclusions drawn from the present investigation are :

1) - The values of the frequency parameter and the behavior of the mode shapes obtained are in excellent agreement with the exact and numerical results available in the literature .

2) - The effects of shear deformation and rotary inertia on mode shapes of the structure are small in the first two modes .

3) - The natural frequencies increase as the rotational speed increases , and they are decreasing as the taper ratio increases .

4) - Existence of a critical taper ratio where the frequencies of a rotating beam reverse the direction of change . The centrifugal effect is more dominant than the softening effect resulting from the decrease of the cross-sectional area .

5) - Timoshenko theory tends to lower the frequencies of the vibration while the effect of shear deformation is generally higher than that of rotary inertia for non-rotating beams , but their relative effects may be reversed for the higher mode frequencies of rotating beams owing to the centrifugal stiffness effects .

6) - The explicit element mass and stiffness matrices eliminate the loss of computer time and round-of errors associated with extensive matrix operations which are necessary in the numerical evaluation of the expressions .

7) - The tapered beam finite element developed in this thesis can be easily integrated into any general purpose finite element code in order to perform dynamic analysis of rotating component such as turbine blades , high speed flexible mechanisms , robot manipulators and helicopter rotors .

REFERENCES

[1] M. Shilhansl, 1958 , J. Applied Mechanics , 25 , 28-30 . ***Bending Frequency of a Rotating Cantilever Beam .***

[2] D. Pruelli, 1972 , J. Applied Mechanics , 39 , 602-604 . ***Natural Bending Frequency Comparable to Rotational Frequency in Rotating Cantilever Beam .***

[3] T. Yokoyama, 1988 , Int. J. Mech. Sci. , 30 (10) , 743-755 . ***Free Vibration Characteristics of Rotating Timoshenko Beams .***

[4] A. V. Krishna Murty and S. Sridhara Murthy, 1977 , Mechanism and Machine Theory , 12 , 311-322 . ***Finite Element Analysis of Rotors .***

[5] B. Downs, 1977 , J. Applied Mechanics , 46 , 737-742 . ***Transverse Vibrations of Cantilever Beam Having Unequal Breadth and Depth Tapers .***

[6] A. S. Sarigul (Aydin) and G. Aksu, 1986 , Mechanism and Machine Theory , 21 (1) , 1-12 . ***A Finite Difference Method for the Free Vibration Analysis of Stepped Timoshenko Beams and Shafts .***

[7] A. W. Lees and D. L. Thomas, 1982 , J. Sound and Vibration , 80 (3) , 355-366 . ***Unified Timoshenko Beam Finite Element .***

[8] J. Dugundji, 1988 , AIAA Journal , 26 (8) , 1013-1014 . ***Simple Expressions for Higher Vibration Modes of Uniform Euler Beams .***

[9] S. C. Lin, 1987 , AIAA Journal , 25 (5) , 765-767 . ***Finite Element Method for a Uniformly Loaded Cantilever Beam with General Cross Section .***

[10] G. R. Heppler and J. S. Hansen, 1988 , AIAA Journal , 26 (11) , 1378-1386 . ***Timoshenko Beam Finite Elements Using Trigonometric Basis Functions .***

[11] F. G. Yuan and R. E. Miller, 1988 , AIAA Journal , 26 (11) , 1415-1417 . ***Higher-Order Finite Element for Short Beams .***

[12] R. Gallagher and C. Lee, 1970 , J. Numerical Methods in Engineering , 2 ,

265-275 . *Matrix Dynamic and Stability Analysis with Non-uniform Elements* .

[13] K. Sato, 1980 , Int. J. Mechanical Sciences , 22 , 109-115 . *Transverse Vibrations of Lineraly Tapered Beams with Ends Restrained Elastically Against Rotation Subjected to Axial Force* .

[14] F. Williams and J. Banerjee, 1985 , J. Sound and Vibration , 99 (1) , 121-138 . *Flexural Vibrations of Axially Loaded Beams With Linear or Parabolic Taper* .

[15] W. Carnegie and J. Thomas, 1972 , J. Engng. Ind. , 94 (1) . *The Coupled Bending-Bending Vibrations of Pretwisted Tapered Cantilever Beam* .

[16] R. P. Goel, 1976 , J. Sound and Vibration , 47 (1) , 1-7 . *Transverse Vibration of Tapered Beams* .

[17] L. A. Taber and D. C. Viano, 1982 , J. Sound and Vibration , 83 (2) , 219-228 . *Comparison of Analytical and Experimental Results for Free Vibration of Non-uniform Composite Beams.*

[18] C. W. S. To, 1979 , J. Sound and Vibration , 63 (1) , 33-50 . *Higher Order Tapered Beam Finite Elements For Vibration Analysis* .

[19] C. W. S. To, 1981 , J. Sound and Vibration , 78 (4) , 475-484 . *A Linearly Tapered Beam Finite Element Incorporating Shear Deformation and Rotary Inertia for Vibration Analysis* .

[20] P. V. de Irassar ,G.M. Ficcadenti and P. A. A. Laura, 1983 , AIAA Journal , 21 (2) , 312-314 . *Vibrations of Nonuniform Beams with one End Elastically Restrained against Rotation*

[21] P. Likins, F. Barbera, and V. Baddeley, 1973 , AIAA Journal , 11(9) , 1251-1258 . *Mathematical Modeling of Spinning Elastic Bodies for Modal Analysis* .

[22] S. V. Hoa, 1979 , J. Sound and Vibration , 67 (3) , 369-381 . *Vibration of Rotating Beam with Tip Mass* .

[23] J. S. Rao and S. Banerjee, 1977 , Mechanism and Machine Theory , 12 , 271-280

Coupled Bending-Torsional Vibrations of Rotating Cantilever Blades - Method of Polynomial Frequency Equation .

[24] W. Carnegie, 1959 , J. Mech. Engng. Sci , 1 (3) . *Vibrations of Rotating Cantilever Blading : Theoretical Approaches to the Frequency Problem Based on Energy Methods .*

[25] Y. A. Khulief and Laejoon Yi, 1988 , Computers & Structures , 29 (6) , 1075-1085 . *Lead-Lag Vibrational Frequencies of a Rotating Beam with End Mass .*

[26] D. C. Kammer and A. L. Schlack, Jr, 1987 , J. Applied Mechanics , 54 , 305-310 . *Effects of Nonconstant Spin Rate on the Vibration of a Rotating Beam .*

[27] A. D. Wright, C. E. Smith, R. W. Thresher and J. L. C. Wang, 1982 , J. Applied Mechanics , 49 , 197-202 . *Vibration Modes of Centrifugally Stiffened Beams*

[28] M. Swaminathan and J. S. Rao, 1977 , Mechanism and Machine theory , 12 , 331-337 . *Vibrations of Rotating , Pretwisted and Tapered Blades .*

[29] P. J. Magari, L. A. Shultz and V. R. Murthy, 1988 , Computers & Structures , 29 (5) , 763-776 . *Dynamics of Helicopter Rotor Blades .*

[30] D. Stori and Y. Aboelnaga, 1987 , J. Applied Mechanics , 54 , 311-314 . *Bending Vibrations of a Class of Rotating Beams with Hypergeometric Solutions .*

[31] Y. A. Khulief, 1989 , J. Sound and Vibration , 134 (1) , 87-97 . *Vibration Frequencies of a Rotating Tapered Beam with End Mass .*

[32] F. S. Tse, I. E. Morse and R. T. Hinkle, 1978 , *Mechanical Vibrations : Theory and Applications .* Second Edition Allyn and Bacon , Inc.

[33] Leonard Meirovitch, 1967 , *Analytical Methods in Vibrations .* Mac Millan Company . New York.

[34] R. D. Blevins, 1979 , *Formulas For the Natural Frequency and Mode Shape .* Litton Educational Publishing , Inc .

[35] J. S. Przemieniecki, 1968 , *Theory of Matrix structural Analysis .* Mc. Graw Hill Book Company .

[36] C. L. Dym and I. H. Shames,1973 , ***Solid Mechanics A Variational Approach*** . Mc. Graw Hill Company .

[37] R. D. Cook , D. S. Malkus and M. E. Plesha, 1989 , ***Concepts and Application of Finite Element Analysis*** , 3rd edition , John Wiley & Sons.

[38] B. Smith, J. Boyle, J. Dongarra, B.Garbow, Y. Ikebe, V. Klema and C. Moler, 1976 , ***Matrix Eigensystem Routines-Eispack Guide, Lecture Notes in Computer Science*** . Berlin : Springer-Verlag.

[39] D. H. Hodges and M. J. Rutkowski, 1981 , AIAA Journal , 19 (11) , 1459-1466 . ***Free-Vibration Analysis of Rotating Beams by a Variable-order FiniteElement Method*** .